ECOSYSTEM IMPACTS OF DIAZOTROPHY IN THE SOUTHWESTERN SOUTH CHINA SEA

Dissertation
Zur Erlangung des akademischen Grades
doctor rerum naturalium (Dr. rer. nat.)
der Mathematisch-Naturwissenschaftlichen Fakultät
der Universität Rostock

vorgelegt von
Sarah C. Weber
Rostock, 2020

https://doi.org/10.18453/rosdok_id00002774

Gutachter:

Prof. Dr. Maren Voss
Universität Rostock, Leibniz-Institut für Ostseeforschung Warnemünde

PD Dr. Stefan Forster
Universität Rostock

Prof. Dr. Tim Rixen
Universität Hamburg, Leibniz-Zentrum für Marine Tropenforschung

Datum der Einreichung: 21. Januar 2020

Datum der Verteidigung: 26. Juni 2020

List of Publications and Submitted Manuscripts

This thesis uses materials from the publications listed below. Author contributions are noted.

I. **Sarah C. Weber[1]***, Ajit Subramaniam[2], Joseph P. Montoya[3], Hai Doan-Nhu[4], Lam Nguyen-Ngoc[4], Joachim W. Dippner[1], Maren Voss[1]. (2019). "Habitat delineation in highly variable marine environments." *Frontiers in Marine Science* 6: 112. doi:10.3389/fmars.2019.00112

[1]Department of Biological Oceanography, Leibniz Institute for Baltic Sea Research Warnemünde, Rostock, Germany, [2]Lamont–Doherty Earth Observatory, Columbia University, Palisades, NY, United States, [3]School of Biological Sciences, Georgia Institute of Technology, Atlanta, GA, United States, [4]Institute of Oceanography, Vietnam Academy of Science and Technology, Nha Trang, Vietnam

SW, AS, and JM conceived and designed the research. All authors contributed to the collection and compilation of data. SW, AS, JM, and HD-N analyzed the data. SW, AS, and JM wrote the manuscript. All authors contributed to content revisions and approved the final text.

Table of contents

List of Tables

List of Figures

List of Abbreviations

19'BF	19' butanoyloxyfucoxanthin
19'HF	19' hexanoyloxyfucoxanthin
ALF	Advanced Laser Fluorometer
Allo	alloxanthin
BGCP	biogeochemical province
CAP	canonical analysis of principal coordinates
CDOM	chromophoric dissolved organic material
ChlMD	chlorophyll maximum depth
CSI-AA	compound specific isotope analysis of amino acids
CTD	conductivity temperature depth
DDAs	diatom diazotroph associations
DIC	dissolved inorganic carbon
DIN	dissolved inorganic nitrogen
DON	dissolved organic nitrogen
DvChla+b	divinyl chlorophyll a + b
ENSO	El Niño southern oscillation
Fuco	fucoxanthin
Glu	glutamic acid
IM	intermonsoon
ITCZ	inter-tropical convergence zone
MKGTW	Mekong/Gulf of Thailand water
MLD	mixed layer depth
MRW	Mekong River water
MSW	maximum salinity water
N, N_2	nitrogen, dinitrogen
NAI	nitrogen availability index
NEM	Northeast monsoon
NH_3, NH_4^+	ammonia, ammonium
$NO_{2/3}$	nitrate + nitrite
OnSW	onshore or continental shelf water
OSW	open seawater (water mass), oceanic seawater (habitat)
PCA	principal component analysis
PC	principal component
PE	phycoerythrin
Peri	peridinin
Phe	phenylalanine
P, PO_4^{3-}	phosphate
POC	particulate organic carbon
POM	particulate organic matter
PON	particulate organic nitrogen
PP	primary production
SCS	South China Sea
Si, SiO_2	silicate
SSS	sea surface salinity
SST	sea surface temperature
SWM	Southwest monsoon
T-S	temperature-salinity
TP	trophic position
UCYN	unicellular cyanobacteria
UpW	upwelling water (upwelled waters)
WTNA	Western Tropical North Atlantic
Zea	zeaxanthin

Summary

Primary productivity in surface oceans is often limited by nitrogen (N), making the process of biological nitrogen fixation (the reduction of N_2 to ammonia) an important input pathway for the marine nitrogen cycle. Nitrogen fixation (or diazotrophy) was once thought to be limited to warm oligotrophic oceans, but the recognized domain of marine diazotrophs continues to expand into physicochemically complex regions, including continental shelves and regions influenced by major rivers. This has lead to a need for the development of new tools for assessing the biogeography and drivers of diazotroph populations, and phytoplankton communities more generally. In this thesis, I present one such tool, which uses a combination of commonly measured environmental variables (salinity, temperature, mixed layer depth, nitrate availability, and chlorophyll max. depth) that reflect both instantaneous and time-integrated processes to define biologically relevant habitats on the scale of shipboard sampling. Using the continental shelf waters of the southwestern South China Sea (SCS) as a test system, I paired this habitat type approach with a multi-scale ecosystem assessment of diazotroph impacts based on a combination of uptake rate measurements and nitrogen stable isotope natural abundance measurements across multiple levels of the planktonic food web (e.g., phytoplankton and four mesozooplankton size fractions). This approach simultaneously provided a rigorous test of the utility of the habitat type method and enabled me to address specific questions concerning the environmental drivers and impacts of diazotrophy on food web structure and energy flow in this shelf ecosystem.

This strategy identified clear habitat-specific trends in phytoplankton community structure, as well as diazotroph distributions and activity. In contrast to previous investigations, we found that aged Mekong River plume waters were not necessary to stimulate N_2-fixation in the region, suggesting that diazotrophy may be more widespread on the SCS shelf than previously thought. Even though rates of N_2-fixation were modest, natural abundance measurements indicated that diazotroph N accumulated in surface waters, comprising up to 70% of N in suspended particles in oligotrophic shelf waters. Trends in the distribution of diazotrophs and their N_2-fixation activity at the habitat scale were mirrored by contributions of diazotroph N to zooplankton biomass, reaching as high as 20%. These results show that the impacts of N_2-fixation in shelf waters of the SCS were significant and persistent enough to

propagate through the planktonic food web, which had implications for both N cycling and food web structure. Compound specific isotope analyses on amino acid N revealed that mesozooplankton trophic position scaled inversely with mixed layer phosphate concentration, suggesting a useful indirect environmental indicator of zooplankton food web structure. Additionally, we found that mesozooplankton reliance on diazotroph N increased concurrently with nitracline depth, directly linking a habitat-defining variable to upper food web processes. These findings demonstrate for the first time the utility of the habitat type approach in evaluating plankton biogeography, activity, and food web dynamics in physicochemically heterogeneous regions.

Zusammenfasung

Die Primärproduktivität der oberen Wasserschichten der Meere wird oft durch Stickstoff (N) begrenzt, was den Prozess der biologischen Stickstofffixierung (die Reduktion von N_2 zu Ammoniak) zu einer wichtigen Quelle für den marinen Stickstoffkreislauf macht. Die Stickstofffixierung (oder Diazotrophie) galt einst als auf warme oligotrophe Ozeane beschränkt, aber die anerkannte Domäne der marinen Diazotrophie schließt mittlerweile auch physikalisch-chemisch komplexe Regionen ein, einschließlich Kontinentalschelfe und Regionen, die von großen Flüssen beeinflusst werden. Dies hat dazu geführt, dass neue Instrumente zur Bewertung der Biogeographie und der Trieber diazotropher Populationen und der Phytoplanktongemeinschaften im Allgemeinen entwickelt werden müssen. In dieser Arbeit stelle ich ein solches Instrument vor. Es verwendet eine Kombination von üblicherweise gemessenen Umweltvariablen (Salzgehalt, Temperatur, Durchmischungstiefe, Nitraklinen-Tiefe und Tiefe des Chlorophyll-Maximums). Diese spiegeln sowohl momentane als auch zeitintegrierte Prozesse wider, um biologisch relevante Lebensräume auf der Skala von Schiffsprobenahmen zu definieren. Das Schelfwasser des südwestlichen Südchinesischen Meeres (SCS) als Testsystem nutzend, habe ich diesen Habitattyp-Ansatz mit einer Multiskalen-Ökosystem-Bewertung der Auswirkungen von Diazotrophie gepaart. Dafür habe ich eine Kombination aus Messungen der Aufnahmegeschwindigkeit und Messungen der natürlichen Abundanz stabiler Stickstoffisotope über mehrere Ebenen des

planktischen Nahrungsnetzes (z.B. Phytoplankton und vier Mesozooplankton-Größenfraktionen) verwendet. Dieser Ansatz lieferte gleichzeitig einen belastbaren Test des Nutzens der Habitattyp-Methode und ermöglichte es mir, spezifische Fragen bezüglich der Umweltfaktoren und Auswirkungen der Diazotrophie auf die Struktur des Nahrungsnetzes und den Energiefluss in diesem Schelfökosystem zu behandeln.

Diese Strategie identifizierte klare Habitat-spezifische Trends in der Struktur der Phytoplankton-Gemeinschaft sowie der Verteilung und Aktivität von Diazotrophie. Im Gegensatz zu früheren Untersuchungen stellten wir fest, dass das gealterte Mekong-Flußfahnenwasser nicht notwendig war, um die N_2-Fixierung in dieser Region zu stimulieren. Das deutet darauf hin, dass Diazotrophie entlang des SCS-Schelfs weiter verbreitet sein könnte als bisher angenommen. Obwohl die N_2-Fixierungsraten gering waren, zeigten Messungen der natürlichen Abundanz von Stickstoffisotopen in Partikeln, dass sich Diazotrophes N im Oberflächenwasser ansammelte, da diese Schwebteilchen in oligotrophen Schelfgewässern bis zu 70% N diazotrophen Ursprungs enthalten. Die Trends in der Verteilung von Diazotrophen und ihrer N_2-Fixierungsaktivität in den verschiedenen Habitaten spiegelten sich in den Anteilen von diazotrophem N an der Zooplankton-Biomasse wider, die bis zu 20% erreichten. Diese Ergebnisse zeigen, dass die N_2-Fixierung in den Schelfgewässern des SCS signifikant und anhaltend genug war, um sich innerhalb des planktischen Nahrungsnetzes zu verbreiten. Dies hatte Auswirkungen sowohl auf den N-Kreislauf als auch auf die trophische Struktur des Nahrungsnetzes. Molekülspezifische Isotopenanalysen von Aminostickstoff zeigten, dass die trophische Position des Mesozooplanktons invers mit der Phosphatkonzentration in der Durchmischungstiefe zunahm, was auf einen nützlichen indirekten Umweltindikator für die Struktur des Nahrungsnetzes des Zooplanktons im SCS hindeutet. Außerdem fanden wir heraus, dass die Abhängigkeit des Mesozooplanktons von diazotrophem N gleichzeitig mit der Nitraklinen-Tiefe zunahm, was eine direkte Verbindung zwischen einer Habitat-definierenden Variablen und Prozessen in den höheren trophischen Ebenen des Nahrungsnetzes herstellt. Diese Ergebnisse zeigen erstmals den Nutzen des Habitattyp-Ansatzes bei der Bewertung von Plankton-Biogeographie, Aktivität und Nahrungsnetzdynamik in physikalisch-chemisch heterogenen Regionen.

1. Introduction

The PhD thesis work presented here is part of the DFG-funded "Nitrogen-fixation in the monsoon impacted Mekong river plume (NiFiM)" project granted to Maren Voss (Leibniz Institute for Baltic Sea Research Warnemünde) to investigate the drivers and ecosystem impacts of nitrogen-fixation in the southwestern South China Sea (SCS). This project was carried out in corporation with Joseph P. Montoya (Georgia Institute of Technology), Ajit Subramaniam (Lamont–Doherty Earth Observatory), Lam Nguyen-Ngoc and Hai Doan-Nhu, (Institute of Oceanography Nha Trang), Rachel A. Foster (University of Stockholm), and Annalisa Bracco (Georgia Institute of Technology). Ship time was granted by the Schmidt Ocean Institute and was comprised of two expeditions to the southwestern SCS in June 2016 and September 2017. Due to uncontrollable political circumstances, the first cruise was restricted to Vietnamese territorial waters (Fig. S1.1) and permission for the second cruise was ultimately withheld.

In the following thesis, I will perform a multi-scale analysis of the southwestern SCS, beginning with establishing the physicochemical conditions of the investigation area (Chapter 3), working through the biogeography and activity of diazotrophs (Chapters 5 and 6), and finally tracing the biogeochemical impacts of diazotrophy through the upper planktonic food web (Chapter 7). This will be achieved with the help of a novel framework based on biologically relevant habitat types, the development and application of which will be addressed in Chapters 2 and 4, respectively.

1.1. Diazotrophy and the nitrogen cycle

Nitrogen (N) is an essential component of all life on Earth and yet ~70% of the global surface ocean is oligotrophic, where phytoplankton growth and primary productivity are limited by N availability (Falkowski 1997). Inputs of "new" N to these waters (as opposed to regenerated N derived from existing organic matter within the euphotic zone) control production of new biomass and its subsequent downward vertical export (Dugdale and Goering 1967; Eppley and Peterson 1979) (Fig. 1.1). This process, referred to as the biological pump, results in the transfer of biologically fixed carbon dioxide (CO_2) from surface waters to the deep ocean and regulates atmospheric CO_2 concentrations (Gruber and Sarmiento 2002). Globally, dissolved inorganic N (DIN) diffused or upwelled from below the thermocline is the largest source of new N to surface waters (Gruber 2008), but at a regional scale within the tropics and subtropics, N inputs from diazotrophy, which refers to the biological reduction of dinitrogen (N_2) to ammonia (NH_3), can exceed that of vertical

DIN transport (Capone 2005; Karl et al. 1997; Mahaffey et al. 2005). Additionally, subthermocline DIN and riverine N inputs are accompanied by significant injections of CO_2, meaning that diazotrophy (N_2-fixation) and atmospheric N deposition are the only forms of new N that can support the net removal of atmospheric CO_2 (Eppley and Peterson 1979). Given the significance of diazotrophy on both the global N and C cycles, and its bearing on processes linked to climate change, there is an obvious need to understand environmental controls on diazotroph populations, the composition of those populations, and their influence on the movement of N through plankton food webs.

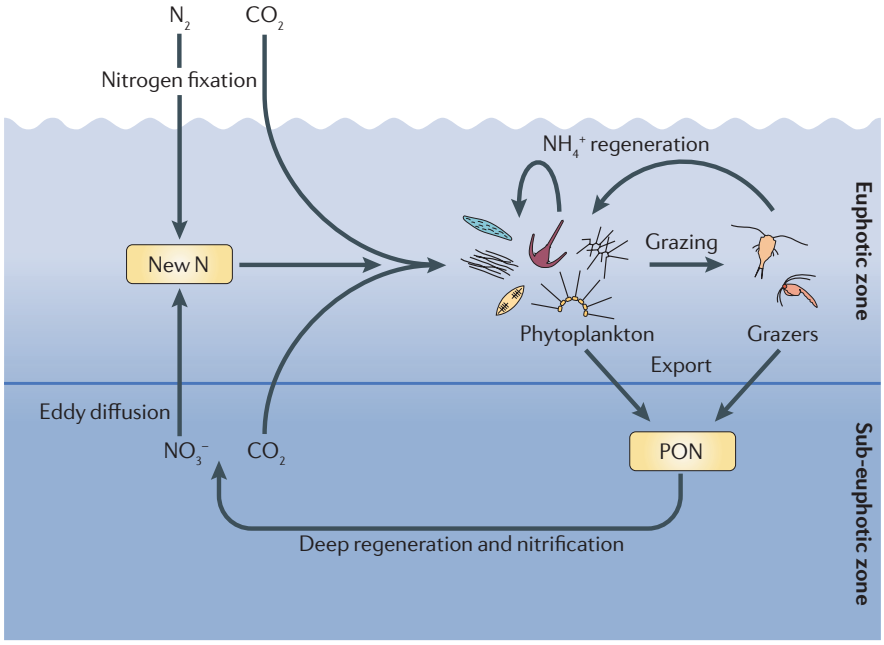

Figure 1.1: Schematic showing the major sources of new N (upwelled/diffused nitrate and N_2-fixation) that support primary production and control the export of particulate organic N (PON) out of the euphotic zone. Production is also fueled by N regenerated within the euphotic zone. Other sources of new N not shown include atmospheric deposition and river outflow. Figure taken directly from Sohm et al. (2011c).

The global significance of diazotrophy was initially realized through studies on large, conspicuous species, namely *Trichodesmium* spp. (Capone et al. 1997; Carpenter 1983) (Fig. 1.2D) and diatom diazotroph associations (DDAs) (see Villareal 1989 and references therein; Villareal 1994) (Fig. 1.2A-C). *Trichodesmium* spp., which are non-heterocystous cyanobacteria that thrive in the warm, oligotrophic waters, essentially drove the narrative on the importance of marine diazotrophy for decades. By contrast, DDAs are less prolific, but represent a highly diverse group in which diazotrophic heterocystous cyanobacteria (*Richelia intracellularis* or *Calothrix rhizosoleniae*) live in presumably facultative symbiosis with various genera of diatoms (*Rhizosolenia*, *Hemiaulus*,

Chaetoceros, *Guinardia*, *Bacteriastrum*) (summarized by Foster et al. 2008). Of these DDAs, *Rhizosolenia–Richelia* and *Hemiaulus–Richelia* associations are the most common (Foster et al. 2008; Villareal 1994).

The development and more frequent application of molecular techniques to identify diazotrophs allowed for a greater appreciation of both diazotroph species and habitat diversity. The most widely used molecular approach enumerates diazotrophs based on *nifH* genes, which encode part of the nitrogenase enzyme responsible for reducing N_2, and enable the identification of species previously undetectable due to their small size and weak fluorescence (Zehr et al. 2016). This includes unicellular groups of cyanobacterial diazotrophs, UCYN-A, B, C (Zehr et al. 2008; Zehr et al. 1998; Zehr and Turner 2001) (Fig. 1.2E), whose abundances, distributions, and N_2-fixation rates can rival that of the more charismatic diazotrophs (Church et al. 2009; Martinez-Perez et al. 2016; Montoya et al. 2004; Tang and Cassar 2019).

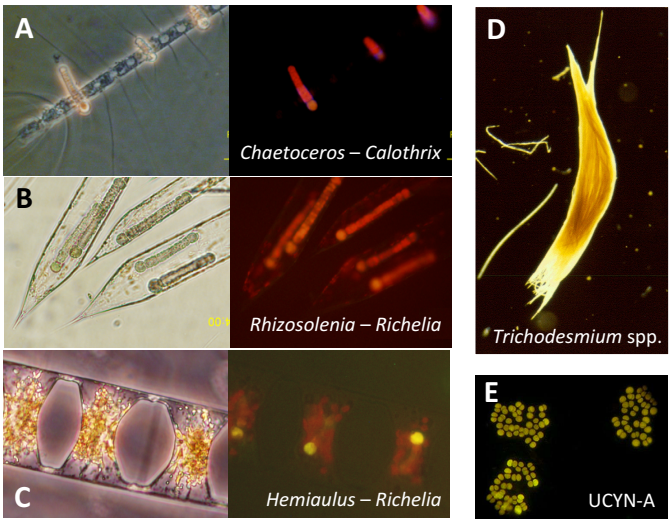

Figure 1.2: (A-C) Paired phase contrast or differential interference contrast **(left)** and fluorescence images **(right)** of the three most common DDAs with **(A)** external and **(B, C)** internal symbionts. *Credit:* Lam Nguyen-Ngoc. **(D)** *Trichodesmium* colony composed of many trichomes. *Credit:* Tracy Villareal. **(E)** Unicellular diazotrophic assemblage. *Credit:* Jonathan Zehr.

A greater understanding of diazotroph diversity has come with an intense interest in understanding the environmental factors that limit N_2-fixation and determine diazotroph habitat space. Global patterns of diazotrophy have gradually emerged (Luo et al. 2012; Sohm et al. 2011c; Tang and Cassar 2019), though the factors regulating diazotroph biogeography are often compounding, complicating the identification of universal controls (Sohm et al. 2011c; Tang and Cassar 2019). Temperature, phosphate (P), and iron are seen as the primary regulators of N_2-fixation, with the majority of activity occurring in warm tropical and subtropical surface waters (Fig. 1.3). In these regions, N:P ratios are below the Redfield ratio of 16:1, indicating an excess of P relative to N according to the average physiological requirements of phytoplankton (Redfield 1958). Additionally, diazotrophs have particularly high iron requirements (Berman-Frank et al. 2001) since nitrogenase, the enzyme that reduces N_2, has a high iron content. Dissolved

iron limits much of the diazotrophic activity in the central and eastern Pacific (Brown et al. 2005; Grabowski et al. 2008; Wu et al. 2001), whereas atmospheric dust inputs from the Sahara Desert (Mahowald et al. 2005) alleviate iron limitation in the North Atlantic (Moore et al. 2009). Iron inputs to this region can be so significant that phosphate is exhausted and becomes limiting (Krauk et al. 2006; Sohm et al. 2008; Webb et al. 2007).

These broad patterns in nutrient limitation are accompanied by regional variation in the dominant diazotroph groups and likely reflect differences in their minimum nutrient tolerances (Fig. 1.3). Unicellular species are most prolific in parts of the North Pacific (Church et al. 2008; Moisander et al. 2010; Tang and Cassar 2019), likely owing to their tolerance of low dissolved iron concentrations (Sohm et al. 2011b; Sohm et al. 2011c), whereas large diazotrophs like *Trichodesmium* spp., which have greater flexibility in P metabolism (Dyhrman et al. 2006), tend to dominate portions of the North Atlantic (Church et al. 2008; Tang and Cassar 2019).

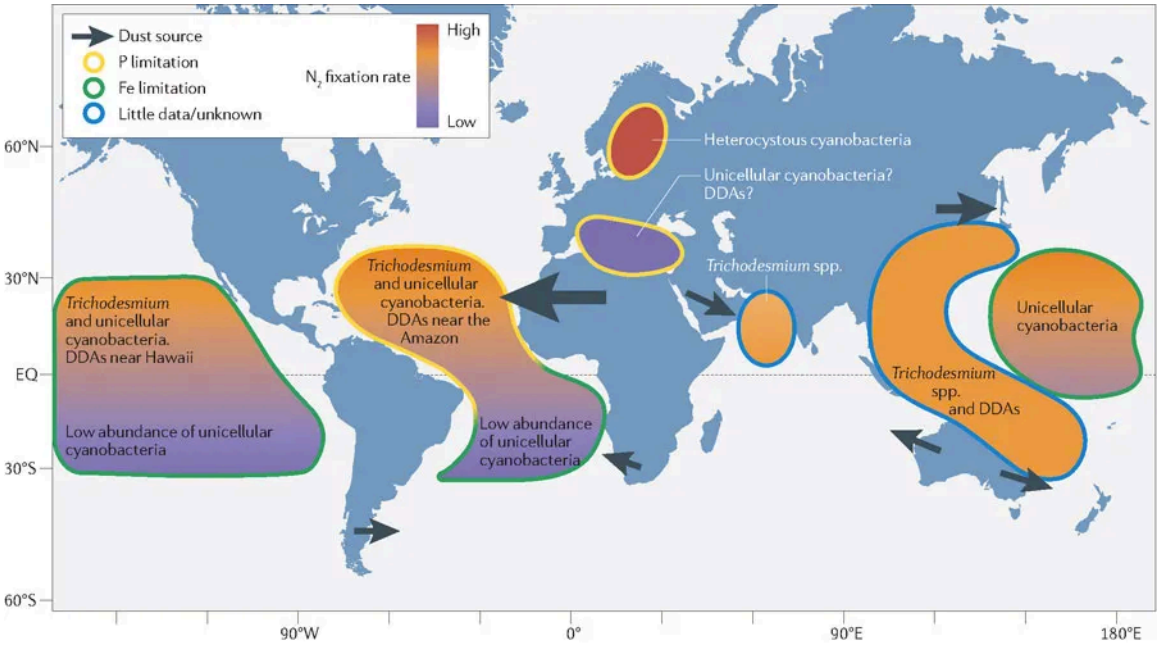

Figure 1.3: Conceptual map summarizing the distribution of N_2-fixation rates, dominant diazotroph species, and limiting nutrients. The fill and outline colors correspond to the relative N_2-fixation rate and principal limiting nutrient, respectively. Figure taken directly from Sohm et al. (2011c).

Global distributions of DDAs are less well-constrained, though *Hemiaulus* associations tend to be more abundant in the North Atlantic, whereas *Rhizosolenia* associations reach their highest abundances in the North Pacific (Foster et al. 2008). Interestingly, both DDAs are commonly associated with the offshore plumes of large tropical rivers (Foster et al. 2007; Foster et al. 2009; Grosse et al. 2010; Voss et al. 2014).

Some of the highest measured DDA abundances have been found in the Amazon River plume in the western tropical North Atlantic (Carpenter et al. 1999; Subramaniam et al. 2008; Weber et al. 2017), where aged plume waters depleted in N but rich in phosphate and silicate stimulate DDA growth (Goes et al. 2014; Subramaniam et al. 2008; Weber et al. 2017). Unfortunately, very little is known about the conditions that foster symbiosis formation and that favor the growth of one particular DDA over another, as DDAs are still systematically under-investigated (Caputo et al. 2018). We do know that the symbioses are highly specific (Foster and Zehr 2006; Janson et al. 1999), and it appears that the degree of the symbiont's dependence on its host, as suggested by genome streamlining (Caputo et al. 2018; Hilton et al. 2013), is reflected in the physical location of the symbiont relative to its host's cell wall. For example, *Calothrix* symbionts attach to the spines of *Chaetoceros compressus* to form external associations and have similar metabolic capabilities to free-living diazotroph species, including the ability to utilize ammonium and nitrate/nitrite (Hilton et al. 2013). By contrast, *Richelia* symbionts reside within the siliceous frustule of *Hemiaulus* and lack genes associated with the uptake and processing of these reduced N species (Hilton et al. 2013); their genomes are effectively streamlined for N_2-fixation. These differences in host-symbiont dependency likely influence the distributions and success of particular DDAs in different environmental conditions, though this question has not been investigated.

The type of diazotroph community present has important implications for the movement of N and C through the food web. *Trichodesmium* spp. are buoyant (Villareal and Carpenter 2003; Walsby 1978) and have few known zooplankton grazers (Conroy et al. 2017; O'Neil and Roman 1992) owing to their chemical defenses (Hawser et al. 1992), making their biomass less prone to export via either passive sinking or zooplankton fecal packaging. In combination with the release of fixed N to their surroundings via either endogenous (Mulholland et al. 2006; Mulholland and Capone 2000; Wannicke et al. 2009) or exogenous (Hewson et al. 2004; O'Neil 1999; Ohki 1999) processes, these mechanisms likely retain *Trichodesmium*-derived N within surface waters (Mulholland 2007). This retained N may be indirectly transferred up the food web through grazing on non-diazotrophic organisms that have utilized this diazotroph-N, including phytoplankton and bacteria (Bonnet et al. 2016a; Bonnet et al. 2016b; Caffin et al. 2018). Since bacteria are too small to be directly grazed by mesozooplankton (Hansen et al. 1997), another trophic step via larger bacterial predators is required to move diazotroph N into the zooplankton food web. This circuitous pathway increases the apparent trophic position of

mesozooplankton (Steffan et al. 2015), and has been demonstrated in the Baltic Sea where diazotrophic cyanobacteria similar to *Trichodesmium* spp. form blooms (Loick-Wilde et al. 2019).

In contrast to *Trichodesmium* spp., DDAs strongly intensify the biological pump since their heavy, siliceous frustules act as ballasts upon their death. DDAs are associated with pulses of sedimenting organic material (Karl et al. 2012; Scharek et al. 1999; Subramaniam et al. 2008), and this process can be so efficient in the offshore waters of the Amazon River plume that the exported C offsets CO_2 outgassing associated with the river outflow (Subramaniam et al. 2008). DDAs are also more palatable than *Trichodesmium* spp., enabling a more direct transfer of diazotroph N into zooplankton biomass (Conroy et al. 2017; Hunt et al. 2016). Less is known about the fate of unicellular groups, but much like DDAs, UCYNs are associated with higher diazotroph N transfer to mesozooplankton (Caffin et al. 2018; Hunt et al. 2016). Additionally, UCYNs release a portion of their fixed N as dissolved N, though comparatively less than *Trichodesmium* spp. (Berthelot et al. 2015), which likely contributes to non-diazotroph primary production.

Despite advances in quantifying the rates of activity and global distributions of major diazotrophs, geochemical models continue to point to an underestimation of global N_2-fixation (Codispoti 2007; Deutsch et al. 2007; Landolfi et al. 2018), which has prompted investigations into regions that were traditionally thought to limit diazotroph growth and activity. Within the last decade in particular, the known domain of diazotrophs has expanded significantly with the discovery of active unicellular groups in Artic waters (Harding et al. 2018; Shiozaki et al. 2018; Sipler et al. 2017), non-cyanobacterial diazotrophs below the euphotic zone (summarized by Bombar et al. 2016; Moisander et al. 2017), and a variety of highly active diazotroph species near upwelling zones (Sohm et al. 2011a; Voss et al. 2006; Voss et al. 2004) and in coastal waters (e.g. Mulholland et al. 2019; Shiozaki et al. 2015; Tang et al. 2019) where DIN concentrations can be significant. These findings continue to challenge the widely held notions that autotrophic N_2-fixation is energetically unfavorable (Falkowski 1983) in the presence of appreciable DIN (Knapp 2012) or that diazotrophs are outcompeted by fast-growing phytoplankton species (Ward et al. 2013).

1.2. Ecosystem partitioning

Interest in diazotrophy in coastal waters along continental shelves continues to grow, given that these regions are highly productive and support massive fishing economies

(Jahnke 2010; Lohrenz et al. 2002; Teh et al. 2017). Even so, shelf ecosystems remain severely understudied and underrepresented in biogeochemical models due in large part to the high variability in physicochemical conditions (Deutsch et al. 2007; Gruber and Sarmiento 1997). The mesoscale and submesoscale features that drive biological productivity and phytoplankton growth in these regions (e.g. coastal upwelling, mesoscale eddies, river outflow, and their associated fronts) introduce incredible heterogeneity, complicating efforts to evaluate phytoplankton biogeography and plankton influence on the local biogeochemistry. There is a clear need for tools that can untangle biologically relevant forcings at these scales.

A common strategy when working with heterogeneous marine systems is to use physical tracers like water temperature and salinity (T-S) to resolve the hydrological structure underlying the chemistry and biology. This approach is very powerful in identifying water masses and quantifying their mixing, but may fail to address processes directly regulating phytoplankton growth and community structure. For example, much of the recent work in the offshore Amazon River plume has used a defined salinity range to categorize habitats and to evaluate phytoplankton biogeography (Goes et al. 2014; Gomes et al. 2018; Subramaniam et al. 2008; Weber et al. 2017). The prevalence of DDAs in "mesohaline" waters (surface salinity of 30 – 35) is an interesting emergent property of the system: salinity itself is unlikely to determine DDA distributions (Subramaniam et al. 2008), since not all mesohaline plume waters have significant DDA populations (Goes et al. 2014; Weber et al. 2017), but rather DDA distributions reflect biogeochemical conditions and their variability (Goes et al. 2014; Gomes et al. 2018; Stukel et al. 2014; Weber et al. 2017). In addition, the Amazon River's chemical composition varies with season (DeMaster et al. 1996), so salinity alone may not be a reliable indicator of biogeochemical conditions (Subramaniam et al. 2008).

As another example, Loick-Wilde et al. (2017) used waters masses based on T-S properties of the South China Sea (Dippner and Loick-Wilde 2011) as a means of both categorizing large phytoplankton datasets and assessing the influence of water mass distributions and their interactions on community composition over multiple seasons and years. This approach, however, groups phytoplankton communities based solely on physical properties of the water, which presents two problems: 1) other environmental factors known to influence phytoplankton distributions (e.g., the availability of nutrients, light, etc.) are not explicitly addressed, and 2) the mixing of water masses is an instantaneous process reflected directly in the T-S properties, whereas significant alterations

to phytoplankton community composition and biomass may take on the order of hours to days. Even though such efforts to use water mass analysis to define phytoplankton habitats have greatly enhanced our understanding of marine systems, there is still room to develop complementary methods of habitat delineation.

For an alternative approach, we can draw inspiration from Longhurst's biogeochemical province (BGCP) concept (Longhurst 1995; Sathyendranath et al. 1995), which has been widely implemented since its development (e.g. Honjo et al. 2008; Reygondeau et al. 2012; Rouyer et al. 2008). Importantly, this approach uses a combination of both physical ocean processes and seasonal cycles of production and consumption – directly reflective of biological activity – to partition the global seascape (Longhurst 1995; Sathyendranath et al. 1995). The resulting provinces have geographically dynamic boundaries that reflect seasonal and climatic fluctuations and which can be used to extrapolate sparse measurements to larger regions. BGCPs operate at the global scale, but the same qualities that have made this concept so successful can be retuned to accommodate ecosystem partitioning on the scale of oceanographic cruises and shipboard sampling.

In this thesis, I will outline such an approach (Chapter 2) and will apply it (Chapter 4) to the southwestern South China Sea (SCS) near the coast of southern Vietnam to assess phytoplankton community structure and to provide a framework on which to evaluate the drivers and ecosystem impacts of diazotrophy. This region is an ideal test system for the following reasons: 1) it is hydrographically complex due to the seasonal influence of both coastal upwelling and discharge of the Mekong River (Voss et al. 2014); 2) it supports a global fishing industry, establishing the area as economically valuable (Teh et al. 2017); and 3) it supports a diverse and active diazotroph community, the drivers of which remain somewhat unclear (Bombar et al. 2011; Grosse et al. 2010; Voss et al. 2006). Additionally, any investigation into this region has the benefit of the immense groundwork laid by a four-year field program stemming from a Vietnamese (Institute of Oceanography Nha Trang) – German (Leibniz Institute for Baltic Sea Research Warnemünde) corporation between 2003 and 2006 (Voss et al. 2014).

1.3. Physical background of the SCS

The South China Sea, one of the largest marginal seas in the western Pacific, is a very physically dynamic and complex system, but understanding the major physical forcings and resulting seasonal patterns is vital to interpreting biogeochemical and biological aspects of the region. Basin-wide changes in the wind field and currents occur

on inter- and intra-annual timescales and with appreciable variability within seasons. The most prominent forcings in the region are the East Asian monsoons, which control both the climate and upper water column dynamics of the SCS. The monsoons are generated by regular meridional migrations of the Inter-Tropical Convergence Zone (ITCZ): during the winter monsoon (Nov – March), the ITCZ lies to the south of the SCS, producing strong NE winds (~9 m/s, Dippner et al. 2007), and during the summer monsoon (June – Sept), the ITCZ has shifted northward (21 – 24°N), switching the direction of the wind field and resulting in SW winds (~6 m/s, Dippner et al. 2007).

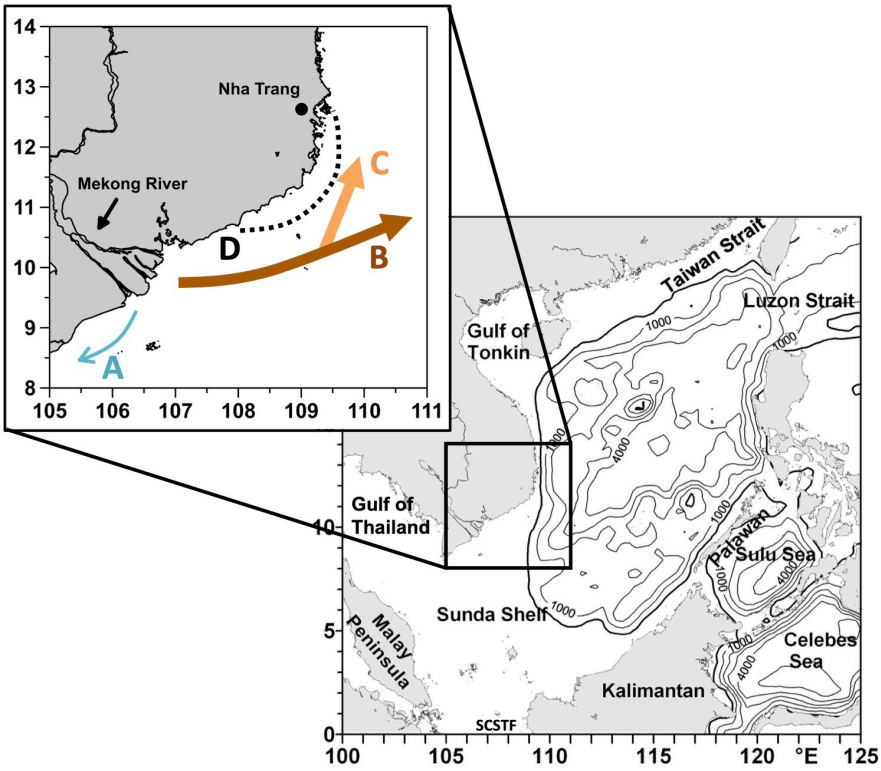

Figure 1.4: Study region in the South China Sea. Bathymetry at 1000m increments is shown by the black lines; thick black line marks 200m. Black box marks the study region. Map courtesy of Joachim Dippner. **(Inset)** seasonal flow direction of the Mekong River along the coast of southern Vietnam: **(A)** winter NE monsoon, **(B)** strong summer SW monsoon, and **(C)** weak summer SW monsoon. **(D)** Area of coastal upwelling during the summer SW monsoon.

The monsoons produce distinct responses in the circulation patterns of the northern and southern regions of the SCS (Wyrtki 1961). The circulation in the southern basin is directly affected by the monsoon winds: the NE winter monsoon (NEM) generates cyclonic circulation, whereas anticyclonic flow results from the SW summer monsoon (SWM). In the north, the combination of inflow from the Luzon Straight and wind stress from the NEM generates cyclonic circulation, which combines with the southern cyclonic gyre to produce

basin-wide cyclonic flow. The cyclonic gyre in the north is maintained in the summer during the SWM, where curl of the wind stress generates dipole circulation in the basin (Chao et al. 1996), and a stretching deformation in the flow pattern of the dipole forms an offshore jet at ~12^{o}N (Dippner et al. 2007; Wu et al. 1998). The SWM winds also generate seasonal upwelling along the eastern Vietnam shelf between 11^{o}N and 16^{o}N (Wyrtki 1961; Xie et al. 2003), which is locally enhanced by the offshore jet (Dippner et al. 2007).

In addition to controlling the major currents of the SCS, the monsoons directly influence both the magnitude and direction of the Mekong River plume outflow. During the SWM season, monsoonal rains intensify the outflow of the Mekong River, accounting for 85% of total annual discharge (Snidvongs and Teng 2006), and ultimately regulates the spatial influence of the offshore river plume. The flow trajectory of the plume is tightly controlled by wind and basin circulation patterns, which force the plume south along the Vietnamese coast during the winter monsoon and to the north parallel to coast during the summer (Fig. 1.4). Depending on the strength of the summer monsoon, the river plume may separate from the shoreline at 11^{o}N and advect offshore (Fig. 1.4) (Dippner et al. 2013). The monsoons are also strongly influenced on interannual timescales by climate phenomena such as the El Niño Southern Oscillation (ENSO). ENSO events are known to cause a substantially weakened SWM (Chao et al. 1996; Zhang et al. 1996), which in turn reduces coastal upwelling (Dippner et al. 2013) and the outflow of the Mekong River (Thi Ha et al. 2018).

1.4. Sources of nutrients to the SCS

The central South China Sea has conditions that are seemingly ideal for N_2-fixation: its waters are warm and permanently stratified (i.e., N-limited), surface concentrations of dissolved phosphate are relatively high (Wu et al. 2003), and the region receives substantial iron inputs from the Gobi Desert (Duce et al. 1991; Mahowald et al. 2005). And yet, diazotroph abundances and rates of N_2-fixation are surprisingly modest (Chen et al. 2019; Chen et al. 2008; Wu et al. 2003). It is hypothesized that organic ligand availability limits dissolved iron concentrations, given that particulate iron concentrations are substantial in surface waters but very low in the dissolved form (Wen et al. 2006; Wu et al. 2003), which ultimately limits N_2-fixation in the central SCS (Wu et al. 2003).

Interestingly, diazotrophy does appear to be stimulated in the southwestern region of the SCS along the southern coast of Vietnam, where the outflow of a major river is in close proximity to an area of seasonal upwelling (Bombar et al. 2011; Grosse et al. 2010; Voss et

al. 2006). Both features are important sources of nutrients to the region and consequently are thought to play significant roles in shaping the local phytoplankton communities and biogeochemistry. The coastal upwelling and the Mekong River outflow both support new production near shore through classical eutrophication (Bombar et al. 2010), but also appear to foster diazotrophy (Bombar et al. 2011; Grosse et al. 2010; Voss et al. 2006), which contributes an important additional source of new N to the SCS (Voss et al. 2014; Voss et al. 2006).

Rates of both primary production and diazotrophy (Fig. 1.5) in the southwestern SCS are higher in the summer during the SWM (compared to the spring intermonsoon) and in normal or La Niña years (compared to post-ENSO years) (Bombar et al. 2010; Grosse et al. 2010; Voss et al. 2006). During the SWM, coastal upwelling is strongest and the Mekong River forms an extensive plume to the NE of its mouth. Voss et al. (2006) suspect that the low N:P ratio (<16) of the upwelled water help establish favorable conditions for diazotrophs, though they note that the highest measured rates occur on the offshore edge of the upwelling area. Interestingly, this is the region where the summer Mekong River plume intersects the upwelled waters (Fig. 1.5). Voss et a. (2006) speculate that the delivery of iron and other micronutrients as well as increased stability of the water column promote the growth of diazotrophs like DDAs and *Trichodesmium* spp., but the relative influence of the aged upwelled waters and the river plume on diazotrophy in this offshore region remains unclear and requires further investigation.

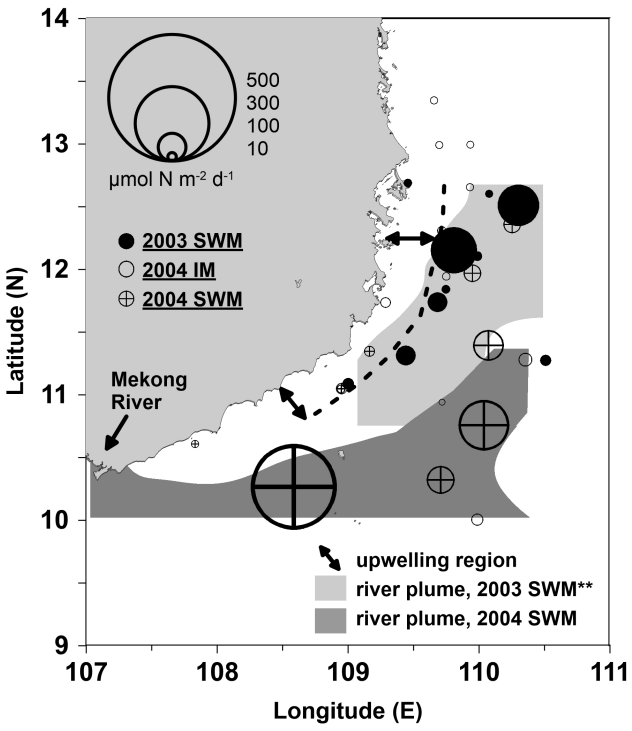

Figure 1.5: Comparison of Mekong River plume coverage (gray shaded areas) and areal rates of N_2-fixation (bubbles) from previous cruises during the 2003 and 2004 SW monsoon (SWM) and the 2004 intermonsoon (IM) seasons. There was no detectable river plume during the 2004 IM season. Bubble size corresponds to areal rate magnitude. The dashed line and arrows mark the coastal upwelling area. Asterisks mark post-ENSO years (2003). Modified figure from Voss et al. (2006).

The role of the Mekong River in stimulating diazotrophy was indisputable, however, in a study by

Grosse et al. (2010) carried out during the spring intermonsoon period (April 2007). Due to the relatively dry conditions during this time of year, river discharge was very low and restricted to the river mouth. It was here in the transitional waters, where salinity was nearing oceanic values and the N:P ratio had dropped below 16:1, that particularly high N_2-fixation activity was measured. Rates of N_2-fixation were up to 10 – 20 nmol N L^{-1} h^{-1}, an order of magnitude higher than average rates measured in the offshore river plume during the SWM (1 – 2 nmol N L^{-1} h^{-1}; Voss et al. 2006) and roughly equal to or higher than rates measured in the most active regions of the Amazon River plume (Subramaniam et al. 2008) Grosse et al. (2010) could confirm that the majority of N_2-fixation activity was carried out by large diazotrophs, but were unable to enumerate actual DDAs, instead reporting on abundances of potential host species (i.e., diatoms capable of forming DDAs). These counts provide a useful first approximation of DDA distributions, and Bombar et al. (2011) confirmed the presence of DDAs with *nifH* gene analyses, but counts of potential hosts may not be wholly representative of symbiotic. Such information would better characterize diazotrophy in this system.

Another aspect of the SCS ecosystem that remains poorly investigated is the influence of diazotrophy on the upper planktonic food web. Diazotroph N can be transferred to higher trophic levels through direct grazing on diazotrophs or through grazing on other organisms reliant on diazotroph N. The dominant pathway of N transfer is dependent on the prevailing diazotroph community (Mulholland 2007) and has implications for the trophic structure of the zooplankton food web as well as the cycling of N and C more generally (Loick-Wilde et al. 2019; Steinberg and Landry 2017). Only a handful of studies have investigated N sources and structure of planktonic food webs in highly heterogeneous systems, such as those influenced by river plumes (Conroy et al. 2017; Loick et al. 2007; Loick-Wilde et al. 2016), whereas most studies have focused on comparatively stable environments such as the central Baltic Sea (Eglite et al. 2018; Loick-Wilde et al. 2019) and the central gyres of the Atlantic (Hauss et al. 2013; Landrum et al. 2011; Mompeán et al. 2016) and Pacific (Hannides et al. 2009). It is unclear if some of the mechanisms driving food web changes in these environments are operating (or are detectable) in other more physicochemically variable systems. For example, recent work by Loick-Wilde et al. (2019) in the Baltic Sea revealed that an increase in the mixed layer depth, N_2-fixation rate, and the late bloom stage of diazotrophic cyanobacteria were associated with a transition from herbivory to carnivory in mesozooplankton. This trophic transition was linked to a shift in the primary inorganic N source for secondary production,

from nitrate-based to primarily diazotroph-N-based. The SCS is an excellent test site for investigating the universality of these findings.

1.5. Questions and hypotheses

This thesis is structured around the following research questions and associated hypotheses:

Q1: What are the relative influences of the Mekong River plume and seasonal coastal upwelling in the southwestern SCS at the time of sampling?

H1a: Both the Mekong River outflow and the coastal upwelling are detectable, but reduced relative to "normal" SWM conditions.

Q2: How do the river plume and upwelling shape the local phytoplankton community and govern the distributions of diazotroph populations?

H2a: Diazotroph abundances are elevated in the Mekong River plume and offshore of the coastal upwelling.

H2b: DDAs are the most active diazotroph group in the study region, particularly in waters affected by the Mekong River plume.

Q3: What are the ecosystem impacts of diazotrophy in southwestern SCS in June 2016 and how does it compare with previous expeditions?

H3a: Rates of N_2-fixation are measurable, but reduced compared to previous SWM conditions, and are highest in the aged river plume waters.

H3b: Diazotroph N can be traced into suspended particles, but does not represent the dominant source of N.

H3c: Diazotroph N makes a measurable contribution to zooplankton biomass where diazotroph abundances and activity are highest.

H3d: Mesozooplankton trophic position increases concurrently with reliance on diazotroph N.

1.6. Tools for quantifying ecological impact of diazotrophy and food web dynamics

Nitrogen stable isotopes (^{15}N, ^{14}N) are powerful tools for quantifying the activity of diazotrophs and for tracking diazotroph derived N through the ecosystem. Two aspects of N stable isotopes make them particularly useful for these purposes: 1) ^{15}N and ^{14}N both occur in natural systems and their ratio is variable and can be measurably altered by biologically mediated processes, usually through isotopic discrimination against the heavier isotope, ^{15}N; and 2) a variety of compounds highly enriched in ^{15}N are readily available for use in tracer experiments to quantify uptake and process rates. The first aspect allows us to use natural fluctuations in the ratio of ^{15}N:^{14}N to follow diazotroph N through the food web, from POM and into zooplankton (which are assumed to graze on POM). The N turnover times or effective integration times of POM and zooplankton are on the order of days to weeks (Landrum et al. 2011; Montoya 2007; Sharp 1983), meaning that isotope analyses of these pools provides information on diazotroph inputs on these scales (Fig. 1.6). They can additionally provide insight into how diazotrophy is influencing food web trophic dynamics, which will be discussed further below. The second aspect means that rates of N_2-fixation can be experimentally determined by measuring the fixation and subsequent incorporation of isotopically labeled N_2 ($^{15}N_2$) into biomass. This provides an estimate of net N_2-fixation activity on the timescale of the experiments (i.e., one day). In combination, N_2-fixation rates and ^{15}N natural abundance measurements provide a considerable range in the temporal and spatial scales over which diazotroph influence on the ecosystem can be assessed.

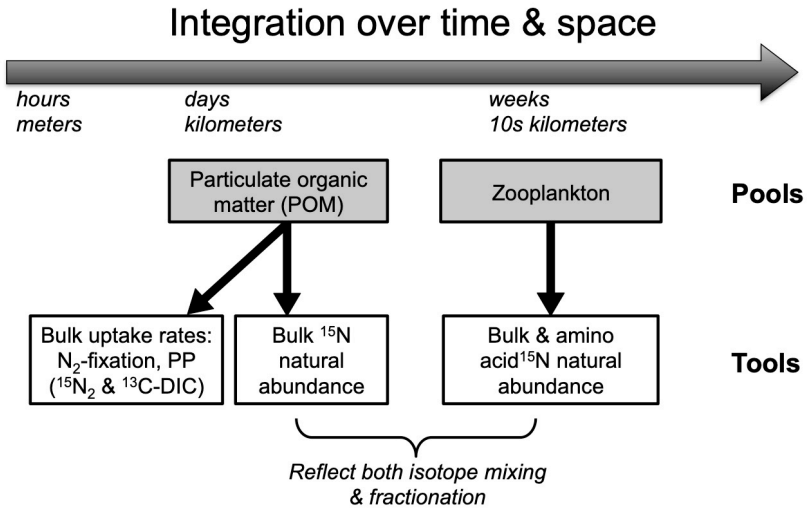

Figure 1.6: Conceptual diagram of the nitrogen pools and isotope tools used to analyze these pools in this thesis, where horizontal position along the arrow relates to the estimated scale lengths over which isotope information is integrated.

Given the analytical difficulties in measuring the absolute isotope ratio ($^{15}N:^{14}N$) in a sample, the natural abundance of ^{15}N is expressed using the delta notation, $\delta^{15}N$, where the isotope ratio of the sample is normalized to a reference, atmospheric N_2:

$$\delta^{15}N\ (‰) = \left(\frac{\left(^{15}N:^{14}N\right)_{sample}}{\left(^{15}N:^{14}N\right)_{atmosphere}} - 1 \right) \times 1{,}000 \qquad \text{(Eq. 1.1)}$$

The process of biological N_2-fixation fractionates only marginally against ^{15}N in N_2, resulting in the generation of diazotroph biomass with a $\delta^{15}N$ signature of -2 to -1‰ (Carpenter et al. 1997; Montoya et al. 2002) or that is slightly depleted in ^{15}N relative to typical biomass. Organisms relying on diazotroph N are thus isotopically distinct from organisms dependent on nitrate (4.5 – 5‰, Liu and Kaplan 1989; Sigman et al. 2000), which provides a natural isotope tracer of diazotroph N within the ecosystem. With careful consideration of the sources and processes acting within the SCS (see Chapter 5), we can quantify the dependence of the food web on diazotroph N.

1.6.1. Food web analysis

Due to their longer life spans, zooplankton act as low-pass filters (Montoya 2007) whose isotopic composition integrates dietary isotopic fluctuations occurring on short time scales. Only sustained isotopic signals, such as consistent grazing on ^{15}N-depleted diazotroph biomass, will result in the propagation of that signal through the planktonic food web. While this gives useful information on zooplankton diet over longer time scales, it can lead to spatial and/or temporal decoupling between the $\delta^{15}N$ of zooplankton biomass and its food source (e.g. O'Reilly et al. 2002).

To complicate things further, the $\delta^{15}N$ signature of zooplankton biomass increases with each trophic transfer by ca. 3.4‰ (Deniro and Epstein 1981; Fry 1988; Minagawa and Wada 1984; Wada et al. 1987) due to isotopic fractionation associated with catabolic and excretory processes (Fig. 1.7) (Montoya et al. 2002). However, this trophic fractionation factor can vary across different samples (Deniro and Epstein 1981; McCutchan Jr et al. 2003; Vander Zanden and Rasmussen 2001), which further complicates isotopic interpretations of food web N-sources and dynamics based on bulk biomass.

Compound-specific isotope analysis of amino acid nitrogen (CSI-AA) circumvents these problems, since information on both the trophic position and the N source to the base of the food web can be derived from a single sample. This is made possible by the considerable variability in the trophic fractionation of amino acids: glutamic acid (Glu) is enriched in ^{15}N by ~8‰ with each trophic transfer, whereas the $\delta^{15}N$ value of phenylalanine

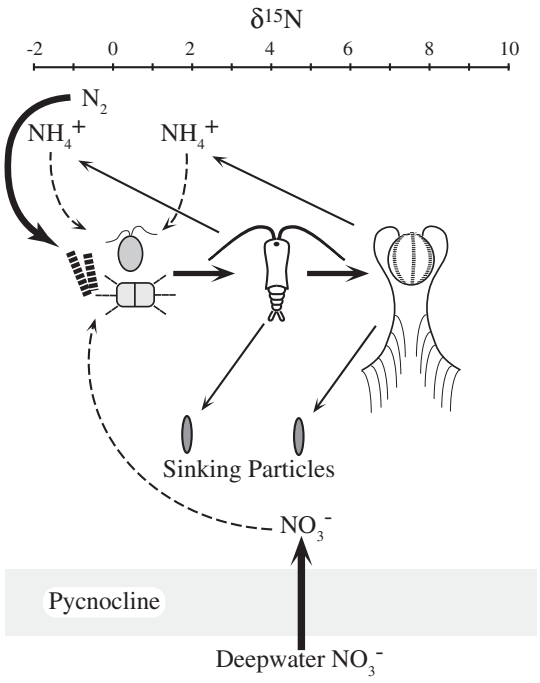

Figure 1.7: Schematic illustrating the major N sources and processes controlling the $\delta^{15}N$ of plankton within the mixed layer. The uptake of NO_3^- and NH_4^+ by phytoplankton is shown with the broken arrows, N_2-fixation and upwelling of NO_3^- are shown with solid heavy arrows, medium solid arrows represent trophic processes, and light solid arrows represent losses of ingested nitrogen to dissolved and solid excreta. The broken arrow representing NO_3^- uptake signifies isotope fractionation associated with the incomplete consumption of NO_3^- (discussed in more detail in Chapters 6 and 7). Figure taken directly from Montoya et al. (2007).

(Phe) remains nearly unchanged and thus reflects the isotopic composition of the primary producers (Fig. 1.8) (Chikaraishi et al. 2009; Chikaraishi et al. 2010; McClelland and Montoya 2002). Thus, a simple comparison of the $\delta^{15}N$ values of Glu and Phe from the same sample (see Eq. 2.5) normalizes the trophic data to the mean $\delta^{15}N$ signature at the base of the food web (Chikaraishi et al. 2009; Chikaraishi et al. 2010; McClelland and Montoya 2002), allowing for an estimation of trophic position and the disentanglement of these two (occasionally opposing) isotopic influences. These findings have been refined and confirmed in numerous field- and lab-based trophic studies on marine zooplankton over the last decade (e.g. Hannides et al. 2009; Mompeán et al. 2016; Steffan et al. 2015).

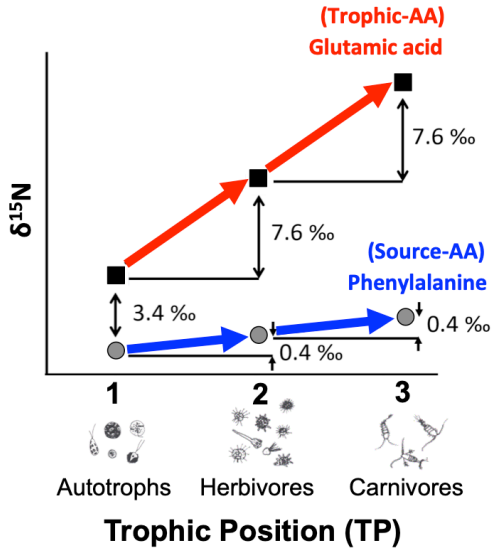

Figure 1.8: Schematic illustrating the relationship between trophic position and the change in $\delta^{15}N$ values of the amino acids glutamic acid (Glu) and phenylalanine (Phe) from the same food web. The initial isotopic offset between Glu and Phe in autotrophs is 3.4‰, and the increase in the $\delta^{15}N$ values of Glu and Phe with each trophic step is 7.6‰ and 0.4‰, respectively. Modified figure from Chickaraishi et al. (2009).

2. Materials & Methods

This section is organized thematically according to chapter content. Note that later chapters may use samples and data from earlier chapters. Where indicated in the text, colleagues performed the sample collection and measurements.

2.1. Physical & chemical characterization

2.1.1. Study Site

Samples were collected aboard the R/V Falkor on cruise FK160603 off of the southern coast of Vietnam in the SCS between 3 – 19 June 2016 (Fig. 2.1). The cruise encompassed a total of 21 stations each comprised of multiple sampling events, where particular events are identified by their unique "station.event" code in the text and some figures.

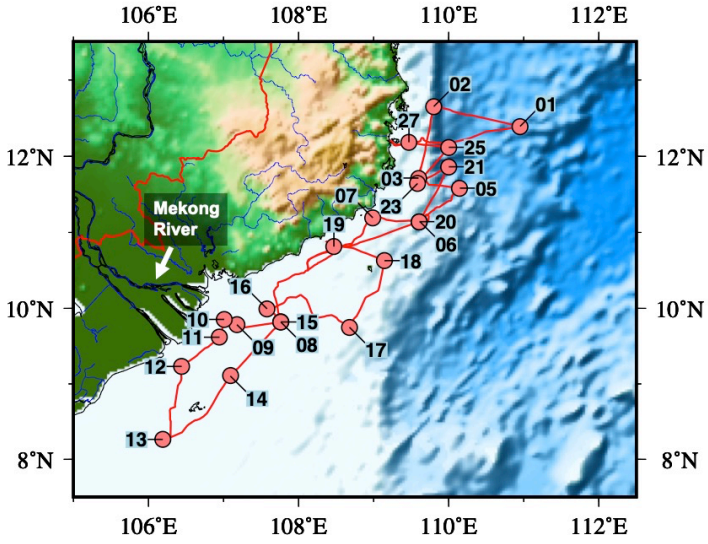

Figure 2.1: Cruise track (red line) and station map (red circles) of cruise FK160603. Stations are labeled according to their station number. Figure generated by Joseph Montoya.

A synoptic view of daily sea surface temperature (SST) was obtained using Multi-scale Ultra-high Resolution (MUR) SST analysis (Chin et al. 2017). The MUR SST is a blended product that utilizes 1-km resolution MODIS retrievals fused with AVHRR GAC, microwave, and in-situ SST data by applying internal correction for relative biases among the datasets. Satellite images were generated by Ajit Subramaniam.

2.1.2. Hydrographic measurements and sample collection

Underway temperature and salinity measurements were collected with a thermosalinograph mounted near the ship's water intake (~5 m depth). A Sea-Bird Electronics CTD-rosette system equipped with a fluorometer and Niskin bottles was used to measure the water column properties and to collect bulk water for analyses. Typically six depths were sampled at each station spanning the surface waters to below the chlorophyll maximum, with three depths at particularly shallow stations. Unless otherwise stated, all chemical, biological, and biogeochmical samples were collected using the CTD-rosette system. Samples for water column nutrient concentrations (nitrate + nitrite, phosphate, silicate) were collected directly from the Niskin bottles and were then immediately filtered through 0.2 cellulose acetate filters and frozen for transport. Samples were thawed for 24 h prior to analysis using a Lachat QuikChem 8000 flow-injection analysis system.

2.2. Habitat type approach

2.2.1. Habitat delineation

"The general approach (to generating habitat types) was to combine a principal component analysis (PCA) with a hierarchical cluster analysis to examine relationships among a defined set of environmental variables. The resulting analysis partitions the stations into statistically robust groups, which we call 'habitats.' This method is flexible and widely applicable, producing habitat types that reflect the biologically relevant physical and chemical drivers of each system to which it's applied. In order to make this approach both straightforward and general, we used the following criteria to identify environmental (or habitat-defining) variables:

1. Use variables that stem from common oceanographic measurements
2. Include biologically relevant variables that are sensitive to both physical and biological processes
3. Include both surface and upper water column properties that can be measured either directly or through proxies
4. Include both measurements that reflect instantaneous processes and others that integrate over time scales relevant to phytoplankton communities

A set of five variables together meet these criteria: sea surface temperature (SST) and salinity (SSS), mixed layer depth (MLD), depth of the chlorophyll *a* maximum (ChlMD), and nitrate availability to surface waters, which is represented here as a nitrate availability

index (NAI). SST and SSS are properties that explicitly address the identity of surface waters, aiding in water mass identification and capturing the influence of water mass mixing. To extend this approach beyond classical water mass analyses, three integrative parameters (MLD, ChlMD, and NAI) derived from vertical profiles were also included," (Weber et al. 2019).

We defined the mixed layer depth (MLD) as the depth of the buoyancy frequency maximum, which reflects the position of maximum stratification and is especially sensitive to sharp gradients in water density. Among other things, MLD is sensitive to the interaction of waters of varying density (e.g. a river plume spreading across marine waters) and vertical advection from upwelling. The mixed layer thickness is also relevant to phytoplankton as it regulates their exposure to nutrients and light.

The depth of the chlorophyll maximum (ChlMD) is an emergent ecosystem property influenced by multiple factors, including light availability, nutrient availability, and phytoplankton motility and physiology – all of which are modulated by hydrodynamics and food web interactions (summarized in Cullen 2015). In open ocean environments, the ChlMD generally occurs around the 1% light level, reflecting a balance between light availability from above and nutrient availability from below. However, in river plumes and upwelling systems where nutrients are delivered to surface waters, ChlMD may be positioned at or near the surface.

Nutrient availability plays a critical function in shaping phytoplankton distributions. We focused on nitrate because nitrogen often limits primary productivity in coastal and oligotrophic marine ecosystems (Dugdale 1967; Falkowski 1997; Howarth and Marino 2006; Ryther and Dunstan 1971) and because of its role in regulating diazotrophs abundances. However, using nitrate concentration in this analysis is challenging given that surface nitrate concentrations can vary from undetectable in offshore oligotrophic waters to several micromolar in areas affected by river plumes and upwelling. Although the nitracline depth can provide insight into nutrient availability in surface waters, the combination of complex hydrography in dynamic systems, variable water column depths, and coarse sampling create significant challenges in explicitly defining the nitracline. To address this complexity, we developed a nitrate availability index (NAI) as a proxy for nutrient availability in surface waters. NAI is defined as:

$$\mathrm{NAI} = \begin{cases} [\mathrm{NO_{2/3}}], & \text{if } [\mathrm{NO_{2/3}}]_{surface} \geq 0.5\mu\mathrm{M} \\ -\mathrm{Z}_{[\mathrm{NO_{2/3}}]} = 2\mu\mathrm{M}, & \text{if } [\mathrm{NO_{2/3}}]_{surface} < 0.5\mu\mathrm{M} \\ -\mathrm{Z}_{bottom}, & \text{else} \end{cases} \qquad \text{(Eq. 2.1)}$$

where $[NO_{2/3}]$ is the sum total concentration of nitrate and nitrite, and Z is water column depth (positive downwards). This definition produces an index that scales directly with nutrient availability for surface phytoplankton: positive NAI values reflect significant surface $[NO_{2/3}]$, indicating a relief from nitrate limitation, whereas negative NAI values reflect a lack of nitrate at the surface. In the absence of surface $NO_{2/3}$, NAI becomes increasingly negative as the nitracline depth increases (see Fig. S2.1).

The cases and the boundary values that define them can be tuned to fit the specifics of the system being analyzed. For the SCS, a boundary value of 0.5 μM $NO_{2/3}$ was used for the Case 1 since it is comparable to K_s values for nitrate uptake in marine phytoplankton, meaning that this $NO_{2/3}$ concentration will support appreciable uptake rates (Eppley and Thomas 1969). For Case 2, we used a boundary value of 2 μM $NO_{2/3}$ because it provides a balance between registering influential features in the near surface and significant shifts in the nitracline and is high enough to be reliably interpolated in coarsely sampled profiles.

For our SCS cruise, all five of the environmental variables could be determined for a total of 30 casts from 21 stations and these casts became the basis for the SCS habitat analysis. To generate the habitat types, a PCA on covariances was performed in combination with a hierarchical cluster analysis of the standardized habitat-defining variables (JMP Pro 14 software, SAS Institute Inc., Cary USA). The significance of differences in variables between habitat types was tested by performing a one-way ANOVA. Since all tests were significant ($p<0.0001$), post hoc Tukey-Kramer tests were run for each of the environmental variables to identify the particular habitats that differed (alpha=0.05; Fig. S2.2).

2.2.2. Validation of habitat types with phytoplankton community analysis

To test the utility of the habitat types, we compared the habitats to surface measurements of phytoplankton community composition. Surface phytoplankton communities were assessed using both diagnostic phytoplankton pigments and microscopic cell counts. Phytoplankton pigments were collected by Ajit Subramanium and analyzed at the Lamont Doherty Earth Observatory (LDEO) in Pallisades, New York, USA using High Performance Liquid Chromatography as described in Van Heukelem and Thomas (2001). One to two liters of water collected from the surface using the CTD rosette were filtered through a GF/F filter and were then frozen in liquid nitrogen until analysis. Seven pigment

classes were evaluated for this assessment: divinyl chlorophyll *a* + *b* (DvChla+b) was used as a proxy for prochlorophytes, 19' butanoyloxyfucoxanthin (19'BF) for pelagophytes and haptophytes, 19' hexanoyloxyfucoxanthin (19'HF) for haptophytes, alloxanthin (Allo) for cryptophytes, zeaxanthin (Zea) for cyanobacteria, peridinin (Peri) for dinoflagellates, and fucoxanthin (Fuco) for diatoms (according to Jeffrey et al. 1997; Vidussi et al. 2001 and references therein).

Direct cell counts were made by the Doan-Nhu and Nguyen-Ngoc labs at the Institute of Oceanography, Nha Trang (ION) in Nha Trang, Vietnam from water (1.5 L) collected with CTD Niskin bottles in the upper 5m of the water column. Samples were fixed with Lugol's solution (5% final concentration) and concentrated down to 2 – 5 mL through gravitational settling, and then enumerated at the species level using a Sedgwick-Rafter counting chamber and an Olympus CX41 microscope (100x magnification). At least 300 cells were counted from each sample to produce an estimated counting error of 11.5%. A total of 135 species or groups of phytoplankton were enumerated.

To assess how well the habitat type groupings are reflected in the phytoplankton communities, both the SCS pigment and cell count datasets were analyzed statistically using PRIMER-6 with PERMANOVA+ add-on software (Primer-E Ltd., Plymouth UK). First, resemblance matrices were generated for both datasets, where chi-squared distances were generated for the pigment data in order to mitigate the effect of large scale differences between habitats (e.g. Faith et al. 1987), whereas for the species-specific cell counts, the classical approach of generating Bray-Curtis dissimilarities on log(x+1)-transformed abundances was followed. PERMANOVAs were then performed on the resemblance matrices to test for significant differences in phytoplankton communities between habitat types. Since both tests were significant ($p<0.001$), a canonical analysis of principal coordinates (CAP) was then performed on each matrix. CAP is a constrained ordination technique that maximizes the explained variance between *a priori* groups (e.g. habitat types) and estimates error using a leave-one-out cross-validation technique (Anderson and Robinson 2003; Anderson and Willis 2003). Canonical correlations were based on 999 permutations ($p<0.001$ for both analyses). The individual pigments or species likely responsible for the observed community differences between habitats were identified based on Pearson correlations. Correlations were calculated on standardized pigment abundances and untransformed cell abundances with respect to their corresponding canonical axes.

2.3. Quantification of diazotroph populations

2.3.1. Microscopic quantification

Diazotroph species were identified in discrete CTD samples from the water column by the Doan-Nhu and Nguyen-Ngoc labs at the Institute of Oceanography, Nha Trang (ION) as outlined above. In addition, vertically integrated plankton samples were collected in vertical tows (100 m to the surface) of a Juday net (45µm mesh). These samples provided sufficient material for enumeration of DDAs and characterization of the symbiosis (rate of association and number of symbionts per host cell). Net samples were fixed with Lugol's solution (5% final concentration) and concentrated down for storage in 30 mL bottles. After species enumeration, formaldehyde solution was added to the samples (4% final concentration) for long-term storage. Net plankton samples were examined using a Leica LDMB microscope with phase contrast and differential interference contrast optics, and equipped with an epifluorescence unit. Cyanobacterial symbionts in DDAs (*Richelia intracellularis* and *Calothrix rhizosoleniae*) were identified and characterized using their pigment autofluorescence under blue light excitation. A digital camera, Olympus DP71, was used for microphotography.

2.3.2. Molecular quantification

Water samples for quantifying *nifH* gene copy abundances were immediately filtered after collection onto 25 mm diameter pore size 0.2 mm Supor filters (PALL Life Sciences, USA, MI) and flash frozen in liquid N_2, and stored at -80 °C until extraction. DNA was extracted and applied in TaqMan qPCR assays as previously described for UCYN-A1, B, and C (Church et al. 2005; Foster et al. 2007; Moisander et al. 2008). Sample collection, preparation, and analysis for the molecular identification of diazotrophs were performed by Andreas Novotny, Marcus Stenegren, and Rachel Foster of the Foster lab at Stockholm University of Stockholm, Sweden.

2.4. Quantifying diazotroph activity and contributions to PON

2.4.1. Suspended particle collection

Suspended particulate organic matter for natural abundance measurements was collected by filtering 1-20 L via gentle pressure filtration (5-10 psi) through pre-combusted (450°C for 2 h) 47-mm GF/F filters. Filters were dried at 60 °C and stored on desiccant for analysis ashore.

2.4.2. Elemental and isotopic analyses

Stable isotope abundance measurements were made by coupled elemental analysis isotope ratio mass spectrometry (EA-IRMS) using a Thermo Scientific Delta V Advantage interfaced to a Flash 2000 elemental analyzer in Warnemünde, Germany or a Micromass Isoprime IRMS coupled to a Carlo Erba NA2500 elemental analyzer in Atlanta, GA, USA. Each analytical run included a size series of elemental (methionine) and isotopic (peptone) standards, which provided a check on the stability of the instrument and allowed for the removal of contributions of any analytical blank from our isotopic measurements (Montoya 2008). We conservatively estimate that the overall analytical precision of the isotopic measurements for both instruments is better than ± 0.2‰. All isotope natural abundances are expressed as δ-values relative to atmospheric N_2 ($\delta^{15}N$) and VPDB ($\delta^{13}C$).

2.4.3. Rate experiments

Experiments to measure nitrogen fixation and primary production rates in bulk seawater were carried out following the methods of Montoya et al. (1996). In brief, experiments were performed in triplicate by filling 4.6-L Nalgene bottles with seawater in the morning, usually between 08:00-11:00 local time. Bottles were then injected with $^{15}N_2$ gas (Cambridge Isotope) and ^{13}C-bicarbonate (Sigma-Aldrich) to achieve isotope enrichments of ca. 7 at% ^{15}N-N_2 and 2 at% ^{13}C-DIC. After ~30 s of shaking, bottles were incubated for 24 h in on-deck flow-through incubators under simulated light conditions. Rate experiments were terminated by gentle pressure filtration through a 10 μm Nitex prefilter (47 mm) followed by a pre-combusted (450°C for 2 h) 25 mm GF/F filter. Material collected on the 10 μm prefilter was then rinsed onto a pre-combusted 25 mm GF/C filter. Filters were then dried at 60˚C and stored over desiccant until analysis ashore.

To calculate volumetric rates (ρ) of nitrogen fixation and primary production, the mass balance approach of Montoya et al. (1996) was used:

$$\rho = V \times [\mathrm{POM}] = \frac{A_{\mathrm{POM_f}} - A_{\mathrm{POM_0}}}{A_{\mathrm{substrate}} - A_{\mathrm{POM_0}}} \times \frac{[\mathrm{POM}]}{\Delta t} \qquad \text{(Eq. 2.2)}$$

where V is the specific rate of fixation (d^{-1}), [POM] is the concentration of PON or POC, Δt is the duration of the experiment, A_{POM0} and A_{POMf} are the initial and final isotopic enrichment of ^{15}N or ^{13}C in POM (atom%), and $A_{substrate}$ is the isotopic enrichment of the substrate pool (N_2 or DIC) immediately after injection of the labeled substrate ($^{15}N_2$ or ^{13}C-DIC). Values for A_{POM0} were calculated based on the elemental concentrations and $\delta^{15}N$ and $\delta^{13}C$ isotopic signatures of PON and POC collected from the same depth.

Detection limits for nitrogen fixation rates were calculated according to Montoya et al. (1996) based on a minimum acceptable change in the $\delta^{15}N$ of PON (4‰ or 0.00146 at%). Given typical values from our experiments (Δt of 1 d, A_{N2} of 6.50 at%, A_{PON0} of 0.366365 at%), the average limit of detection for specific rates (V_{min}) of N_2-fixation was approximately 2.38×10^{-4} d^{-1}. Since the minimum detectable volumetric rate (ρ_{min}) is strongly influenced by PON concentration, which can vary between replicates, ρ_{min} was calculated individually for each replicate. The volumetric rate for a particular replicate was considered to be below the detection limit if it was lower than its respective ρ_{min}. Among all of our 176 samples, only a handful of the >10-µm size fraction samples were below the detection limit.

Volumetric rates of nitrogen fixation and primary production are given in the units of nmol N L^{-1} d^{-1} and µmol C L^{-1} d^{-1}. Areal rates were calculated by performing trapezoidal integration from the surface to the bottom of the mixed layer or to the deepest sampled depth, as indicated in the text.

2.4.4. Diazotroph contribution measures

The impact of diazotrophy on the water column was assessed using both the natural abundance of ^{15}N in suspended particles and rate measurements. To minimize the influence of nitrate fractionation from uptake by phytoplankton on the $\delta^{15}N$ signatures of POM, discrete $\delta^{15}N$-POM measurements were integrated through the mixed layer (as opposed to the whole water column or upper 100 m). This mixed layer, mass- and depth-weighted $\delta^{15}N$ value for each station ($\delta^{15}N\text{-}PON_{ML}$) was calculated using the trapezoidal integration method of Landrum et al. (2011).

The relative contribution of diazotroph N ($\%N_{diazo}$) to $\delta^{15}N\text{-}PON_{ML}$ values was calculated using a simple linear mixing model:

$$\%N_{diazo} = 100 \times \left(\frac{\delta^{15}N\text{-}PON - \delta^{15}NO_3^-}{\delta^{15}N_{diazo} - \delta^{15}NO_3^-} \right) \qquad \text{(Eq. 2.3)}$$

where $\delta^{15}N$-PON is the $\delta^{15}N\text{-}PON_{ML}$ for each station, $\delta^{15}N_{diazo}$ is the isotopic endmember of -2.0‰ for recently fixed nitrogen (Montoya et al. 2002), and $\delta^{15}NO_3$ is the isotopic endmember of 5.0‰, which is the value measured for upwelled nitrate off the coast of Vietnam (Loick et al. 2007) and is roughly equal to the global mean value for nitrate in deep waters (Liu and Kaplan 1989). As another precaution against the influence of nitrate fractionation, stations where the nitracline (NAI) was shallower than the MLD were excluded from the $\%N_{diazo}$ calculation, which included Stns. 9, 10, and 11 of the MRW

habitat, Stn. 13 of OnSW, and Stn. 7 of UpW. OSW Stn. 6 was also excluded based on findings in Chapter 7, which hypothesized that biomass (POM and zooplankton) at this station was primarily supported by isotopically heavy nitrate advected from the upwelling region. Redfield stoichiometry (C:N = 6.7) was used to estimate the percentage of areal primary production that could be supported by the areal rates of nitrogen fixation ($\%PP_{diazo}$).

2.5. Food web analysis

2.5.1. Sample collection

Zooplankton for elemental, bulk isotope, and compound specific isotope analyses were collected in vertical tows around local noon and local midnight with a 0.5 m^2 ring net (200 μm mesh size) equipped with a USBL transponder to provide position and depth information. The upper 100 m of the water column was sampled, or to about 10 m above the bottom at shallower stations. Animals were size-fractionated using a graded series of Nitex sieves with mesh sizes of 2000 μm, 1000 μm, 500 μm and 250 μm and dried at 60°C for 48 h. Dry samples were ground to a fine powder, then stored in pre-combusted aluminum foil (450°C for 2 h) at -20°C for the duration of the cruise.

At selected stations, additional samples of POM for CSI-AA were collected by gentle pressure filtration of 20-60 L of seawater from either the surface or the chlorophyll-maximum through a series of pre-weighted 47-mm polycarbonate filters (Whatman Nuclepore, 0.2 μm) that were exchanged when fully loaded. These samples were quickly frozen at -20°C and dried at 60°C ashore.

2.5.2. Bulk isotope analyses and quantification of diazotroph N

Zooplankton samples for elemental and bulk isotope analyses were analyzed using an EA-IRMS as outlined in section 2.4.2. Samples with elemental C:N ratios outside of the expected range for zooplankton (C:N of 4.0 – 5.4, Steinberg and Saba 2008) (Fig. S2.3) were assumed to be contaminated with fish (especially high in N) or large phytoplankton (especially high in C), and were thus excluded from further analyses. Contamination was confirmed with visual inspection where possible.

As in section 2.4.4, station averaged $\delta^{15}N$ values for POM were used to estimate the contribution of diazotroph N to POM ($\%N_{diazo}$) (Eq. 2.3), though with some modifications. Discrete $\delta^{15}N$-POM measurements were instead integrated through the zooplankton net tow

depth (δ^{15}N-POM$_{tow}$) to provide an estimate of the isotopic composition of the autotrophs in the upper water column that supported the local zooplankton populations.

The estimated relative contribution of diazotroph N to bulk zooplankton (zp) was calculated as:

$$\%N_{diazo} = 100 \times \left(\frac{\delta^{15}N_{zp} - \delta^{15}N_{reference\ zp}}{\delta^{15}N_{diazo} - \delta^{15}N_{reference\ zp}} \right) \quad \text{(Eq. 2.4)}$$

where $\delta^{15}N_{reference\ zp}$ was 5.8‰ for the small (250-500 µm) and 6.0‰ for all larger mesozooplankton size fractions (500-1000 µm; 1000-2000 µm; and >2000 µm) based on analysis of similar samples from the Vietnamese upwelling region during strong upwelling in July 2004 (Loick et al. 2007).

2.5.3. Compound-specific stable isotope analysis of amino acids (CSI-AA)

Due to the resource intensive nature of this approach, CSI-AA analyses were performed on only a subset of POM and zooplankton samples, which included POM from both the surface and Chl. *a* maxima (if not located at the surface) and mesozooplankton from the 1000-2000 µm size fraction. This particular size fraction was chosen because it provided good coverage across the various habitats (zooplankton in the larger size fractions were not always present at adequate abundances) and because samples from this size fraction had no signs of phytoplankton contamination. In total, nine POM samples from six stations and 17 zooplankton samples from 14 stations were selected for CSI-AA analysis.

For detailed methods on how plankton samples were prepared and analyzed for individual AA δ^{15}N measurements, refer to the Master's thesis of Melvin Bach and the Methods section of Loick-Wilde et al. (2019). Of the 12 AAs that were derivatized and analyzed, I report here on only the two AAs most widely used for N-source and trophic level assessments, glutamic acid (Glu) and phenylalanine (Phe), respectively (McClelland and Montoya 2002).

2.5.4. Estimation of TP and ∑V for plankton samples

The average TP of the subset of POM samples (from the surface and deep Chl. *a* maxima) and of zooplankton samples (size fraction 1000-2000 µm) were estimated based on the isotopic contrast between Glu and Phe, which is generally accepted as the best pair of AAs for TP estimates in mesozooplankton (e.g. Chikaraishi et al. 2009; Mompeán et al. 2016). We used the most widely used equation after Chikaraishi et al. (2009) as follows:

$$TP_{Glu/Phe} = (\delta^{15}N_{Glu} - \delta^{15}N_{Phe} - 3.4)/7.6 + 1 \quad \text{(Eq. 2.5)}$$

where 3.4 is the average difference between $\delta^{15}N_{Glu}$ and $\delta^{15}N_{Phe}$ in primary producers, and 7.6 is the trophic enrichment factor (TEF) of $\delta^{15}N_{Glu}$ - $\delta^{15}N_{Phe}$.

Detritivory may also be a common feeding mode, though one which cannot be resolved by TP estimation alone (Steffan et al. 2017). Rather, the degree of microbial reprocessing of food in the animal's diet can be estimated by the microbial re-synthesis proxy ∑V (McCarthy et al. 2007). ∑V quantifies the extent of $\delta^{15}N$-AA alteration of detrital material before it's consumed by an animal and thus provides an integrated measure of the full range of trophic behavior of an animal. Note that ∑V is only considered to be a robust proxy for microbial re-synthesis if unrelated to the TP proxy, since trophic effects influence both estimations (Ohkouchi et al. 2017).

2.5.5. Statistical analyses

Differentiating between the mixing of isotopically unique N sources supporting production and isotopic fractionation resulting from biological processing is known to be particularly challenging in complex systems (Fry 2006; Glibert et al. 2019). Since the sources and processes acting on the DIN pool are highly system specific (Montoya 2007), there exists no defined method for distinguishing the influences of major sources from transient processes. For our study area, we have used the highly significant relationship between the bulk $\delta^{15}N$ values of all five plankton compartments and MLD to identify outliers influenced by transient processes. The MLD is known to play an integral role in regulating the supply of DIN to surface waters and consequently the relative contributions of (subthermocline) nitrate and diazotroph nitrogen (when DIN is strongly limiting, Hutchins and Fu 2017) to POM – the two major sources of isotopically unique N in POM of the SCS. This regulatory role of MLD has previously been shown in the SCS (Voss et al. 2006) and in the central Baltic Sea (Loick-Wilde et al. 2019), making it ideal for our purpose here. Using this relationship between plankton bulk $\delta^{15}N$ measurements and MLD, we could not distinguish low $\delta^{15}N$ values attributable to fractionation processes from those produced by high diazotroph N inputs, but anomalously high $\delta^{15}N$ outliers became visually apparent as significant positive deviations from this relationship. Stn. 6 was found to have experienced an unusually intense isotope fractionation event (discussed further in Chapter 7), given that all plankton fractions were highly enriched in ^{15}N (see Fig. 7.1). For this reason, all samples from Stn. 6 were excluded from further statistical analyses.

A correlation-based principal component analysis (PCA) and post hoc bivariate linear correlations were used to visualize and identify the biotic and abiotic factors that

affect the mean N-source and trophic position of the 1000-2000 μm size fraction of zooplankton across the four different habitat types and by proxy their respective phytoplankton communities. All 13 variables (shown in Table 7.1) were available at 15 stations across the four habitat types, though Stn. 1 had to be excluded from the analysis. At this station, there was an uncharacteristically large time gap (8 h) between nutrient and zooplankton sampling, during which surface waters changed appreciably as evidenced by variable T/S profiles (not shown), making it unclear if the chemical conditions measured earlier in the day were representative of the conditions sampled much later.

Since the mesozooplankton (1000-2000 μm size fraction) isotopic measurements and proxies are integrated over the depth interval sampled by our net tows (100 m or shallower depending on the water column depth), the environmental variables were also depth-integrated where appropriate in order to relate them more directly to the zooplankton measures. Given the strong relationship between bulk $\delta^{15}N$ values of plankton and the MLD and the role of the MLD in regulating nutrient supply to the phytoplankton community (Gattuso et al. 2015; Hutchins and Fu 2017; Jewett and Romanou 2017; Paerl and Huisman 2008; Roy et al. 2011) and vertical migration of zooplankton (Eglite et al. 2018; Schulz et al. 2012) in the upper water column, we integrated the environmental variables over the mixed layer for the PCA. We had additionally tested other integration depths including the net tow bottom depth and to the depth of the Chl. *a* maximum, but did not produce meaningful relationships with the N-source and trophic position proxies of the mesozooplankton (not shown). Therefore we only report on the PCA with the MLD-integrated environmental values.

The number of factors (or principal components, PCs) included in the PCA was based on the a priori criterion to cover the environmental variables and zooplankton measures in Table 7.1, some of which had previously been shown to explain much of the phytoplankton community structure in this system (Weber et al. 2019). Note that the PCA in this study is used predominantly as an exploratory and visualization tool, and we have performed post hoc linear correlations between the environmental variables and the zooplankton measures to further elucidate their relationships and confirm their strength and significance (Fig. S2.4). The inclusion of the zooplankton measures in the PCA preserves the relationship of the environmental variables (compared to when these variables are evaluated alone, Fig. S2.5), so for ease of discussion, the full PCA has been included here. The PCA was generated using JMP Pro 14 (SAS Institute Inc., USA) and analyzed using PRIMER-6 Software (Primer-E Ltd., UK).

3. Characterization of the study site

3.1. Physical characterization

Sampling occurred in the wake of a particularly strong ENSO event in 2015/16, which was one of the three strongest events since 1948 based on MAE and Niño3.4 indices. The post-ENSO conditions resulted in a weaker SWM in 2016, which in turn lowered the annual discharge of the Mekong River (Fig. S3.1) (Thi Ha et al. 2018). Additionally, the timing of the cruise prior to the peak SWM season meant that sampling occurred before the river's high flow period (Thi Ha et al. 2018). The combination of these two factors resulted in a modest river outflow during the cruise, which manifested as a slight drop in sea surface salinity (SSS) near the river mouth and adjacent coastline (Fig. 3.1A).

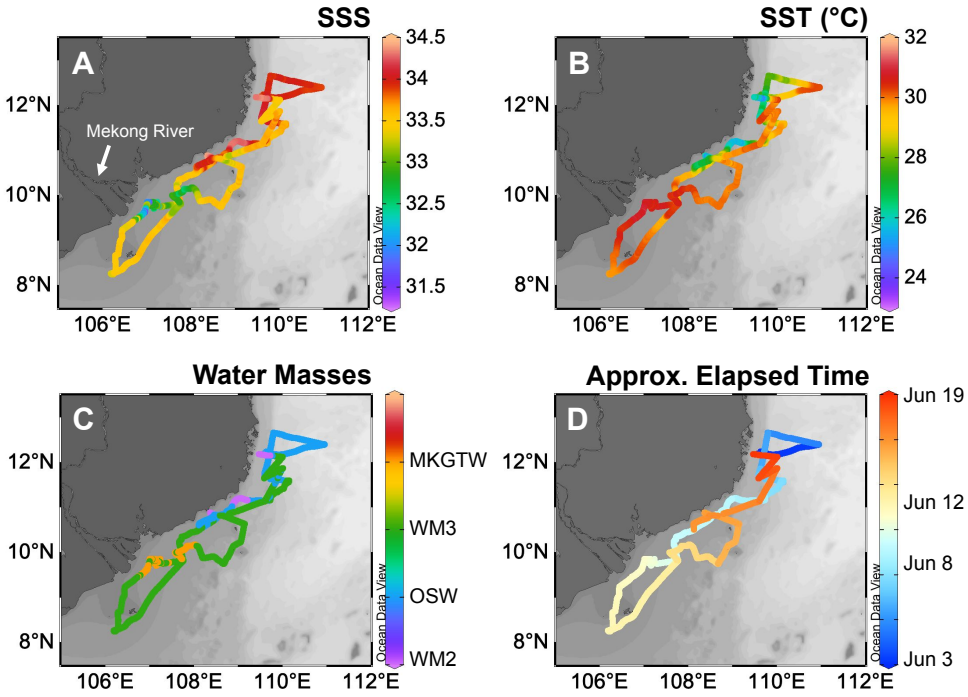

Figure 3.1: Underway sea surface salinity (SSS) **(A)** and temperature (SST) **(B)** collected along the cruise path. Surface distributions of water masses **(C)** based according to modified definitions from Dippner & Loick-Wilde (2011): Open Sea Water (OSW), Mekong/Gulf of Thailand Water (MKGTW), WM2: mixed water between Maximum Salinity Water (MSW) and OSW, WM3: mixed water between OSW and MKGTW. Panel **(D)** shows the approximate elapsed time over the cruise, where blue indicates the start of the cruise and red the end.

It is very difficult, however, to definitively differentiate the Mekong River plume from the nearby Gulf of Thailand water and surrounding coastal waters using either T-S properties or remote sensing techniques. This has lead to ambiguity in how to define the river plume and assess its influence on the region: Voss et al. (2006) used a SSS cutoff of

33.2 (Fig. 3.2), whereas Dippner & Loick-Wilde (2011) used a more conservative value (32.9) in their water mass definitions, but acknowledged the impossibility of differentiating the plume from Gulf of Thailand water and named the water mass Mekong/Gulf of Thailand Water (MKGTW) (Fig. 3.1C, see also Fig. S3.2). Dippner & Loick-Wilde (2011) also implemented a mixed water mass (WM3) to capture mixing of MKGTW with Open Sea Water (OSW). Fortunately, the spatial delineation of the sampled 2016 river plume was largely insensitive to the definition used, and did not extend nearly as far North or East as the river plumes during either the 2003 (a post-ENSO year) or 2004 SWMs (Figs. 3.1C, 3.2, and S3.3). When taken together, all lines of evidence indicate that both the post-ENSO and early SWM timing of the cruise minimized the influence of the Mekong River on the investigation area.

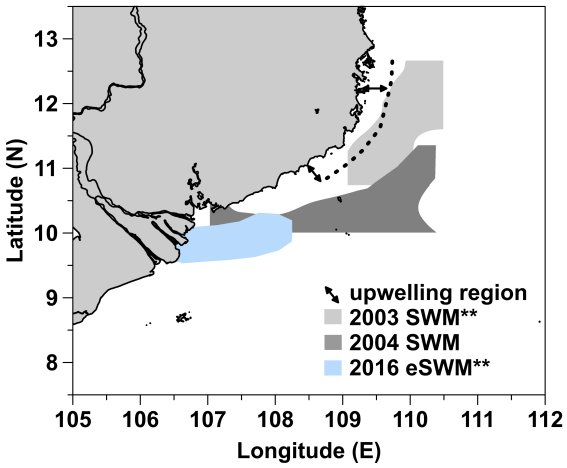

Figure 3.2: Comparison of Mekong River plume coverage between cruises from the 2003 and 2004 SWM season (July) and from the 2016 early SWM season (June, this study). Asterisks mark cruises that occurred during post-ENSO years. The river plume was defined by surface salinity < 33.2. The dashed line and arrows mark the coastal upwelling area. Figure was modified from Voss et al. (2006).

The weakened state of the SWM in 2016 also has implications for the coastal upwelling strength, which is primarily determined by wind speed through Ekman transport (Dippner et al. 2007). Even though the 2016 SWM winds were likely reduced compared to SWM winds during "normal" or La Niña periods (Fig. S3.4), the surface expression of upwelling was easily detectable based on the relatively high SSS (Fig. 3.1A) and low sea surface temperature (SST) signatures (Fig. 3.1B), considering that upwelling transports salty, cold waters from depth. When these underway SSS and SST measurements were converted into water masses according to modified definitions from Dippner and Loick-Wilde (2011) (Fig. 3.1C, S3.2), the distribution of 2016 surface water masses actually looked more similar to that observed in July 2004, a climatically "normal" year. This becomes clear when assessing the presence of Water Mass 2 (WM2), a mixed water mass between OSW and the Maximum Salinity Water (MSW), the latter of which is the core of the upwelling water (Dippner and Loick-Wilde 2011; Dippner et al. 2007). WM2 was detected at the surface in the coastal upwelling zone

in 2004 and 2016, but not in 2003, which suggests that the upwelling signal was relatively strong at the time of sampling in 2016.

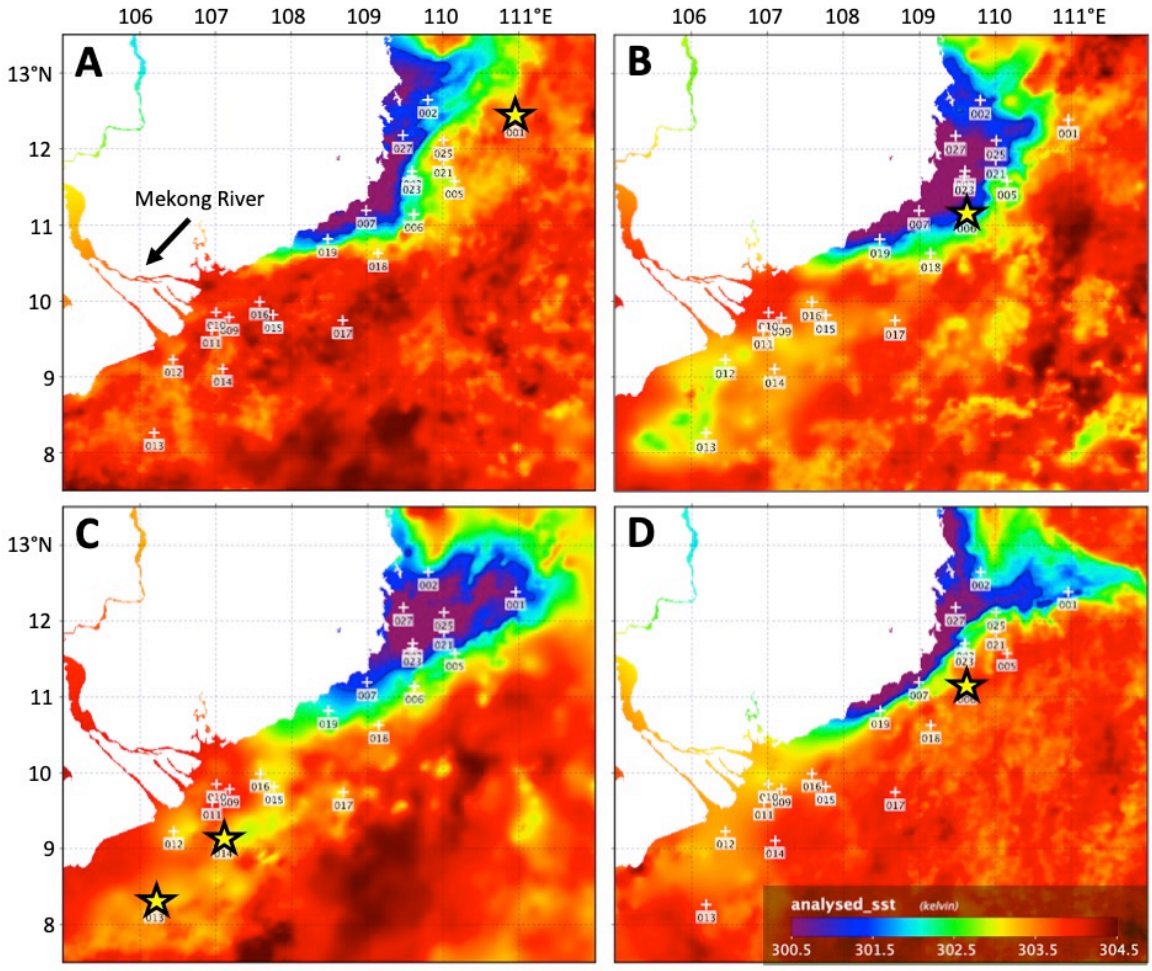

Figure 3.3: Compilation of sea surface temperature (SST) satellite images generated using MUR SST analysis by Ajit Subramaniam. Each panel represents a daily map that in combination encompass a 13-day period (roughly the cruise length): June 4 **(A)**, June 8 **(B)**, June 12 **(C)**, June 16 **(D)**. The yellow stars in each panel designate the stations that were sampled on that particular day. Note that Stations 6 and 20 are coincident in space and were sampled on June 8 **(B)** and June 16 **(D)**, respectively.

Based on the water mass analysis alone, however, it is difficult to determine the full extent of upwelling influence on surface waters, as well as the variability of this influence. Dippner et al. (2007) had previously defined the thickness of the coastal upwelling zone based on the Rossby radius of deformation (Gill and Donn 1982), but once near the surface, upwelled waters can be advected offshore through a combination of local winds and currents. As a result, the surface expression of upwelling may extend well beyond the core upwelling zone, which greatly complicates surface water characterization. An image compilation of satellite-based SST measurements documents this variability over a 13-day period during our June 2016 sampling (Fig. 3.3), and shows considerable small-scale

fluctuations in the position of the upwelling front. Stations located North of 10.5°N were variably influenced by upwelling over the course of the cruise, and only two of the most coastal stations in this northern region (Stns. 7 and 27) were consistently within the heart of the upwelling. Interestingly, the SST images also capture the gradual development of an offshore jet at ~12.5°N. This jet is a well-documented feature associated with the stretching-deformation caused by the SWM current pattern (Wu et al. 1998), and is known to enhance the coastal upwelling (Dippner et al. 2007).

3.2. Surface nutrient distributions

Despite the prevalent SST signals in Fig. 3.3, coastal upwelling appears to have had a minimal influence on surface nutrient concentrations (Fig. 3.4), indicating that nutrients were mostly or fully consumed before reaching the surface, as previously documented (Bombar et al. 2010; Loick et al. 2007; Voss et al. 2006). Only at Stns. 7 and 27 along the northern coast were nutrient concentrations elevated relative to surrounding waters. At these stations, N:P was below the Redfield ratio (16:1) (Fig. 3.4D), indicating N-limitation in upwelled waters, which is in line with the findings of Voss et al. (2006).

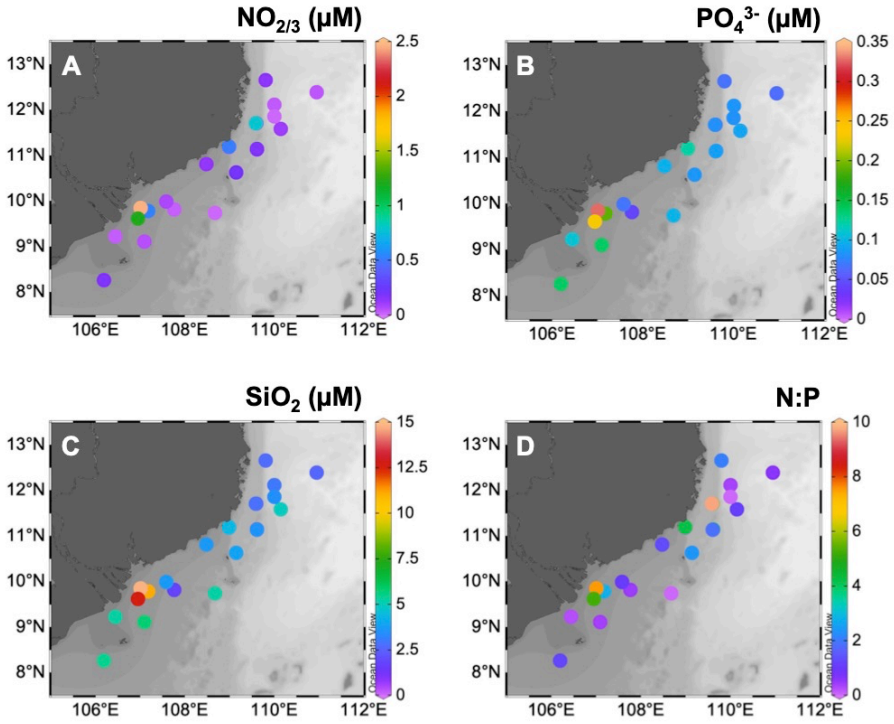

Figure 3.4: Surface nutrient concentrations of **(A)** nitrate + nitrite, **(B)** phosphate, **(C)** silicate, and **(D)** N:P at the sampled stations.

The Mekong River was an unambiguous nutrient source at three stations near the river mouth (Stns. 9 – 11), though plume waters were already severely N-limited with N:P below 8 (Fig. 3.4D) and $NO_{2/3}$ concentrations < 2.5 μM (Fig. 3.4A). The Mekong River plume was previously shown to have a N:P ratio of ~32 and $NO_{2/3}$ concentrations > 20 μM at 0 salinity in the late summer (Grosse et al. 2010), suggesting that significant N removal (and perhaps P addition through particle adsorption) had occurred upstream of these three stations. The river was also a clear source of SiO_2, though SiO_2 was in excess relative to the physiological needs of diatoms (Si:P ratio of 15:1, Brzezinski 1985) at all stations, with Si:P ratios ranging between 30 – 60 (not shown). Taken together, surface waters were N-limited with an excess of PO_4^{3-} and SiO_2, indicating that the region was theoretically primed for diazotrophs and DDAs in particular, barring other (micro)nutrient limitations.

3.3. Summary

The overall picture developing from this brief assessment is of a unique situation in June 2016 relative to previous investigations: both the Mekong River plume and upwelling were detectable, but the modest river outflow resulted in the spatial separation of these two features. This constellation may help us to untangle the relative influences of the river plume and coastal upwelling on diazotrophs and planktonic food web structure. However, the physicochemical variability within the spatial and time scales of our research cruise, which very likely affected phytoplankton growth, were not well-represented by water masses alone.

4. Habitat delineation

Now that I have established that both the coastal upwelling and Mekong River plume are detectable and variably shape the surface physicochemical conditions, the question remains on how to characterize our sampling stations in a way that both captures this heterogeneity and is biologically relevant. To answer this question, we developed a method for delineating habitat space that utilizes commonly available measures that variably integrate over both time and the vertical water column (see Methods). These defining variables (SSS, SST, MLD, ChlMD, and NAI) are known to influence or reflect influential drivers of phytoplankton distributions and community composition. This habitat approach was designed to be both flexible and adjustable in order to make it applicable to numerous systems, and was successfully applied to the Amazon River influenced region of the North Atlantic, as demonstrated by Weber et al. (2019) and Montoya et al. (In press). Here, I am presenting and discussing the outcome of applying this approach to the southwestern SCS.

4.1. Results & Discussion

4.1.1. Habitat types

Applying the habitat type analysis to the SCS dataset successfully generated habitats and achieved a high degree of separation of stations among those habitats. The first two PCs of the PCA explained 86.8% of the total variance, demonstrating that our set of habitat-defining variables is comprehensive and highly relevant. PC1 accounted for 54.3% of the variation and was primarily driven by the emergent properties MLD, ChlMD, and NAI (Fig. 4.1). PC2 explained 32.5% and was driven primarily by the surface properties of SST and SSS. Combining the PCA and cluster analysis, the approach generated four habitat types, which we have termed Mekong River water (MRW), onshore or continental shelf waters (OnSW), upwelling waters (UpW), and oceanic seawater (OSW). PC1 accounted for most of the separation between MRW, OnSW, and OSW habitats, whereas PC2 was important in distinguishing UpW from OnSW and MRW habitats.

Based on their environmental properties and locations, the habitat types largely reflect the three primary end members in the sampling area: the Mekong River (MRW), and oceanic waters (OSW), and coastal upwelling (UpW). MRW stations were located near the mouth of the Mekong River (Fig. 4.2), overlapping with the previously identified plume

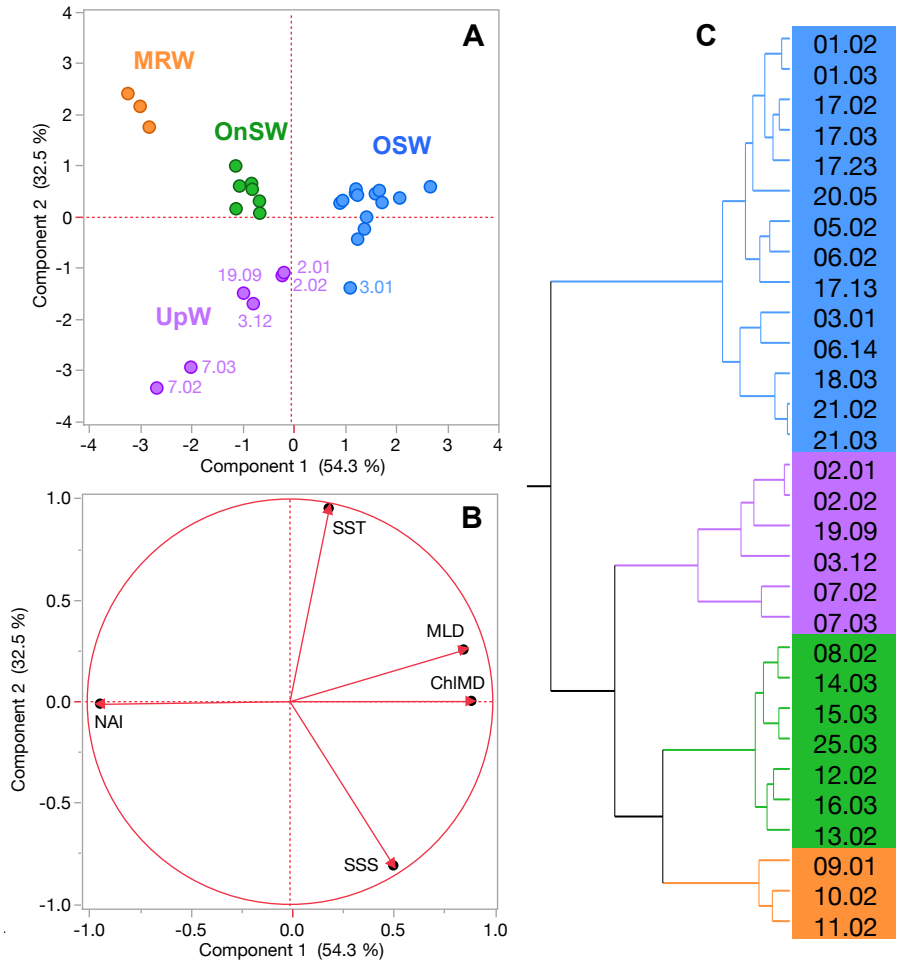

Figure 4.1: **(A,B)** Principal component analysis of CTD casts based on the habitat type defining variables. The score plot **(A)** is a scatter plot of each cast's score according to the first two principal components, where % explained variation is listed on the respective axes. The loading plot **(B)** shows the unrotated loading matrix between the analyzed variables and the first two principal components. The closer a variable's loading value is to 1, the greater the effect of the variable on that component. **(C)** Wards-mean hierarchical cluster analysis based on the habitat-defining variables. Habitat types are identified by color: Mekong River water (MRW), on-shelf water (OnSW), upwelled water (UpW), and oceanic seawater (OSW).

location (Fig. 3.1), and were characterized by the combination of relatively shallow MLDs and Chl. *a* maxima, high NAI, and fresh, warm surface waters (Table 4.1), which are consistent with the properties of a river plume. In contrast, OSW stations were located farther offshore and had properties typical of oligotrophic oceanic conditions, including the deepest MLDs and Chl *a* maxima, the lowest NAI, and SST and SSS values characteristic of surface oceanic waters in the region. Properties of UpW stations were varied, but were nonetheless symptomatic of upwelling. These stations had generally shallow MLDs and ChlMD, higher nutrient availability than OSW stations, but were saltier and cooler at the surface than either MRW or OnSW waters. Importantly, these UpW stations were located

along the northern coast of our sampling area, consistent with the typical location of the monsoon upwelling (Fig. 3.1, 3.2). In contrast to the other habitats, OnSW is not an end member per se, but is comprised of shelf waters that are transported from the Gulf of Thailand and mixed in differing proportions with the other three end members (Fig. 3.1C) (Dippner and Loick-Wilde 2011). Based on SSS and SST, OnSW is most similar to OSW, but has shallower MLDs, ChlMD, and nitraclines since it occupies the shelf.

In addition to simply describing the sampled region, these statistically significant habitat types and the environmental variables that define them provide a means for evaluating the major physical processes acting on the region, as well as their variability. In accordance with the findings in the previous chapter, the habitat types show that both the Mekong River and coastal upwelling were clearly discernable in the region but geographically restricted (Fig. 4.2).

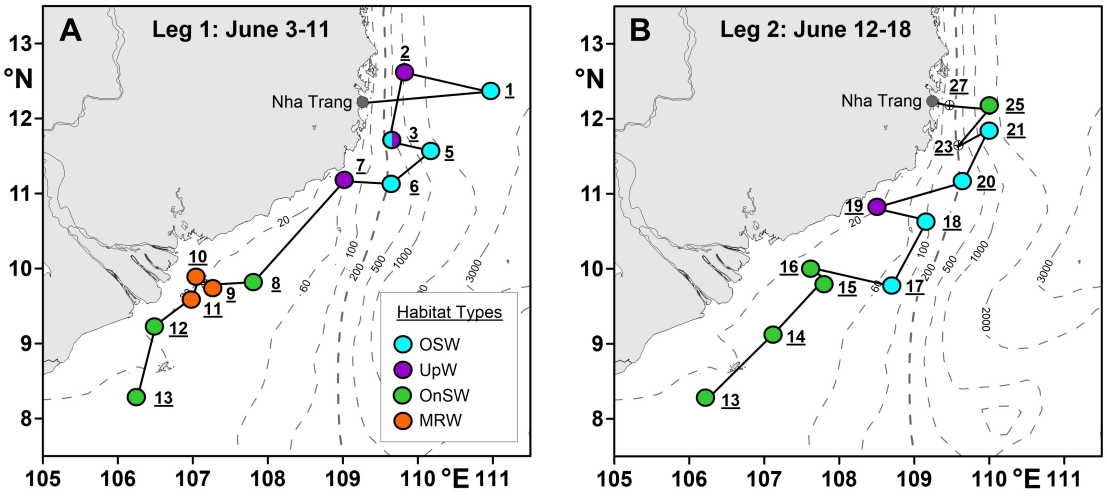

Figure 4.2: Station maps from leg 1 **(A)** and leg 2 **(B)** including the cruise track off southern-central Vietnam. Note that Stns. 8 from leg 1 and Stn. 15 from leg 2 are coincident in space but were sampled several days apart. This is also the case for Stations 6 and 20. Colors indicate habitat types after Weber et al. (2019) (see legend). Waters at Stn. 3 transited from OSW to UpW over the duration of sampling. Dashed lines indicate the bathymetry.

"Whereas the influence of the Mekong River was rather coherent across the affected stations, the expression of upwelling was both patchy and variable in PCA space, as seen in the distribution of the UpW CTD casts within the PCA score plot (Fig. 4.1A). In combination with the vectors mapped in the loading plot (Fig. 4.1B), the relative positions of the casts in the PCA score plot reflect the environmental variables driving the casts' distributions. The UpW subgroup farthest from the other casts (corresponding to two casts from Stn 7) has the strongest upwelling signal from the youngest/least altered upwelled waters sampled (coolest SST and shallowest MLD and ChlMD). The remaining UpW casts

(Stns 2, 3, and 19) extend towards the center of the PCA plot with properties more similar to those of OSW and OnSW stations. This pattern suggests that the upwelled waters at these stations are characterized by relatively greater age/mixing compared to Station 7.

In addition to geographic heterogeneity, we also see clear evidence of temporal variability in the expression of upwelling. At Station 3, two casts (3.01 and 3.12) sampled within 9 hours and 1 km of one another were classified into different habitat types (Fig. 4.2). Cast 3.01 is an edge case whose properties place it uniquely on the border between OSW and UpW habitats (Fig. 4.1A). The SST and SSS of both casts are nearly identical and indicative of aged/altered upwelled water, whereas all of the integrated properties differ, making cast 3.01 similar to OSW waters (deeper MLD and ChlMD and a negative NAI)," (Weber et al. 2019).

4.1.2. Phytoplankton communities

We can now assess the relevance of these habitats to surface phytoplankton distributions using two complementary metrics of community composition: diagnostic pigments and species-specific cell counts. These two metrics provide complementary assessments of the phytoplankton communities, where diagnostic pigments offer a coarser view on composition with the identification of higher taxonomic groups (Vidussi et al. 2001). Though some of the diagnostic pigments occur in multiple groups of phytoplankton (e.g. Zeaxanthin, a marker for cyanobacteria, is also a common photo-protectant in eukaryotic phytoplankton, Kana et al. 1988), they give a broad community overview that importantly includes prochlorophytes (DvChla+b). Despite being capable of reaching appreciable abundances in oligotrophic waters, prochlorophytes are notoriously difficult to quantify with traditional microscopy due to their small size. Complementing this high-level assessment, microscopy-based cell counts provide an extremely detailed view of the larger (>2μm) phytoplankton community.

To answer the question of habitat relevance statistically, CAP was applied to both community datasets, constraining the analysis on habitat types. This approach allows for comparison of the phytoplankton communities across habitat types both visually with the construction of ordination plots and numerically with an error analysis through cross-validation. The CAP results reveal that despite the differences in resolution and coverage between the two community metrics, the habitat type groupings were largely relevant to the local phytoplankton. Ordination of community data achieved appreciable separation of the

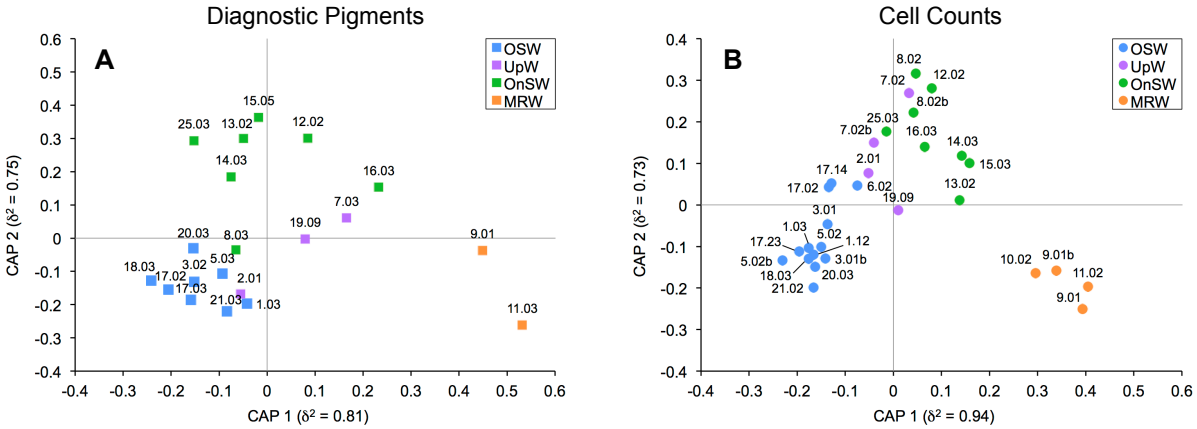

Figure 4.3: Canonical analysis of principal coordinates (CAP) ordination for diagnostic pigment **(A)** and species-specific cell count **(B)** community data for each sampling event. Markers are colored according to their habitat types. δ^2 is the canonical correlation of a given axis.

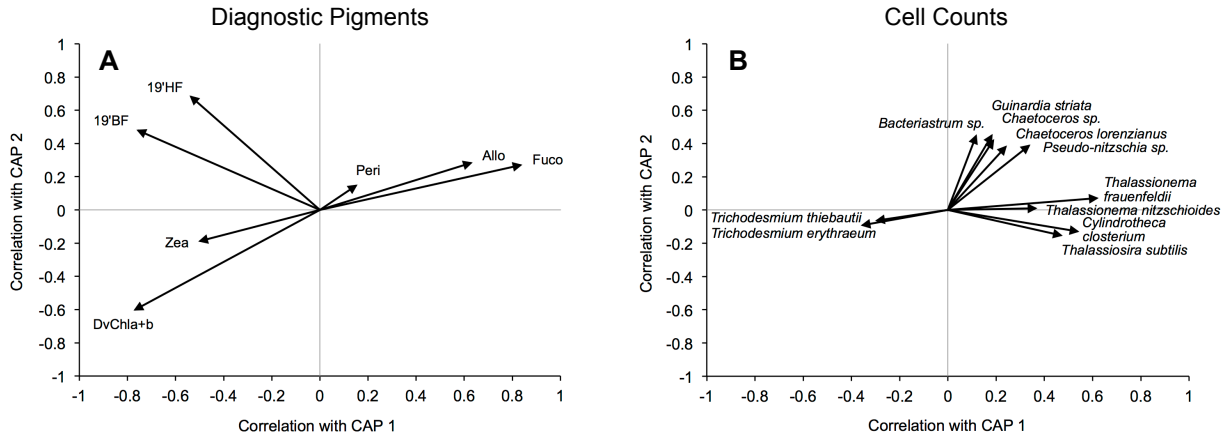

Figure 4.4: Biplots of the correlations of phytoplankton pigments **(A)** and species cell counts **(B)** with their respective canonical axes (see Fig. 4.3). The cell count biplot **(B)** shows only the phytoplankton with a Pearson correlation of $|r| \geq 0.3$ that also comprised $\geq 2\%$ of the total abundance of the habitat with which they best correlate. For example, the four species correlating most strongly and positively with CAP 1 made up $\geq 2\%$ of the community sampled in MRW casts. UpW was not explicitly considered.

stations between the MRW, OnSW, and OSW habitats for both community metrics, whereas the UpW habitat was consistently poorly defined. In both analyses, CAP 1 primarily separated MRW from OnSW and OSW (correlation coefficients of $\delta^2 = 0.81$ and 0.94 for pigments and cell counts, receptively), whereas CAP 2 chiefly separated OnSW from MRW and OSW ($\delta^2 = 0.75$ and 0.73, respectively). The ordination results were supported by cross-validation given the 80% success rate by the analysis to correctly classify pigment samples into their pre-determined habitat types and the 72.4% success rate for cell count samples (Table 4.2). The majority of the error in both analyses is attributable to the UpW habitat, with only 33.3% and 25% of samples correctly assigned for the pigment and cell count datasets, respectively.

Table 4.2: Classification success of pigment and cell count community samples to their pre-defined habitat types. The ratios in the total row are the total number of correctly sorted samples (events) over the total number of samples analyzed for each dataset. A 25% success rate would be expected if results were no better than random.

Habitat Type	% Classification Success	
	Pigments	Cell Counts
MRW	100	75
OnSW	71.4	75
UpW	33.3	25
OSW	100	84.6
Total	80 (16/20)	72.4 (21/29)

These results indicate that there is no distinct UpW community, though this is not altogether surprising. The habitat analysis revealed that there is considerable heterogeneity in the expression of upwelling at UpW stations (Fig. 5A) and that the upwelling signal itself was somewhat weak at the time of sampling. The combination of a variable influence of upwelling and lag in phytoplankton community responses behind changing environmental conditions likely prevented the development of a single, characteristic UpW community. The high error rates associated with the UpW habitat make it difficult to draw definitive conclusions about the specific events that were misclassified during cross-validation, particularly those that were reclassified as UpW. It is notable, however, that some of the same UpW stations were misclassified for both the pigment and cell count datasets (Table 4.3). For example, Stn 2.01, which was the most OSW-like out of the UpW casts in the habitat analysis (Fig. 4.1A, B), was consistently reclassified as OSW by the error analysis. It's plausible that at this station, the upwelling was so weak and/or recent that the resulting changes in the physical/chemical conditions of the waters had not significantly altered the (already-present) oceanic phytoplankton community. Similarly, there may be evidence of lags in community response to changing conditions at Stns. 8.03

and 13.02. The habitat type analysis classified these stations as OnSW but their phytoplankton communities are more similar to that of OSW communities (Table 4.3).

Compared to the UpW habitat, CAP could easily define the other three habitats, of which MRW and OSW received the highest classification success rates (Fig. 4.3, Table 4.2). Unlike OnSW, these MRW and OSW habitats reflect distinct end members in the SCS, and phytoplankton in these waters likely experience stronger or more consistent selective pressures on the basis of nutrient availability (among other things). For example, according to our NAI, the OSW surface waters are very limited in nitrate. The CAP biplots identified two groups of phytoplankton that correlated strongly with these nitrate-limited OSW waters: prochlorophytes (DvChla+b; Fig. 4.4A) and *Trichodesmium* spp. (Fig. 4.4B) – both of which contain Zeaxanthin. These two phytoplankton groups are known to thrive in "blue" waters and possess adaptations for oligotrophic conditions (e.g. large surface-area-to-volume ratio and the ability to fix N_2, respectively), making them well suited to the OSW habitat.

Table 4.3: Events that were misclassified during the canonical analysis of principal coordinates (CAP) cross-validation routine. Events marked with * belong to a station that was misclassified in both the pigment and cell count community datasets, whereas events marked with ** came from the same sampling event within a station.

Pigments			Cell Counts		
Event	Original habitat type	Reclassified habitat type	Event	Original habitat type	Reclassified habitat type
			10.02	MRW	UpW
8.03	OnSW	OSW	13.02	OnSW	OSW
14.03**	OnSW	UpW	14.03**	OnSW	UpW
2.01**	UpW	OSW	2.01**	UpW	OSW
7.03*	UpW	OnSW	7.02b*	UpW	MRW
			19.09	UpW	OSW
			3.01	OSW	UpW
			6.02	OSW	UpW

"Conversely, species with a broader salinity-range tolerance that are well adapted to nutrient-replete environs correlated with the MRW habitat (e.g. *Thalassionema* spp., *Cylindrotheca closterium*, and *Thalassiosira subtilis*; Fig. 4.4B). Though MRW phytoplankton formed their own distinct communities, they also shared many similarities with the OnSW communities (e.g. *Thalassionema* spp.; Fig. 4.4B), likely due to the higher nutrient availability that often occurs in coastal waters. This is also seen in a broader sense with the pigment biplot, where diatoms (Fuco) and cryptophytes (Allo) appear to correlate strongly with both habitats (Fig. 4.3A, 4.4A). Despite these commonalities, there were a

handful of neritic species common to the SCS (summarized in Voss et al. 2014) that were particularly abundant in the OnSW waters, including *Bacteriastrum* sp., *Guinardia striata*, *Chaetoceros* spp., and *Pseudo-nitzschia* sp. (Fig. 4.3B, 4.4B). Importantly, these results in particular and those of the CAP analyses in general further support distinguishing the OnSW waters as a distinct habitat, even though it represents a mix of the system's end members," (Weber et al. 2019).

Since we have established the relevance of the habitat types to the local phytoplankton communities, we can use these classifications as an aid to frame hypotheses about the habitat type and phytoplankton community structure when some of the necessary data are missing. In the dataset used here, two stations (Stns 23.02 and 27.01) were excluded from the habitat analysis due to a lack of nutrient data necessary to calculate NAI. There are, however, samples for phytoplankton cell counts from both of these stations and pigment samples from Stn 23.02. Since the habitat types were shown to be statistically significant with CAP, the phytoplankton communities at these two stations can be used to infer their habitat types using the sample add-in routine (in PRIMER).

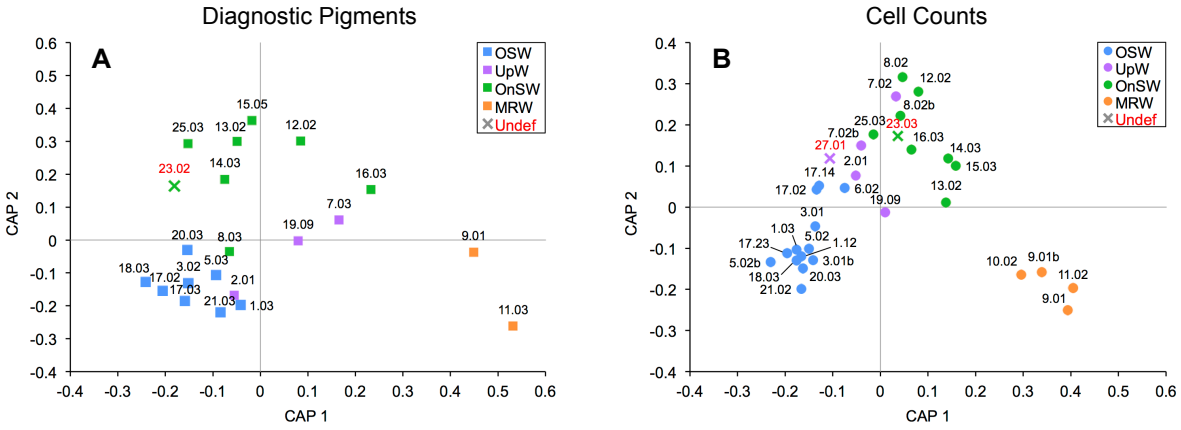

Figure 4.5: Post-hoc addition of phytoplankton samples with undefined habitat types into CAP ordination plots for diagnostic pigment **(A)** and species-specific cell count **(B)** community data. Added samples are labeled in red and their marker color matches that of the closest habitat.

With this routine, samples are placed in ordination space based on their community composition and their distance to the nearest habitat type centroid is used to determine their likely habitat. The routine placed Stn 23.02 closest to the OnSW centroid in both analyses (Fig. 4.5), whereas Stn 27.01 was placed nearest the UpW centroid in the cell count analysis (Fig. 4.5B). The consistency across both community metrics for Stn 23.02 is encouraging,

though the result is somewhat surprising given that the other available environmental data place it cleanly into the OSW habitat (SST: 30.2°C, SSS: 33.5, MLD: 42 m, ChlMD: 48 m). This outcome may reflect a recent transition of the waters at this station from OnSW to OSW, meaning that even though the waters physically and chemically look oceanic, representative species like *Trichodesmium* spp. have not yet grown in.

As for Stn 27.01, the high classification error rates for the UpW habitat (Table 4.2) make it difficult to draw anything conclusive, but this result is consistent with the proximity of the station to the northern coastline where upwelling was observed (Fig. 4.3). In fact, this station location was the most consistently influenced by the upwelling over the course of the cruise based on satellite SST (Fig. 3.3), and the environmental data we do have (SST: 25.9°C, SSS: 34.3, MLD: 5 m, ChlMD: 47 m) place Stn 27.01 well within the UpW habitat.

In summary, we have demonstrated a simple yet powerful approach for delineating habitat space in a highly dynamic and heterogeneous region. This approach, which used only commonly measured environmental variables that inherently integrate over multiple timescales, generated habitats that were highly relevant to the local phytoplankton growing in the SCS shelf waters, and provided insights into the spatial and temporal coupling between environmental drivers and the response of the phytoplankton community.

5. Diazotroph distributions

Since I have shown that the habitat types are both useful and relevant to the surface phytoplankton community as a whole, I will now use the delineated habitats as an aid to more specifically evaluate the biogeography of the major groups of diazotrophs. Following convention, the sampled diazotrophic community was subdivided into two size fractions based on cell diameter, >10 μm and <10 μm, which is reflected in the enumeration methods, as well as with the uptake rate measurements in the following chapter. The larger size fraction was enumerated with microscopy and included DDAs and *Trichodesmium* spp., whereas abundances of the small size fraction were estimated based on *nifH* gene copy abundances of unicellular groups: UCYN-A1, B, and C.

5.1. Results & discussion

Our survey of diazotroph populations confirms previous studies that the western shelf region of the southern SCS supports a diverse community of nitrogen-fixing organisms, even early in the SWM season. Nutrient conditions were widely favorable for diazotrophs given the very low/ undetectable surface $NO_{2/3}$ concentrations in OnSW and OSW waters (Fig. 3.4A) and the low N:P ratio (<16:1) in all habitats (Fig. 3.4D). Evaluation of diazotroph distributions revealed broad similarities between groups as well as group-specific patterns of cell and *nifH* abundances across the habitat types. For all of the diazotrophs and potential assemblages presented here, the highest abundances were often measured in the offshore OSW habitat, whereas counts in the OnSW and UpW habitats tended to be the most variable (Fig. 5.1, Fig. S5.1). These distributions reflect both the physicochemical conditions and the variability of those conditions within the habitats, and mirror results of the CAP analysis (Figs. 4.3, 4.4), which revealed that the OnSW and in particular UpW phytoplankton communities were the least well defined.

Counter to previous results from Bombar et al. (2011) and Moisander et al. (2008), unicellular groups were both highly abundant and widely distributed in the sampled region (Fig. 5.1, Fig. S5.1). Interestingly, both of those studies were carried out during the intermonsoon season (April), when river outflow is lowest, coastal upwelling is absent, and rates of nitrogen fixation tend to be relatively low (Voss et al. 2006). Bombar et al. (2011), who restricted their survey to the river mouth given the low river outflow, detected unicellular groups B and C only in oligotrophic waters (SSS > 33.5), and Moisander et al. (2008), who surveyed approximately the same geographic region as this study, measured

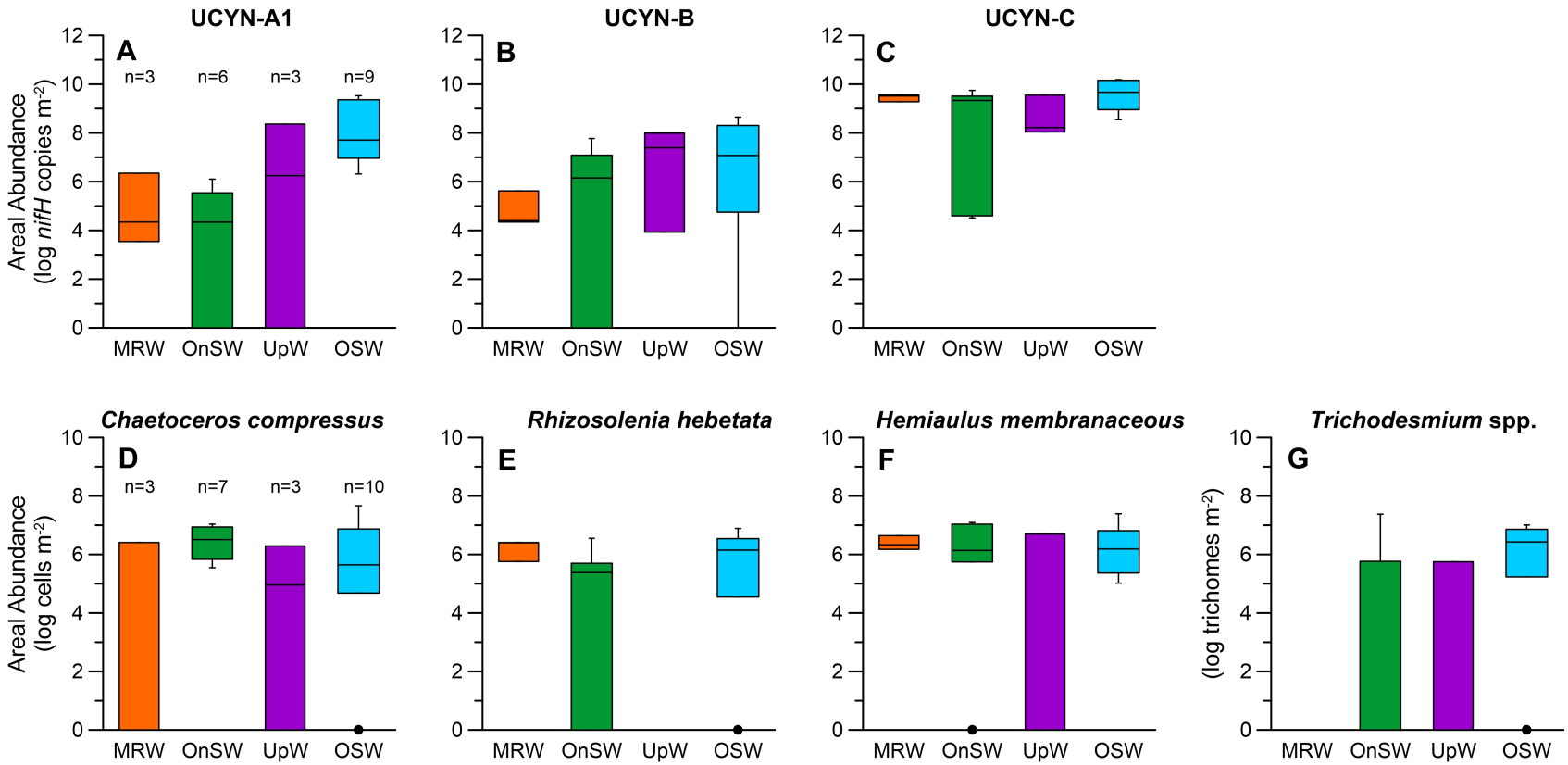

Figure 5.1: Box plots of areal abundances of the most prevalent groups of unicellular diazotrophs based on *nifH* gene copies **(A-C)**, DDA host species based on cell counts **(D-F)**, and *Trichodesmium* spp. based on trichome counts **(G)**, where boxes are colored by habitat type. The number of samples "n" included in each habitat is given in panel **A** for **A-C** and in panel **D** for **D-G**. Outliers are shown as black circles.

low abundances across nearly all samples despite prevailing oligotrophic conditions. These results suggest that the SWM plays a critical role in increasing unicellular diazotroph abundances in all regions of the SCS, including oligotrophic waters. Though UCYN-C was surprisingly widespread in 2016 (Fig. 5.1C, Fig. S5.1C), UCYN-A1 and B tended to have lower abundances in the MRW habitat compared to OSW, but were still consistently detectable (Fig. 5.1 A-B, Fig. S5.1A-B). Some groups of unicellular diazotrophs are known to tolerate higher nutrient levels (see nutrient amendment experiments in Appendix, Fig. S 8.3) and tend to favor cooler waters (Messer et al. 2016; Moisander et al. 2010; Needoba et al. 2007; Stenegren et al. 2017), but temperature dependence is unlikely to explain the lower MRW abundances given the very minor SST differences between MRW and OSW habitats (Fig. 3.1B). Competition with coastal phytoplankton may be a more likely explanation.

Much like the unicellular groups, the large diazotroph species often had their highest abundances in OSW waters. As expected, *Trichodesmium* spp. represent the extreme case, where trichomes were completely absent from the river plume waters and highly variable in the shelf and upwelling region, reflecting their preference for warm, oligotrophic conditions (Capone et al. 1997; Carpenter 1983). Upwelled waters were particularly unfavorable for DDA host species, with *Rhizosolenia hebetata* completely absent from all UpW stations. These host abundances represent the three major species capable of forming DDAs, but the cell counts in Fig. 5.1D-F tell us nothing about which hosts were actually infected with *Calothrix* or *Richelia* and thus fixing N_2. All three of these host species are known to live independently of diazotrophic symbionts, which has complicated previous efforts to assess DDA biogeography in the SCS (Grosse et al. 2010). Due to statistical considerations, infection rates (% of host population infected) for this study were determined from vertical net tows performed in the upper 100m or through the entire water column if shallower. The host infection rates in these depth-integrated tows were then applied to the areal host abundances derived from CTD samples collected over the same depth interval. Though not ideal, this combined dataset nonetheless gives an unprecedented view into DDA formation and proliferation. Very few studies have considered the consequence of host-symbiont association strength on the biogeography of DDAs (Caputo et al. 2018), and the highly heterogeneous physicochemical conditions of the southwestern SCS presents a unique opportunity to do so.

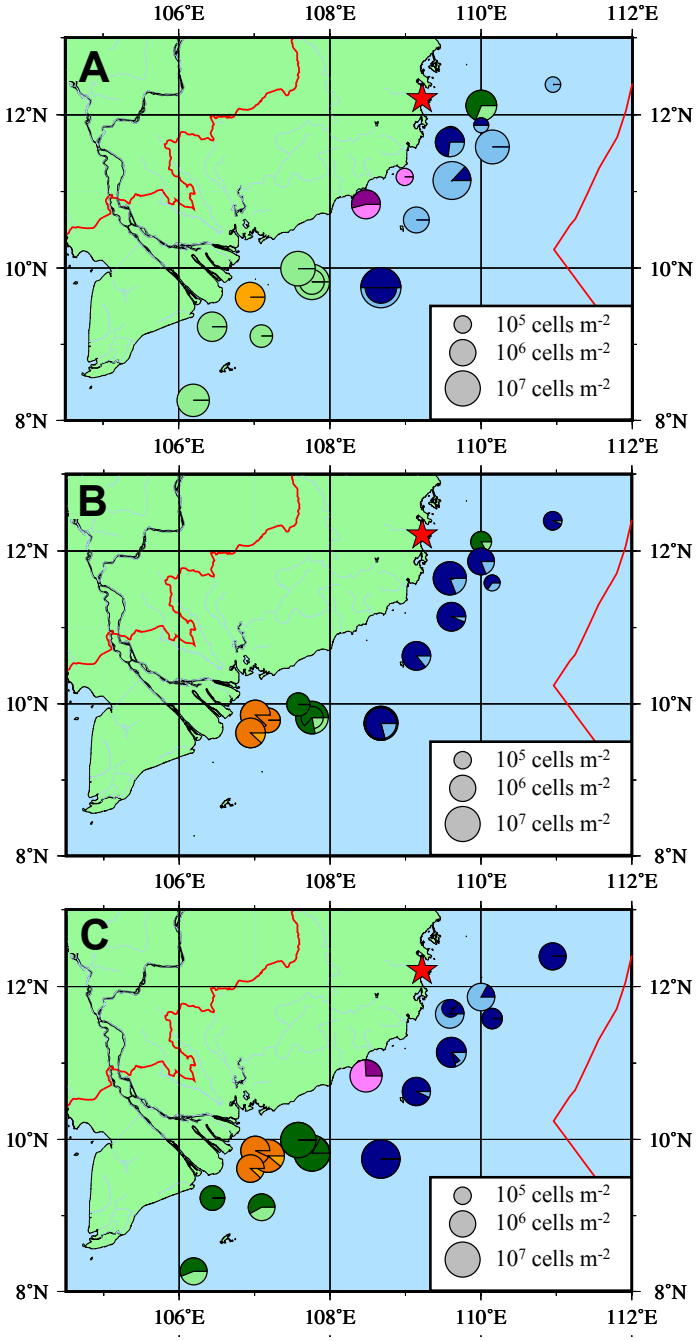

Figure 5.2: Abundance and symbiont infection rate of the three most widely distributed DDAs: **(A)** *Chaetoceros compressus*, **(B)** *Rhizosolenia hebetata*, and **(C)** *Hemiaulus membranaceus*. Circle areas are proportional to areal abundance of hosts (cells m^{-2}) calculated by integrating counts from CTD samples, and the dark wedges represent the proportion of the population at each station carrying one or more symbionts. Infection rates were determined from vertically-integrated net tows. Colors of bubbles refer to the habitat types. Plots were generated by Joseph Montoya.

Variation in the distributions of DDA-capable host species (Fig. 5.1) and their rates of infection (Fig. 5.2) do appear to be consistent with differences in host–symbiont association strength. For example, *Chaetoceros compressus*, which is commonly found living independently in SCS coastal waters (Voss et al. 2014) and only weakly associates with its externally-located *Calothrix* symbiont (Caputo et al. 2018; Hilton et al. 2013; Sournia 1970), had one of the broadest distributions of the host species but some of the lowest infection rates in nutrient replete habitats (Figs. 5.1D and 5.2A). *Chaetoceros compressus* infection was particularly low or at 0% in the river plume and neighboring shelf waters, but infection rates tended to increase in the OSW habitat where nitrate availability (NAI) was lowest. Interestingly, their infection rates were highest at Stn. 17, where the highest diversity of DDA species was found (Hai Doan-Nhu, personal communication). These results suggest that *Chaetoceros compressus* is well adapted to the shelf waters of SCS and may be able to extend its distribution to more oligotrophic conditions through DDA formation.

In contrast, the hosts *Rhizosolenia hebetata* and *Hemiaulus membranaceus* appear to rely heavily on their internally located *Richelia* symbionts (Villareal 1992) to thrive in the SCS. Only small portions of their populations were asymbiotic and host abundances were highest when associated with symbionts (Fig. 5.2B-C). Diazotroph infection was particularly high near the Mekong River mouth and in the offshore waters of the OSW habitat (Fig. 5.1E-F), whereas hosts were absent or uncommon in the upwelling region (Fig. 5.2B-C). Both species were often infected with multiple symbionts, and it was not uncommon for *Rhizosolenia hebetata* to have three or more *Richelia* trichomes (not shown), likely a consequence of its large cell volume.

The high infection rates of *Rhizosolenia hebetata* and *Hemiaulus membranaceus* hosts indicate that their cell counts represent good approximations of DDA abundances, meaning that when converted to cell carbon and summed with estimates of *Trichodesmium* spp. biomass, the proportional contribution of large diazotroph biomass to the standing stock of phytoplankton (determined through microscopy, cells > ca. 5 μm) can be calculated. These estimates, based on surface measurements (shown in Fig. 5.3), indicate that large diazotrophs make up a rather small percentage of the standing biomass at the majority of stations (generally < 3%). Only in the oligotrophic OSW habitat, which is largely defined by the deepest MLDs and lowest NAI values (Table 4.1), do diazotroph relative abundances exceed 25% and reach as high as 55% of the standing biomass.

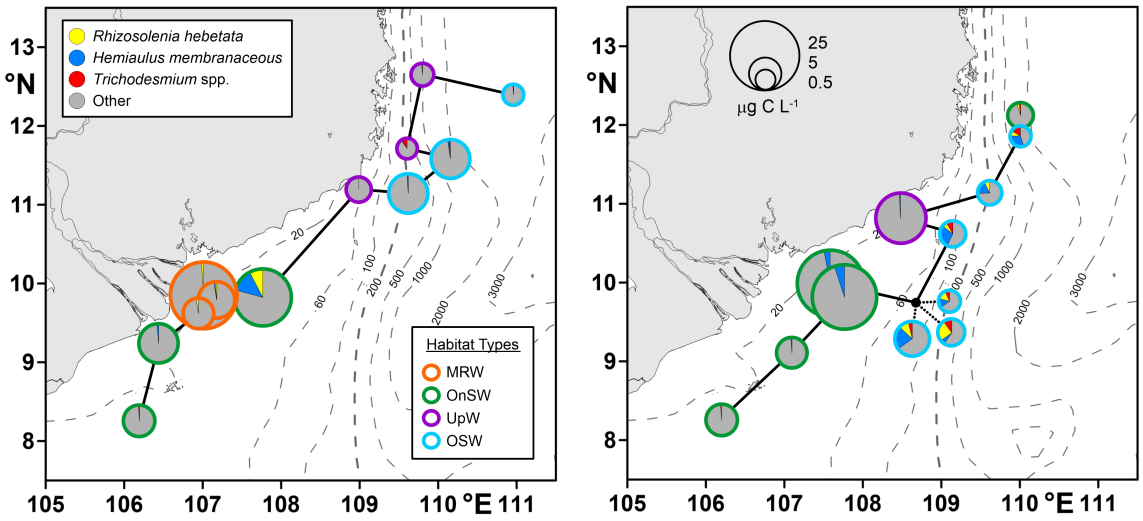

Figure 5.3: Proportion of major species of large diazotrophs in surface phytoplankton communities based on cellular carbon content on Legs 1 **(A)** and 2 **(B)**. Pie chart diameter is proportional to the total community carbon concentration at each station and the colored ring around each pie chart corresponds to the station habitat type. Bathymetry is shown with the dashed lines.

In summary, the Mekong River plume does appear to be an important habitat for diazotrophs, both for unicellular groups and now definitively for DDAs, which is in line with previous studies (Bombar et al. 2011; Grosse et al. 2010; Voss et al. 2006). Even so, the highest absolute and relative abundances of diazotrophs were found in the offshore oligotrophic waters of the OSW habitat, which appears to be unaffected by the river plume and very minimally influenced by aged upwelled water (i.e., Stn. 6, investigated in the following chapters). These findings suggest that there is a greater inherent capacity for N_2-fixation in the oligotrophic SCS than previously recognized. We also saw evidence that the generated habitats (and the variables used to define them) were relevant to diazotroph biogeography, given that the distributions of diazotrophs considered here varied distinctly with habitat type, which indicates that the habitat type approach is likely a meaningful way to evaluate similarly heterogeneous ecosystems. And finally, my analysis (albeit preliminary) on a possible link between DDA symbiosis strength, DDA biogeography, and host infection rates, points to an area of research that deserves far more attention. Surprisingly little is known about the factors that shape DDA distributions, which is likely a consequence of an increasing dependence on *nifH* analyses to survey DDA populations. While this approach is less resource (i.e. human) intensive, it cannot provide valuable information on asymbiotic host populations, nor on the infection intensity or number of symbionts per host. Without this information, we likely miss the nuanced relationships

between DDA distributions and environmental conditions, information that becomes ever more pertinent as we continue to explore diazotrophy in more physicochemically complex regions.

6. Diazotroph activity & contributions to POM

6.1. Results

6.1.1. Rates of N_2-fixation and primary production

In all habitats of the SCS, volumetric rates of nitrogen fixation (N_2-fixation) and primary production (PP) were highest in the surface waters and tended to decrease with depth (Fig. 6.1). The highest nitrogen fixation activity was measured in OSW waters with a maximum of 19.4 ± 6.1 nmol L^{-1} d^{-1} in the <10-µm size-fraction (Fig. 6.1D). By comparison, the highest rates of primary production were measured in the MRW habitat, with a maximum value of 22.0 ± 13.4 mmol L^{-1} d^{-1} in the >10 µm fraction (Fig. 6.1E). With the exception of PP in the MRW habitat, activity across all habitats was consistently

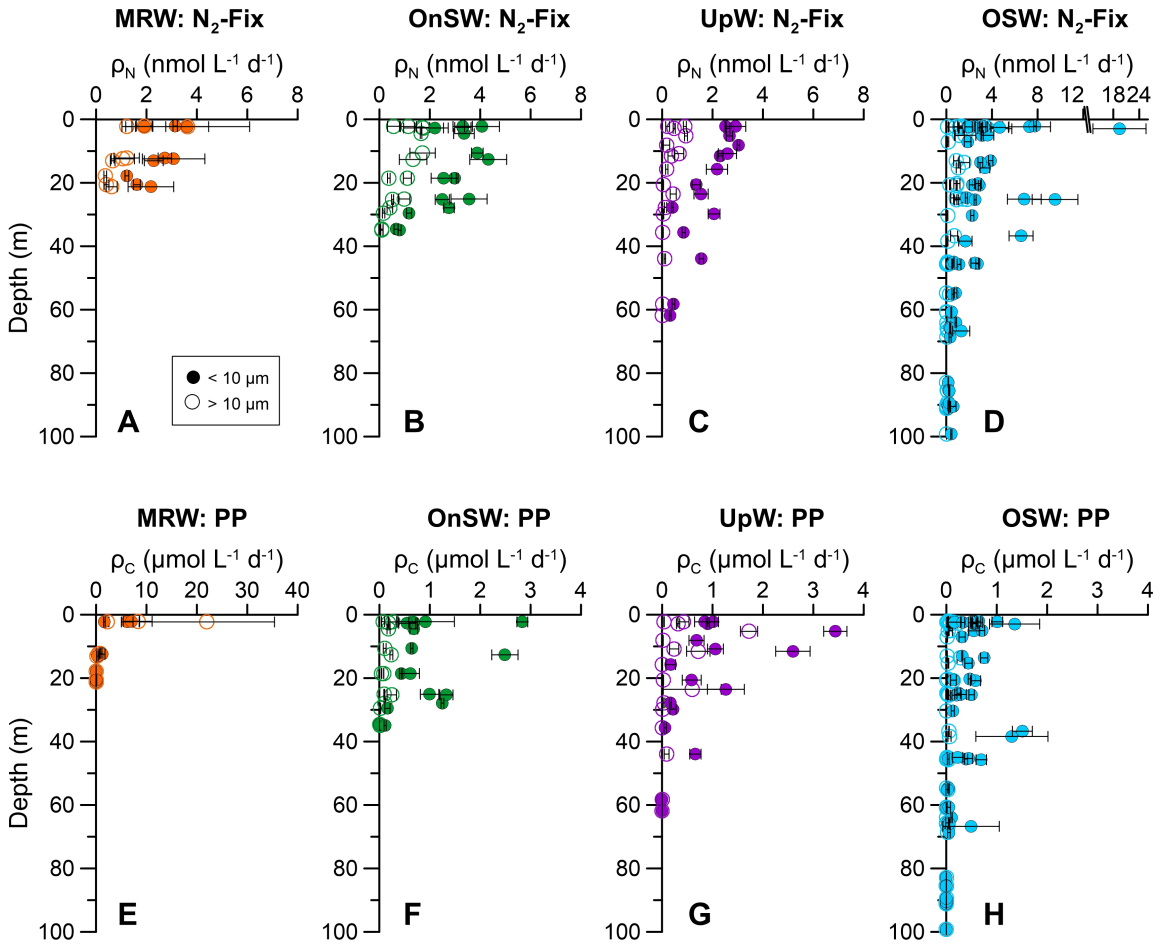

Figure 6.1: Vertical distributions of volumetric rates (mean ± std dev of replicates) of nitrogen-fixation (N_2-Fix; **A-D**) and primary production (PP; **E-H**) in the top 100 m of the water column by habitat type. In each panel, the activity of the smaller size fraction (<10 µm) is shown with a solid circle, and that of the large size fraction (>10 µm) is shown with a larger, open circle. Note the unit difference between N_2-fixation and PP rates, as well as the scale changes in panels **D** and **E** for N_2-fixation and PP rates, respectively.

highest in the <10-µm size-fraction. In the UpW habitat, the variation in PP rates among the two size fractions reflects heterogeneity of rate profiles among stations, such that at a given station, the smaller size fraction was still consistently more active than its respective larger size fraction (Fig. 6.1G).

Patterns in both the relative magnitude and contribution of the small and large size fractions to total activity among habitats were preserved when rates were vertically integrated through the deepest depth sampled (Table S6.1, Fig. 6.2). Areal rates of nitrogen fixation were highest in OSW waters (274 ± 164 µmol N m^{-2} d^{-1}) and were driven by the small size fraction, whereas total primary production was highest at MRW stations (125 ± 86 mmol C m^{-2} d^{-1}) and were predominantly attributable to the large size fraction.

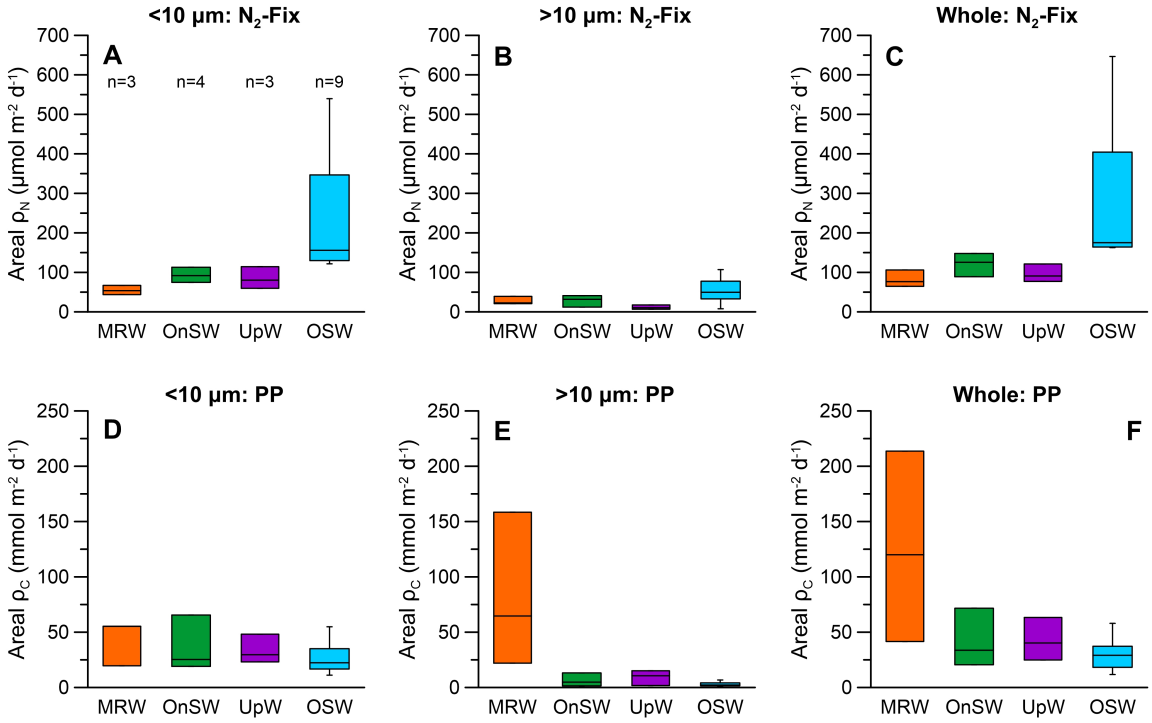

Figure 6.2: Box plots of areal rates of nitrogen fixation (N_2-Fix; **A-C**) and primary production (PP; **D-F**) integrated to 100 m or the deepest depth sampled. Areal rates are shown across the four habitats and are displayed according to size fraction, where "whole" rates are the additive combinations of rates from the small and large size fractions. Note the difference in units between the top panels and bottom panels. In panel **A**, "n" is the number of profiles included in each habitat and applies to all panels.

Comparison of the water column areal rates of N_2-fixation and PP to Redfield stoichiometry provides an additional means of assessing diazotroph impact in terms of the fraction of community primary production supported by diazotrophy ($\%PP_{diazo}$). $\%PP_{diazo}$ varied markedly among habitats (Fig. 6.3), with the lowest diazotroph contributions at MRW and UpW stations and the highest measured at OSW stations, regardless of size

fraction considered. The total diazotroph community and the smaller size-fraction specifically contributed <5% to PP at all stations within the MRW, OnSW, and UpW habitats. By comparison, they accounted for roughly 2 – 12% of PP in OSW waters. Interestingly, at most of the OSW stations, $\%PP_{diazo}$ was significantly higher in the larger size-fraction, with large diazotrophs at most OSW stations supporting 10 – 31% of total PP.

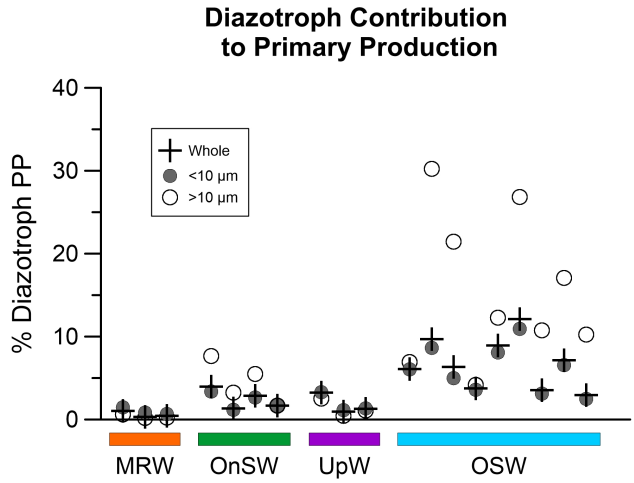

Figure 6.3: Contribution of diazotroph PP to whole community PP based on areal rates of activity. Values are grouped by habitat type and displayed according to their size fraction (see legend). Note that the $\%PP_{diazo}$ value for "whole" is *not* the additive combination of $\%PP_{diazo}$ values of the <10-µm and >10-µm size-fractions.

6.1.2. ^{15}N natural abundance in suspended particles

The $\delta^{15}N$ signatures of PON, which can be used to determine the relative contributions of isotopically distinct N sources to the particulate pool, varied considerably in the top 100 m of the water column, ranging from -0.8 to 6.7‰ (Fig. 6.4A). PON tended to be the most depleted in ^{15}N at the surface and within the top 70 m and $\delta^{15}N$ increased with depth, becoming more similar to the $\delta^{15}N$ end member value for global nitrate (5‰, Liu and Kaplan 1989). Of the four habitats, OSW had the largest variation in $\delta^{15}N$-PON values as well as the most negative signatures, which tended towards the end member for diazotroph biomass (-2‰, Montoya et al. 2002).

With these two end members, I could quantify the role of diazotrophy in supporting biomass production on the timescale of particle turnover (Fig. 6.4B). This was achieved by applying a linear mixing model (Eq. 2.3) to the depth- and mass-weighted average $\delta^{15}N$ of POM from the mixed layer at each station, taking care to exclude stations whose POM $\delta^{15}N$ values may have been influenced by phytoplankton nitrate uptake. The diazotrophic contribution to particles ($\%N_{diazo}$) ranged from 14 to 72% across all considered stations, but with marked differences across habitat types. The UpW habitat had modest diazotroph contributions (16 – 23%), while some OnSW stations had relatively higher contributions that nonetheless remained below 46%. The OSW habitat showed the highest contributions

from diazotrophy, with the majority of the stations giving $\%N_{diazo}$ values between roughly 50 – 70%.

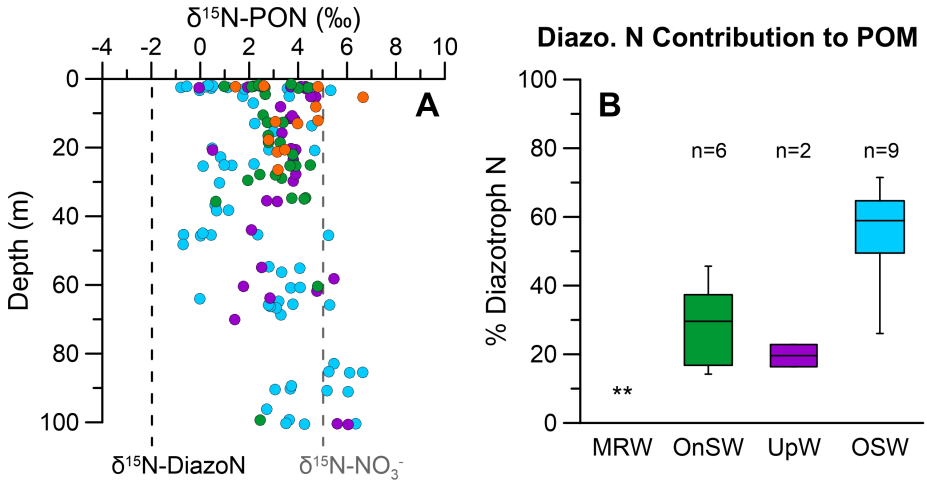

Figure 6.4: **(A)** $\delta^{15}N$ signatures of POM from the top 100m, where markers are colored by habitat type. The dashed lines represent the $\delta^{15}N$ values of the two primary "new" nitrogen sources to phytoplankton, diazotroph biomass (black) and subthermocline nitrate (grey). **(B)** Box plots of the contribution of diazotroph N to mixed layer-integrated POM across the four habitat types. "n" represents the number of profiles included in each habitat type. Stations whose $\delta^{15}N$-POM values were likely influenced by nitrate fractionation are not included in the $\%N_{diazo}$ calculations (see Methods).

6.2. Discussion

Our habitat type classification in Chapter 4 has proven to be an effective means of delineating the SCS into habitats supporting distinct phytoplankton communities and diazotroph assemblages, but the utility of this tool for evaluating biological rates of C and N fixation, as well as the general biogeochemistry of the region, remains an open question. The benefit of this method is in identifying sampling sites affected by the major regional forcings (i.e. upwelling and river outflow) that shape local conditions and phytoplankton communities (Weber et al. 2019), specifically providing insight on how these forcings support or suppress diazotrophy and more generally influence N and C cycling. Previous studies have shown that Vietnamese coastal, shelf and offshore waters of the southwestern SCS support modest rates of nitrogen fixation, though with strong seasonal variation (Voss et al. 2006). Conditions during the SWM are more favorable for nitrogen fixation than during the spring IM period. The interaction of the Mekong River plume with aged, seasonally upwelled waters appears to promote diazotrophy (Bombar et al. 2010; Voss et al. 2006) and occurs only during the SWM season (Hu et al. 2000). The conditions prevailing

during the early stages of the 2016 SWM sampling present an unusual situation in which both the coastal upwelling and river plume were detectable, but their interaction was minimal due to low outflow of the Mekong River. In combination with the large spatial coverage of the 2016 cruise, this dataset gives us the opportunity to better resolve the roles of these two forcings in influencing diazotrophy.

6.2.1. Rates of N_2-fixation and primary production

Rates of N_2-fixation and PP were measurable at all stations, though with distinct patterns in activity among habitats. Whole community rates reveal offshore oligotrophic waters as a regional hotspot for N_2-fixation (274 ± 164 μmol N m^{-2} d^{-1} on average, Table S6.1, Fig. 6.2C), which agrees well with diazotroph distributions (Fig. 5.1). OSW activity is elevated compared to world ocean basin averages (Luo et al. 2012), but still well below that of diazotroph bloom conditions. The highest activity occurred at OSW Stn. 17 (646 μmol N m^{-2} d^{-1}), whose waters also had the highest diversity of DDAs of all sampled stations (Nguyen-Ngoc et al. *in progress*). It is difficult to identify the confluence of factors that lead to such favorable conditions at this station, but the elevated activity demonstrates the potential of the diazotrophic community in the SCS prior to peak season.

The Mekong River plume, by contrast, supported much lower, but significant, rates of N_2-fixation (82 ± 21 μmol N m^{-2} d^{-1}, Table 6.1, Fig. 6.2C). Nitrogen fixation in these waters was surprising given the elevated DIN concentrations in the plume, conditions typically thought of as unfavorable for diazotrophy (see Knapp 2012). In fact, diazotrophy was commonly detected in waters with appreciable $NO_{2/3}$ concentrations (>0.5 μM), including the river plume proper and upwelled waters (up to 3.6 μM) and in deeper offshore waters (up to 9.5 μM, Fig. S6.2A). Importantly, low N:P ratios (below Redfield ratio) prevailed at nearly all sampled locations (Fig. S6.2B), allowing diazotrophs to remain competitive and active. Along with previously measured rates in this region (Grosse et al. 2010; Voss et al. 2006), our results add to mounting evidence that DIN is a weaker regulator of diazotrophy than previously thought (Knapp 2012; Mulholland et al. 2019; Mulholland et al. 2001), and serve to further expand the known domain of active diazotrophs (Mulholland et al. 2019).

Our size-specific rate measurements can provide insight into which organisms are actively fixing nitrogen; for example, we can directly resolve the relative contributions of small (UCYN-A1, B, C) and large diazotrophs (DDAs, *Trichodesmium* spp.) to whole community rates of nitrogen fixation. However, a number of caveats, in particular with the

N_2-fixation rates, must first be considered. The rates presented here represent *net* as opposed to *gross* activity since ^{15}N labeling was quantified for only the particulate fraction. Our rates thus provide an estimate of the realized contribution of diazotrophy to particles over the timescale of the experiments. Recycling of diazotroph-derived N (as autochthonous DIN and DON) can occur rapidly relative to the experiment length (24 hr) (Klawonn et al. 2019; Mulholland et al. 2014), meaning that some labeling of non-diazotrophic organisms likely occurred in our incubations. Since this non-diazotroph ^{15}N was initially derived from nitrogen fixation, these rates therefore represent the realized *community* impacts of diazotrophy.

In the early SWM of the SCS, the smaller size fraction was often more active than the larger, a surprising result given that DDAs and *Trichodesmium* in particular tend to fix N_2 at higher rates than UCYN varieties (e.g. Caffin et al. 2018). Nonetheless, there are regions of the ocean where UCYNs dominate community N_2-fixation (Church et al. 2005; Montoya et al. 2004; Zehr et al. 2001), and the southwestern SCS may be one such system given the high abundances of UCYNs encountered on this cruise (Fig. 5.1A-C). Of course, our partitioning by size fraction is rather coarse, and there may be additional factors or organisms contributing to the higher activity in small particles. For example, non-cyanobacterial diazotrophs (NCDs), which were not explicitly enumerated in this study, can be prevalent throughout the water column (e.g. Bird et al. 2005; Fernandez et al. 2011; Moisander et al. 2014), but little is known about their ecology and activity (Bombar et al. 2016; Moisander et al. 2017). Most studies to date (see summary in Moisander et al. 2017) indicate that NCDs are often inactive or have very modest nitrogen fixation rates, though they may become significant when integrated over the entire water column (Benavides et al. 2018). It is also possible that activity in the small size fraction was overestimated either through breakage of large cells/trichomes during filtration or via the recycling of labeled fixed N (especially as NH_4^+), which may be preferentially assimilated by bacteria and pico-cyanobacteria (Caffin et al. 2018). That said, the methods used here are well-established and have previously shown minimal evidence of bias from mechanical handling (e.g. Montoya et al. 2004). Even with these caveats, these data show the importance of the smaller size fraction in contributing to community rates of both N_2-fixation and PP in all regions of the southwestern SCS.

6.2.2. Diazotroph contribution to primary production

The clear habitat-specific trends in PP and N_2-fixation are reflected in our estimates of the role of diazotrophy in supporting biomass production ($\%PP_{diazo}$). Even though diazotrophs were present (Fig. 5.1) and active (Fig. 6.2) in all habitats, their contributions to biomass production varied considerably (Fig. 6.3). Whole community $\%PP_{diazo}$ was ≤ 4% in all but the OSW habitat, where it reached as high as 12.3% (7.2% on average). To put these figures into perspective, many studies from tropical and subtropical oceanic regions have reported $\%PP_{diazo}$ values (based on net areal rates) that are generally < 5-6% (summarized by Berthelot et al. 2017), and are rarely upwards of 10% (Berthelot et al. 2017; Montoya et al. In press). Though we did not measure nitrate-uptake rates on this cruise, earlier estimates from the same area (Bombar et al. 2010) indicate that OSW N_2-fixation rates would account for more than 30-50% of new production, which further strengthens the narrative of the OSW habitat supporting ecologically significant diazotroph activity.

Examining differences in $\%PP_{diazo}$ estimates between size fractions (Fig. 6.3) reveals major shifts in phytoplankton community composition and N-acquisition strategies across habitats, strongly supporting findings from the CAP analysis in Chapter 4. In the DIN-replete river plume, where CAP had revealed the presence of large, chain-forming coastal diatom species (Fig. 4.4B) (Weber et al. 2019), community rates of PP were strongly driven by the larger size fraction (Fig. 6.2E) and diazotrophy contributed very little to local production (Fig. 6.3). Moving offshore, CAP identified *Trichodesmium* spp. as characteristic of the OSW habitat (Fig. 4.4B) (Weber et al. 2019), and while rates of N_2-fixation in the large size fraction were modest (Fig. 6.2 B), diazotrophy supported up to 30% (18% on average) of PP in large particles at OSW stations (Fig. 6.3).

6.2.3. Diazotroph contribution to POM

The $\delta^{15}N$ of POM provides another means of assessing the community impact of diazotrophy, but on longer timescales than the rate experiments, likely on the order of days to weeks (Landrum et al. 2011; Montoya 2007; Sharp 1983). N_2-fixation typically generates PON with a $\delta^{15}N$ of -2‰, making it isotopically distinguishable from nitrate-based production ($\delta^{15}N$ = ~5‰) and allowing for the quantification of diazotroph N inputs to POM ($\%N_{diazo}$) (Fig. 6.4B). Low $\delta^{15}N$ values can arise through other processes though, complicating this interpretation. Here, I briefly consider other potential sources of N to our

POM samples and describe the steps I have taken to more accurately constrain diazotroph inputs to suspended particles.

One potential major source of N to the region is the Mekong River, which delivers allochthonous particulate and dissolved N (DIN and DON) directly to coastal waters. An assessment of the terrestrial versus marine origins of POM using δ^{13}C-POC signatures in combination with POC:PON ratios (see Chapter 6 supporting material) revealed that the POM we sampled is reflective of marine OM or *in situ* growth (δ13C > -24‰ and C:N < 10; e.g. Savoye et al. 2003; Thornton and McManus 1994). The river was, however, a clear source of DIN at MRW stations (Fig. 3.4A, Table 4.1). Since the incomplete consumption of nitrate can generate isotopically light PON (ε = 5 – 10‰; Montoya and McCarthy 1995; Waser et al. 1998), we cannot unambiguously identify the source of the low δ^{15}N signals in these waters, so MRW stations were excluded from the $\%N_{diazo}$ calculations. Similarly, any stations with significant $NO_{2/3}$ within the mixed layer were disregarded, which included some UpW and OnSW stations (Fig. S6.1). Riverine DON is another potential source of allochthonous N to the region, and even though DON was not quantified in this study (and to my knowledge, unreported for the Mekong River), riverine inputs were likely insignificant over much of the study region. Based on other physicochemical measures, the river had minimal influence beyond the MRW habitat (see Fig. 3.1, Chapter 4), and considering that only a small fraction of DON is actually labile (~12%, Bronk 2002), effects of riverine DON on OnSW, UpW, and OSW particles were likely minimal. Nitrification can also produce ^{15}N-depleted N, though the isotopic imprint from fractionation is transferred to particles only when the transformation of the NH_4^+ pool to NO_3^- is incomplete (Clark et al. 2008). We unfortunately could not quantify NH_4^+ during the cruise, but NH_4^+ tends not to accumulate in the oligotrophic euphotic zone outside of diazotroph bloom conditions, and likely did not significantly influence mixed layer POM at the considered stations.

Compared to these other potential sources of isotopically light N, atmospheric deposition can be significant in the SCS (Duce et al. 2008; Kim et al. 2014; Yang et al. 2014). Effects from this process, which involve inputs of reactive N species (e.g. NO_3^-, NH_4^+, DON) with variable isotopic signatures (-7.5 to 3.7‰, Yang et al. 2014), have shown to support primary production in range of marine environments (e.g. Baker et al. 2007; Paerl 1997), but are greatest near areas of high population density with burgeoning economies (Duce et al. 2008). For this reason, most studies have focused on the coastal waters of China in the northern SCS, where atmospheric inputs have been implicated in

stimulating production both near the coast (Wu et al. 2018) and offshore (Kim et al. 2014). By comparison, very little is known about the magnitude of atmospheric inputs to our study region, even though the Mekong Delta region of Vietnam is expected to become a more significant source of anthropogenic N in the coming decades (Duce et al. 2008). If there had been a local trend in atmospheric N deposition on the scale of our study site, we would expect inputs to be greatest near shore and perhaps to the south, closer to (and downwind of, Fig. S3.4) the largest center of population in Vietnam. This would mean that particles from OnSW stations would have lower $\delta^{15}N$ signatures than those from OSW stations, but we measured the opposite trend. Additionally, we experienced no precipitation during the cruise, as it took place before the start of the region's rainy season, which eliminates inputs through wet deposition. For these reasons, atmospheric deposition alone cannot explain the measured trends in $\delta^{15}N$-POM, and even though it likely did contribute some ^{15}N-depleted N to surface waters, diazotrophy must have been the dominant ^{14}N source to OSW suspended particles. As an extreme case, even if I were to assume that dry atmospheric deposition influenced all stations evenly and accounted for all of the mixed layer diazotroph N signal from UpW and some OnSW stations (~20%), diazotroph N would still comprise 20-50% of POM from the majority of OSW stations (Fig. 6.4B).

Despite having to reduce the number of stations included in the $\%N_{diazo}$ calculation, this POM-based estimate of diazotroph contributions still revealed clear trends across three of the habitat types. In line with both the rates of nitrogen fixation (Fig. 6.2) and diazotroph abundances (Fig. 5.1), $\%N_{diazo}$ was consistently highest in the OSW habitat, where it varied between 20 and 80% (Fig. 6.4B). In fact, $\%N_{diazo}$ increased significantly with both log-transformed areal rates of N_2-fixation (r^2=0.50, p<0.007; Fig. S6.3A) and the relative contribution of large diazotrophs to total biomass (r^2=0.63, p<0.0004; Fig. S6.4B) when all measures were integrated over (or were derived from) the mixed layer. These two relationships indicate that community rates of diazotrophy are influencing particles on a timescale relevant to suspended particle turnover, and that $\%N_{diazo}$ is reflective of both the standing stock of diazotroph biomass, as well as the cumulative impact of nitrogen-fixation. In terms of magnitude, the $\%N_{diazo}$ values presented here are similar to values measured in regions with prominent diazotroph populations. For example, $\%N_{diazo}$ values based on integrated measures reached 60% and 80% in the *Trichodesmium* dominated Arabian Sea (Capone et al. 1998) and subtropical North Atlantic (Landrum et al. 2011), respectively, and up to 100% in the offshore waters of the Amazon plume (Loick-Wilde et al. 2016; Montoya

et al. In press; Weber et al. 2017) where populations of DDAs and *Trichodesmium* were highest (Goes et al. 2014; Weber et al. 2017).

6.2.4. Comparison of diazotroph contribution measures

Our two measures of diazotroph contribution to the ecosystem, $\%PP_{diazo}$ and $\%N_{diazo}$, provide information on distinct time scales: rate measurements reflect physiological activity over one day while stable isotope abundances integrate nitrogen inputs over longer periods, from days to weeks (Fig. 1.6). Both measures were highest at OSW stations, but diazotrophs appear to make much larger contributions to POM (typically 5-fold higher) relative to corresponding estimates of diazotrophy-based PP (Fig. 6.5A). Such a mismatch appears to be common and has been documented in other systems, including the oligotrophic Arabian Sea (Capone et al. 1998) and North Atlantic (Carpenter et al. 1999; Montoya et al. 2002), and more recently in the Amazon River-influenced region of the western tropical North Atlantic (Montoya et al. In press). Such an offset must indicate differential cycling of N and C within the mixed layer (Montoya et al. In press), such that diazotroph N is retained in the upper water column over time and has a persistent influence through its support of recycled production. This would mean that even modest but sustained inputs of diazotroph N could have a large isotopic influence on particles.

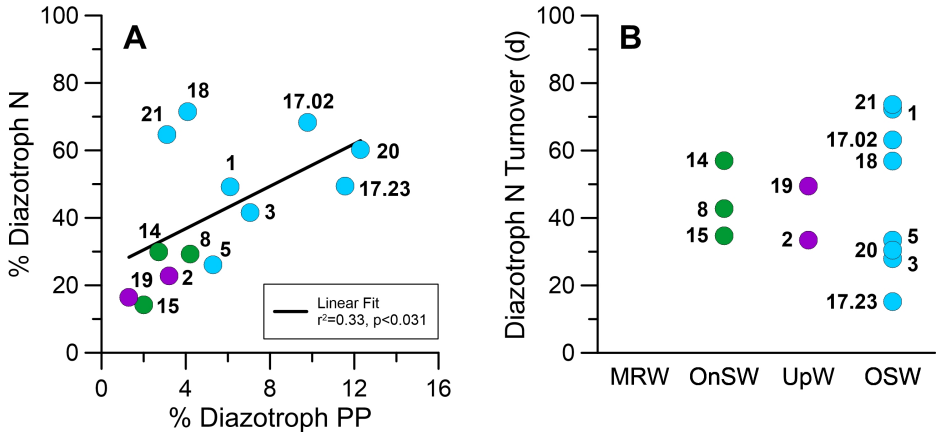

Figure 6.5: **(A)** Relationship between the percentage of diazotrophic nitrogen in POM ($\%N_{diazo}$) to rate-based impact of diazotrophy ($\%PP_{diazo}$) within the mixed layer. The linear fit is shown with the black line (see plots for details). **(B)** Ecosystem turnover of diazotroph N in mixed layer particles based on areal rates of N_2-fixation (see text). Markers in both panels are labeled with their station number and colored according to habitat type.

Perhaps most surprising is that despite the contrast in their magnitude and effective integration times, $\%PP_{diazo}$ and $\%N_{diazo}$ were linearly correlated in the SCS (Fig. 6.5A, r^2=0.33, p<0.031), meaning that the rates of net N_2-fixation must persist over timescales

relevant to bulk particles. Such a relationship was not found in the similarly heterogeneous waters (Weber et al. 2019) of the offshore Amazon River plume (based on reanalyzed data from Montoya et al. In press), and indicates a much tighter coupling in the SCS between daily new production via diazotrophy and the standing stock of biomass dependent on diazotroph N.

This significant relationship between $\%PP_{diazo}$ and $\%N_{diazo}$ begs the question: How long would it take for diazotrophs to generate the ^{15}N-depleted signal measured in suspended particles? Since I can calculate the areal concentration of diazotroph N in particles and have measured corresponding areal rates of nitrogen fixation, ecosystem turnover times of diazotroph N can be estimated for each station according to the following:

$$\text{Diazotroph N Turnover (d)} = \frac{\%N_{diazo} \times \text{Areal ML PON}}{\text{Areal ML } \rho_N} \qquad \text{(Eq. 6.1)}$$

where "Areal ML PON" is the areal concentration of PON (μmol N m^{-2}) within the mixed layer and "Areal ML ρ_N" is the areal rate of N_2-fixation (μmol N m^{-2} d^{-1}) within the mixed layer. Based on this calculation, it would take between two weeks and 2.5 months for nitrogen fixation to generate the isotopically light N signals in PON (Fig. 6.5B). The large variation in turnover times within the OSW habitat reflects the typical disconnect that occurs between $\%PP_{diazo}$ and $\%N_{diazo}$ estimates (due to their inherent difference in integration times), though in the case for the SCS, that disconnect was not severe enough to preclude an ecosystem-level relationship between the two measures. The particularly long turnover times at some OSW stations may be symptomatic of abating diazotroph communities, where activity is low relative to the integrated diazotroph impact on POM, and would be an interesting hypothesis to test further. Such an ecosystem-normalized approach to assessing diazotroph contribution measures could provide information on the trajectory of the diazotroph community (growing vs. abating) in a range of marine environments.

Overall, the turnover times calculated here are surprisingly long considering the variability in conditions in these dynamic waters, but it's worth noting that they represent upper-end estimates since they are based on net activity. Net rates of N_2-fixation into particles underestimate the overall impacts of diazotrophy because they exclude the unquantified release of dissolved N by diazotrophs. The magnitude of this underestimation is difficult to assess given the known variability in the relationship between net and gross N_2-fication rates among various environments and phytoplankton communities. For

example, dissolved N release from diazotrophs tends to be highest in *Trichodesmium*-dominated waters, but varies between 10 and 80% of the gross rate of N_2-fixation (Benavides et al. 2013; Berthelot et al. 2017; Bonnet et al. 2016a; Glibert and Bronk 1994; Konno et al. 2010). In contrast, UCYNs appear to more efficiently transfer diazotrophic N to the planktonic food web (Caffin et al. 2018), and are not strongly associated with dissolved N build-up in the natural ecosystem (Berthelot et al. 2017). The diazotroph communities encountered in the SCS during our cruise were quite diverse in this regard (Fig. 5.1), but it is likely that dissolved N release was highest in OSW waters, where *Trichodesmium* spp. abundances (Figs. 5.1G, 5.3), net N_2-fixation rates (Fig. 6.2), and $\%N_{diazo}$ (Fig. 6.4B) were also highest.

It is also possible that these rates are partially underestimated due to methodological error, but this is not likely to be a significant factor. Some studies have found that the "bubble" method (Montoya et al. 1996) of measuring N_2-fixation underestimates rates due to the slow or incomplete dissolution of the $^{15}N_2$ gas bubble meant to label the dissolved N_2 substrate pool (see Wannicke et al. 2018). The alternative "enriched water" method, in which filtered seawater is pre-enriched with $^{15}N_2$ and added directly to experimental bottles (Mohr et al. 2010), has been shown to produce areal rates 2 – 6 fold higher in certain cases (Grosskopf et al. 2012; Mohr et al. 2010). Other studies, however, have found no significant difference between the two methods (see meta-analysis by Wannicke et al. 2018 and references therein) and have emphasized the impracticality of using the "enriched water" method in chemically diverse waters, such as those sampled in this study. Additionally, the degassing step involved in preparing the pre-enriched water likely alters the water's chemistry, though some groups avoid this issue by employing the "bubble removal" method, where the $^{15}N_2$ gas bubble is removed after an initial incubation period and the enrichment of the N_2 pool is measured directly (see Jayakumar et al. 2017). Based on theoretical calculations by Wannicke et al. (2018), I estimate that with the classical method we used, the error associated with incomplete bubble equilibration during our 24 h incubations was less than 10% and is thus smaller than other likely sources of error.

In summary, the diazotroph contribution indices presented here captured coherent variation in diazotroph behavior among habitat types on both short and long timescales, and both indices support the conclusion that diazotrophy is a regionally important N source to the southwestern SCS. Nonetheless, consideration of gross N_2-fixation rates and quantification of processes like atmospheric N deposition would likely generate more robust diazotroph N turnover times, and bear further study in the SCS and in marine ecosystems

more generally. Our lack of information on these two factors in the SCS is unfortunately symptomatic of larger issues surrounding the accurate quantification of global N inputs from diazotrophy.

6.2.5. Cruise comparison of activity

The rates of N_2-fix and PP measured here represent only a snapshot in time, but activity measured during previous investigations of the area allow us to place our 2016 data into a broader context temporally. In Voss et al. (2006), the authors analyzed a region that was geographically very similar to that in this study (Fig. 6.6) during post-ENSO SWM conditions in 2003, as well as the IM and "normal" SWM seasons in 2004 (Table 6.1). Voss et al. (2006) grouped their stations into two categories, offshore and upwelling, and while the comparison of upwelling stations across all years/seasons is straightforward, their offshore conditions during the 2003/04 SWM season have no clear analogue in this study. During the 2003/04 study, the Mekong River plume extended much farther offshore than in 2016, influencing waters south of the upwelling area and in the same geographic location as

Table 6.1: Comparison of integrated rates to previous cruises.

	2003* Jul (SWM) Post-ENSO	2004* Apr (IM) --	2004* Jul (SWM) --	2016† Jun (eSWM) Post-ENSO
Nitrogen Fixation (μmol N m^{-2} d^{-1})				
MRW	--	--	--	80.2 ± 21.8
OnSW	--	--	--	136.2 ± 33.5
UpW	41.6 ± 37.0	16.3 ± 6.0	19.1 ± 9.9	81.2 ± 16.1
OSW/ Offshore	84.5 ± 76.3	14.1 ± 12.0	115.0 ± 112.8	234.2 ± 164.4
Primary Production (mmol C m^{-2} d^{-1})				
MRW	--	--	--	140.1 ± 98.3
OnSW	--	--	--	44.1 ± 29.1
UpW	18.5 ± 8.0	9.7 ± 5.6	117.5 ± 66.8	37.6 ± 22.5
OSW/ Offshore	19.7 ± 17.0	6.4 ± 3.4	36.8 ± 35.8	22.9 ± 11.7
% PP_{diazo}				
MRW	--	--	--	0.5 ± 0.3
OnSW	--	--	--	2.5 ± 1.3
UpW	1.3 ± 0.7	0.9 ± 0.8	1.7 ± 1.7	2.0 ± 1.6
OSW/ Offshore	4.1 ± 3.1	0.8 ± 0.8	1.5 ± 1.5	7.2 ± 3.4

* Voss et al. 2006 (integrated to 40m)
† This study (integrated to 20m in MRW, 40m for the rest)
IM = intermonsoon, (e)SWM = (early) southwest monsoon

the oligotrophic waters sampled during the 2004 IM and 2016 eSWM cruises. Based on SSS alone, the "offshore" conditions of Voss et al. (2006) in 2003/04 were more similar to those sampled in the 2016 OnSW habitat.

It should also be noted that the rate experiments performed by Voss et al. 2006 used much shorter incubation times, generally 6 h, which were then converted to daily rates by assuming 12 h of N_2-fixation and PP activity in a day. While this short incubation time may decrease detrimental bottle-effects on the active community, it does make the experiments more sensitive to underestimation errors associated with the "bubble method," and could potentially lead to a 20% labeling underestimate (Wannicke et al. 2018). Additionally, assuming 12 h of N_2-fixation may underestimate daily activity, since the natural population is still partially active at night (Grosse et al. 2010). This could mean that methodical

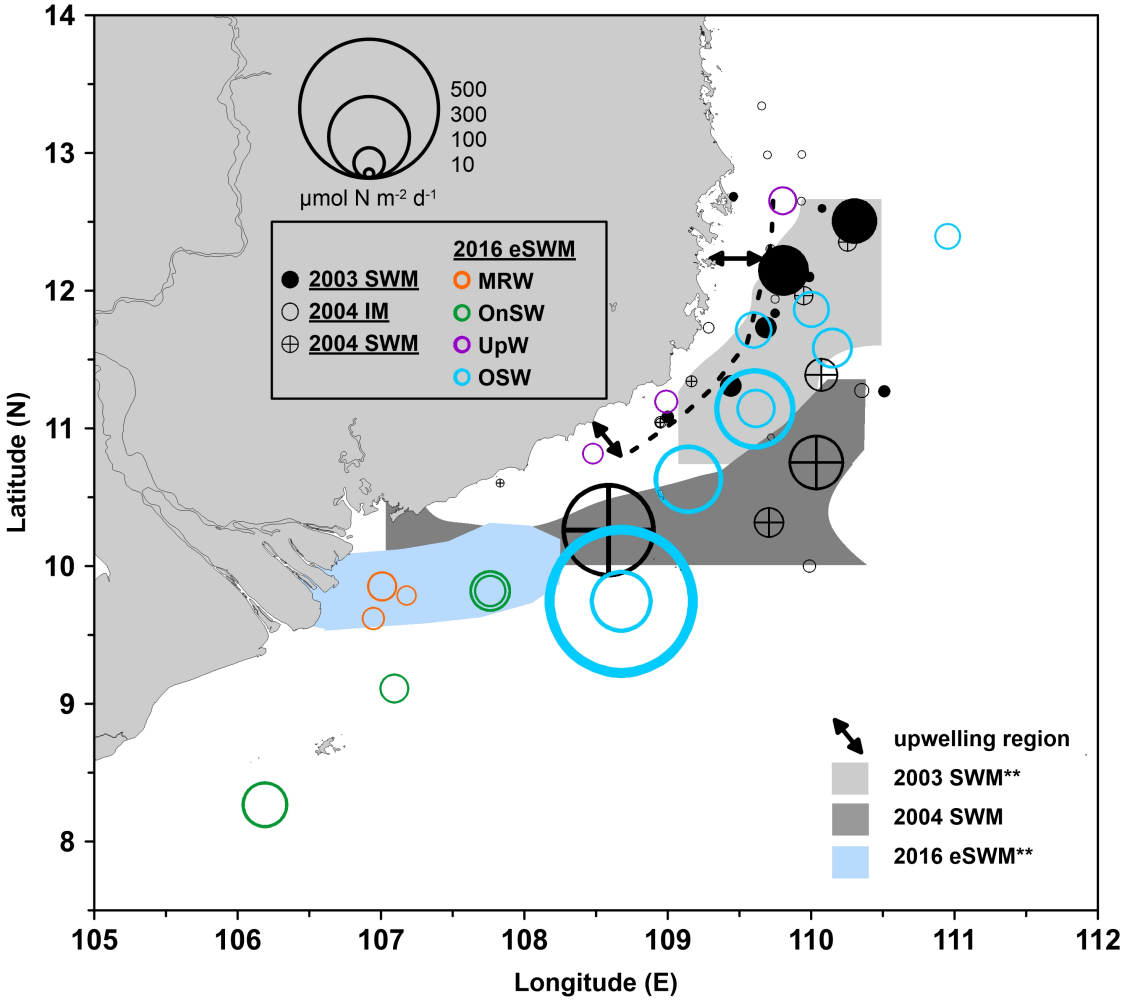

Figure 6.6: Comparison of river plume extension (shaded regions) and areal rates of N_2-fixation (bubbles) between field campaigns in 2003-2004 and 2016. All rates have been integrated to 40 m where possible. Rate magnitude scales with bubble size; bubbles are colored according to the cruise and habitat (see legends). Asterisks mark post-ENSO years.

differences between the 2003/04 and 2016 campaigns contributed to the observed variation in activity.

With these distinctions and caveats in mind, integrating the two datasets over the same water column depth (where possible) reveals some interesting similarities and differences between the years and seasons. As expected, 2016 was more similar to the 2003/04 SWM conditions, with much higher rates of both N_2-fixation and PP in all 2016 habitats than in the 2004 IM season (Table 6.1). Despite the reduced plume influence in 2016, we measured higher rates of N_2-fixation in both the upwelling and OSW/offshore waters (Fig. 6.6, Table 6.1), which further indicates that the plume may not be necessary to support elevated rates in this region. N_2-fixation rates in offshore waters in 2003/04 are more comparable to what was measured in the MRW and OnSW habitats in 2016. The 2004 SWM upwelling area stands out as being particularly productive, which was previously ascribed to higher upwelling intensities in 2004 compared to 2003 (Dippner et al. 2007; Voss et al. 2006). Despite the clear upwelling signal in 2016, PP rates in 2004 surpassed those measured in all habitats in 2016 except for MRW, and likely reflect the ENSO-related weakening of upwelling in 2016. The importance of diazotrophy in the comparatively unproductive OSW region in 2016 is further underlined when examining $\%PP_{diazo}$ values across years and seasons, which indicate that diazotrophs supported a much greater share of community PP in offshore waters in 2016.

Taken together, our data indicate that even over such varied conditions, the Mekong River plume is an important habitat for diazotrophs. In the context of my study, results from 2003/04 clearly support the conclusion of Voss et al. (2006) that the offshore river plume fostered higher rates of diazotrophy relative to the upwelling region, but the findings from 2016 bring into question how elevated the 2003/04 river-associated activities were relative to those in oligotrophic waters outside of the plume and upwelling influence. The differences in rates of N_2-fixation (and abundances of diazotrophs) measured between cruise legs in 2016 reveal the variability in diazotrophy in oligotrophic waters, but importantly also highlight the potential of these waters to support appreciable diazotrophic activity over the course of (at a minimum) days, based on the timescale of particle turnover. A broader sampling region, as was originally planned for this project, into oligotrophic waters outside of the Vietnamese territorial waters in all years would have provided a more comprehensive picture of the southwestern SCS.

One question that remains, however, is why the oligotrophic OSW waters in our study region supported appreciable abundances of active diazotrophs, whereas waters of the

central SCS seemingly do not. Wu et al. (2003) had previously hypothesized that N_2-fixation activity in the central SCS is ultimately limited by a deficit in organic ligands, which enable the dissolution of iron for biological consumption. Though this theory is yet to be tested directly, it is supported by the surprisingly low concentrations of dissolved iron in the central SCS (Wen et al. 2006) despite significant aeolian iron inputs (Duce et al. 1991; Mahowald et al. 2005) and measurable inorganic phosphate (which would have also been depleted if the low dissolved iron concentrations were due to consumption) (Wu et al. 2003). More importantly, this points to a possible mechanism behind the stimulation of diazotrophy in oligotrophic shelf waters, through the delivery of ligands and/or dissolved iron. Since both the Mekong River and upwelling very minimally affect the OSW habitat, the most likely source of ligands and dissolved iron would be from the Gulf of Thailand waters, which we know influence the region based on the water mass analysis (Fig. 3.1C). Perhaps high exposure to land and allochthonous inputs along with the current flow pattern in the Gulf of Thailand increase the dissolved iron concentrations in these waters. Though this remains speculation, this mechanism in stimulating diazotrophy along the Vietnamese shelf waters should be explored further.

7. Diazotroph inputs to the planktonic food web

This section includes collaborative work carried out with Dr. Natalie Loick-Wilde and her Master's student Melvin Bach. All of the zooplankton samples and POM amino acid samples used here were both collected and analyzed by Bach and Dr. Loick-Wilde. Bach laid the groundwork for this chapter in his thesis, "Nitrogen sources and trophic dynamics in zooplankton of the South China Sea." With the help of Dr. Loick-Wilde, I have used a portion of his dataset and have expanded his initial analysis, placing the work into broader context with the habitat type analysis and other datasets presented in here in this thesis. Dr. Loick-Wilde and I have also identified environmental drivers of zooplankton nitrogen sources and trophic position, further developing the story. Together, this work provides a further test of the habitat type approach and caps my investigation into the ecosystem impacts of diazotrophy in the SCS in June 2016.

7.1. Results

7.1.1. Relationship of bulk $\delta^{15}N$ values of plankton compartments and environmental variables

We extended the habitat type approach, which resolved the factors affecting the distribution of phytoplankton communities (Weber et al. 2019), to biogeochemical processes by identifying habitat-specific nitrogen sources for particles and mesozooplankton. Among all environmental variables considered here, MLD had the most consistent and significant linear relationship with the depth-integrated bulk $\delta^{15}N$ values of all five planktonic compartments (Fig. 7.1). With the exception of samples from Stn. 6, bulk $\delta^{15}N$ values in all compartments decreased with increasing MLD. The ranges of bulk $\delta^{15}N$ values were similar among all size fractions and varied between 4.3 – 7.5‰ (Fig. 7.1). We found no clear trend with size or time of sampling (day- or nighttime). Samples from Stn. 6 had consistently high bulk $\delta^{15}N$ values in all five planktonic compartments including POM_{tow}, which is in stark contrast to the otherwise comparatively low bulk $\delta^{15}N$ values at the other OSW habitat stations (Fig. 7.1).

Interestingly, a consistent and large offset of several ‰ occurred between the $\delta^{15}N$ values in POM_{tow} and the four mesozooplankton size fractions, with POM_{tow} having much lower bulk $\delta^{15}N$ values than the mesozooplankton (Fig. 7.1). Applying a simple isotope mixing model, this offset in bulk $\delta^{15}N$ values between POM_{tow} and mesozooplankton identified clear habitat type specific differences in the contribution of diazotroph N to the

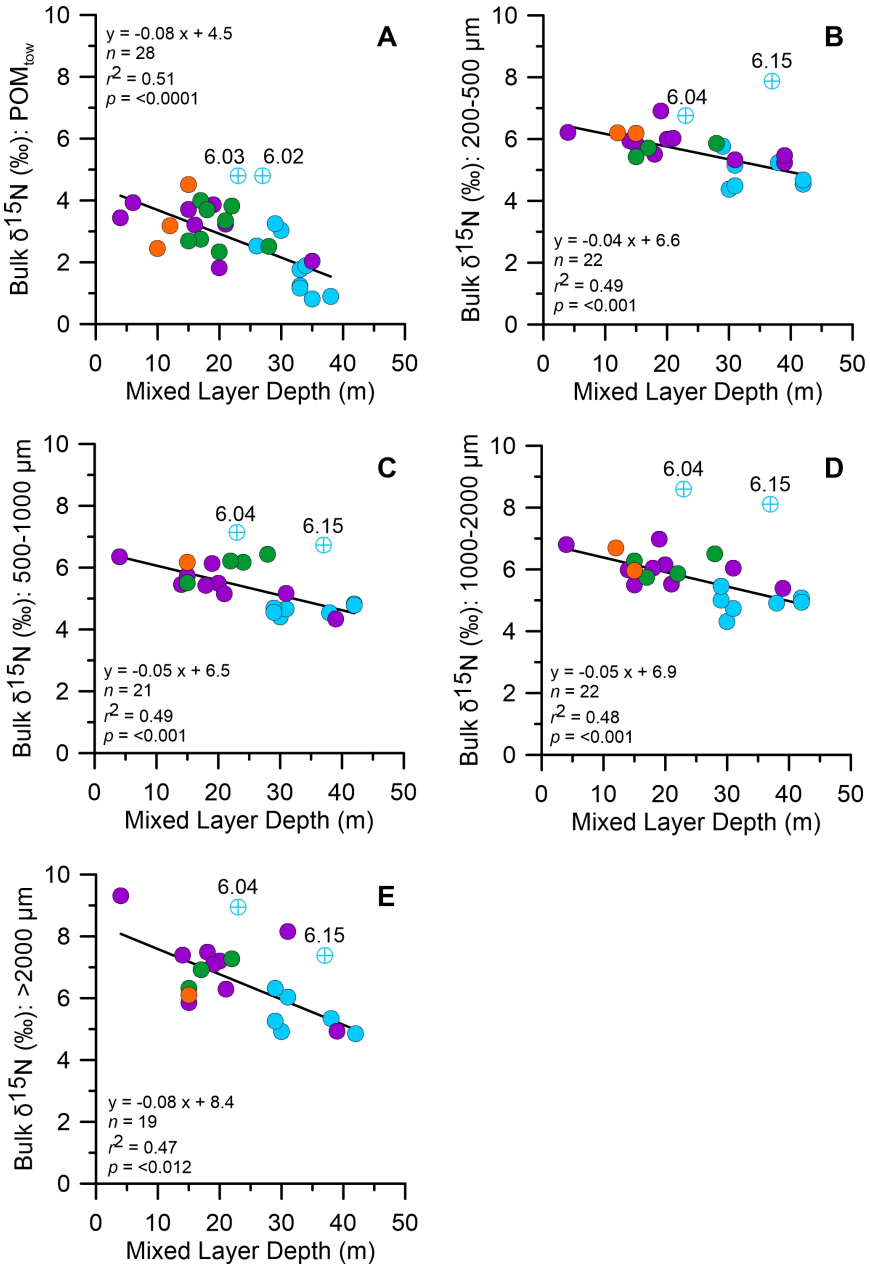

Figure 7.1: $\delta^{15}N$ patterns of depth-integrated and concentration-weighted POM_{tow} samples and of four net-plankton size fractions versus mixed layer depth (m): **(A)** POM_{tow}, **(B)** 250-500 µm, **(C)** 500-1000 µm, **(D)** 1000-2000 µm, and **(E)** >2000 µm. Colors correspond to the habitat types. Included are the regression lines and regression details. Regressions exclude all samples from Stn. 6, which are marked by the circled-cross and labeled with event numbers. Samples with high C:N were excluded completely.

different plankton compartments (Fig. 7.2). POM_{tow} included up to 60% of N from N_2 fixation at OSW habitat type stations. In contrast, mesozooplankton received at most 20% of their nitrogen from N_2-fixation in OSW waters. But while the mixing model identified diazotroph N inputs in suspended particles at MRW, OnSW, and UpW habitat type stations, diazotroph N was hardly incorporated into mesozooplankton outside the OSW waters.

Finally, the anomalous Stn. 6 was the only OSW type station without clear diazotroph N inputs into either particles or mesozooplankton (data not shown).

7.1.2. Nitrogen source and food web structure proxies in mesozooplankton

A subset of the POM and zooplankton were additionally analyzed with CSI-AA, which included samples from most habitat types (except from UpW waters for POM). Of the zooplankton samples, only the 1000-2000 µm mesozooplankton size fraction was analysed (Fig. 7.3). From these analyses, the N source proxy δ^{15}N-Phe and the food web structure proxy TP were determined for both pools.

The δ^{15}N-Phe values of POM and zooplankton samples confirmed the pattern from the bulk δ^{15}N values and revealed large differences among stations in both compartments (Fig. 7.3). The δ^{15}N-Phe values in POM from both surface and deep Chl. *a* maxima were clearly lower than the values in zooplankton (Fig. 7.3) and ranged from -2.0‰ to 1.6‰ with a median value of 0.6‰, which is in between the δ^{15}N endmember value for Phe in N_2-fixing *Trichodesmium* (-3.6 ‰, McClelland et al. 2003) and the δ^{15}N values for deep water nitrate (5.0 ‰, Liu and Kaplan 1989). The δ^{15}N Phe values in the zooplankton size fraction 1000-2000 µm covered a much wider range from 0.8 – 7.1‰ with a median value of 4.5‰ (Fig. 7.3). For POM, no clear habitat type specific expression of δ^{15}N-Phe values was found, although the minimum value was measured in surface waters at an OSW station

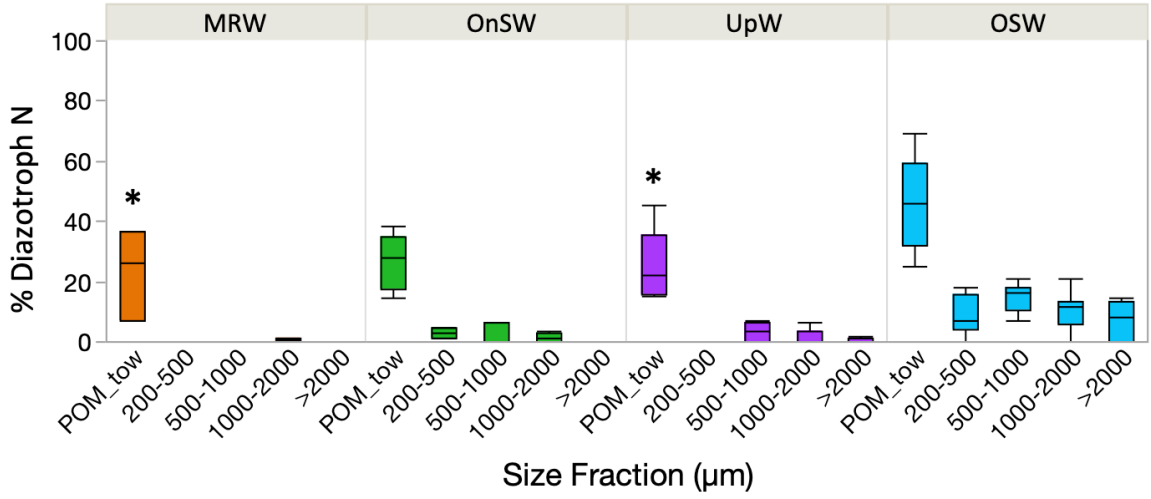

Figure 7.2: Diazotroph N (%) contribution to POM and zooplankton samples according to a simple isotope mixing model based on δ^{15}N patterns of depth-integrated and concentration-weighted POM samples and of four net-plankton size fractions, grouped by habitat type. Colors correspond to the different habitat types. Samples with anomalously high δ^{15}N values (identified in Fig. 7.1) were excluded. Asterisks indicate samples that likely have falsely high $\%N_{diazo}$ contributions due to nitrate fractionation.

(Stn. 17). In contrast, the mesozooplankton δ^{15}N-Phe values showed a stronger relationship with habitat types, with values clearly below 5‰ mainly at OSW stations and values close to or >5‰ mainly at MRW, OnSW, and UpW stations (Fig. 7.3).

The estimated trophic position (TP) of POM samples using the $TP_{Glu/Phe}$ approach ranged from 1.1 to 1.6 with an average of 1.4 ± 0.2 (Table 7.1, Fig. 7.3), thus mostly reflecting material of autotrophic and mixotrophic origin. The TP of zooplankton in the 1000-2000 µm size fraction ranged from 1.7 to 2.5 with an average of 2.1 ± 0.3 (Table 7.1, Fig. 7.3), reflecting mainly herbivorous and some omnivorous feeding behaviors (OSW Stns. 1, 3, 17, and 18). Note that the waters at Stn. 3 transitioned from OSW to UpW during the time that we occupied the station (Chapter 4), but the zooplankton samples (event 3.03) were collected during the OSW phase. Interestingly, no clear signal of predominantly carnivorous feeding behavior (TP ≥ 3.0) was found in any of the zooplankton samples.

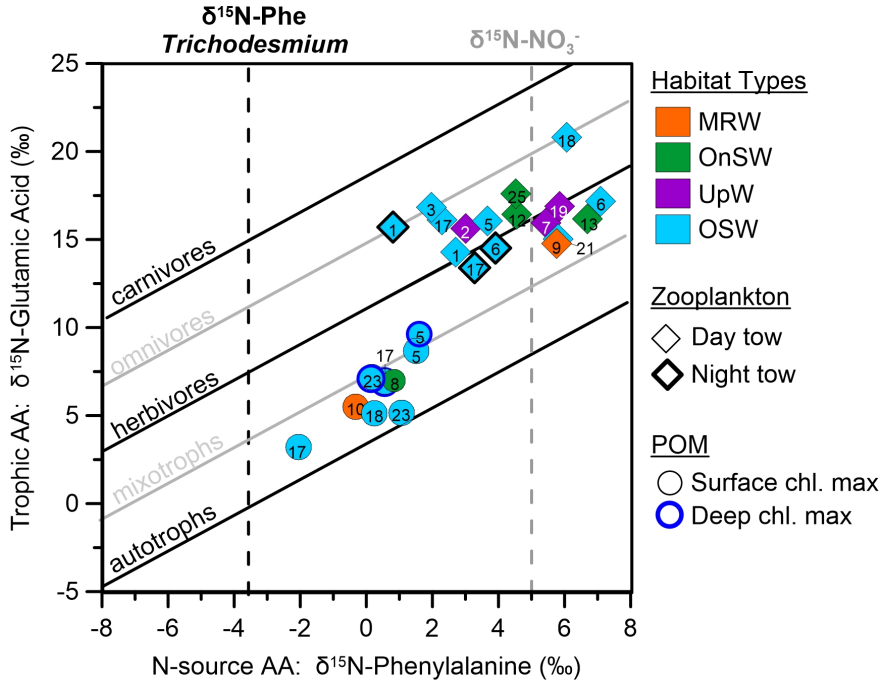

Figure 7.3: δ^{15}N-Glu (trophic AA) versus δ^{15}N-Phe (N-source AA) of discrete POM samples (circles) from surface waters and from the deep Chl. *a* maximum (if not at the surface) and of the 1000-2000 µm zooplankton size fraction from day- and night-time tows (diamonds). Isolines indicate the trophic position (TP) and marker colors correspond to the different habitat types. The vertical black dashed line indicates the δ^{15}N-Phe values of N_2-fixing *Trichodesmium* (McClelland et al. 2003); the vertical grey dashed line indicates the δ^{15}N value for deep water nitrate (Liu and Kaplan, 1989).

Table 7.1: Habitat characteristics, nutrient, and Chl. *a* fluorescence found in the surface mixed layer and biogeochemical variables of the mesozooplankton size fraction 1000-2000 µm from the upper 100 m (or to the bottom if shallower). Chl. *a* from the water column sensor is in relative units. Overlined variables have been integrated through the mixed layer. All variables were included in the principal component analysis.

											$\delta^{15}N$			
Habitat	Event	MLD	$\overline{Temp}$	$\overline{Sal}$	NAI	$\overline{PO_4^{3-}}$	$\overline{SiO_2}$	$\overline{DIN}$	ChlMD	$\overline{FL}$	$bulk_{zp}$	Phe_{zp}	Glu_{zp}	TP_{zp}
MRW	9.01	15	30.76	32.46	0.5	0.17	9.68	0.16	6	0.18	6.0	5.8	14.8	1.7
OnSW	12.02	22	30.33	33.33	-22.0	0.11	5.23	0.00	21	0.04	5.9	4.5	16.4	2.1
OnSW	13.02	28	29.85	33.38	-27.9	0.14	5.35	0.38	15	0.03	6.5	6.7	16.2	1.8
OnSW	25.03	15	30.76	33.43	-40.0	0.08	2.94	0.00	34	0.01	6.3	4.5	17.6	2.3
UpW	2.02	14	29.00	33.90	-44.9	0.07	2.70	0.27	46	0.00	6.0	3.0	15.6	2.2
UpW	7.03	4	25.29	34.23	-29.2	0.10	4.08	0.03	13	0.02	6.8	5.4	15.9	1.9
UpW	19.09	19	25.64	34.13	-27.8	0.13	4.38	0.33	22	0.06	7.0	5.8	16.9	2.0
OSW	3.01	30	26.72	34.04	-54.8	0.05	2.53	0.04	55	0.01	6.0	2.0	16.8	2.5
OSW	5.02	21	29.37	33.69	-67.3	0.08	4.40	0.21	75	0.01	6.0	3.7	16.1	2.2
OSW	17.03	30	30.21	33.56	-50.8	0.07	3.61	0.20	64	0.01	4.3	2.3	16.1	2.4
OSW	17.13	26	30.11	33.55	-85.3	0.09	4.37	0.19	56	0.01	4.7	3.3	13.5	1.9
OSW	18.03	38	29.13	33.78	-50.5	0.08	3.48	0.19	47	0.03	4.9	6.1	20.8	2.5
OSW	21.03	33	28.06	34.00	-49.5	0.11	3.73	0.31	45	0.04	5.0	5.8	15.0	1.8

Since detritivory may influence TP estimations, a proxy for the impact of this process, ΣV, was also investigated. When calculated for mesozooplankton samples, ΣV approximates the degree to which δ^{15}N-AA values in the food source were modified by heterotrophic microbial reprocessing (McCarthy et al. 2007). The highly significant relationship between ΣV and TP values for the majority of mesozooplankton samples implied that microbial processes were not a significant source of variation in our data set (Ohkouchi et al. 2017). The sample from Stn. 18, however, was a clear exception, where the anomalously high ΣV value of 2.8 relative to the TP of 2.5 strongly indicated the incorporation of a microbially altered diet (Fig. S7.2).

7.1.3. Statistical analyses to identify environmental controls on food web structure

A PCA and post hoc linear correlations were used to visualize and identify the environmental controls on the planktonic food web structure according to N-source proxies and TP estimates from the mesozooplankton size fraction 1000-2000 μm across different habitats. All 13 variables from the 13 stations included in the PCA (Table 7.1) were described by the first two PCs, which explained 63.2% of the total variation (Fig. 7.4). PC 1 (43.7% of variability) broadly represented the chemical/biological context, and environmental variables related to nutrient availability were particularly important drivers of this axis (primarily phosphate concentrations, with less contributions from silicate concentrations and NAI values). Additionally, both the N-source and TP proxy from the 1000-2000 μm mesozooplankton size fraction (δ^{15}N-Phe$_{zp}$ and TP$_{zp}$) were major contributors to PC1 but correlated inversely with one another. PC 2 (19.5% of variability) was driven predominantly by physical environmental variables, primarily temperature and to a lesser degree by MLD and salinity (Fig. 7.4B).

Among the leading abiotic variables, δ^{15}N-Phe$_{zp}$ had significant positive relationships with $\overline{PO_4^{3-}}$ (r^2=0.57, p<0.5) and NAI (r^2=0.30, p<0.5) (Fig. S7.1). In contrast, TP$_{zp}$ was significantly inversely correlated with $\overline{PO_4^{3-}}$ (r^2=0.63, p<0.5) and $\overline{SiO_2}$ (r^2=0.40, p<0.5). Both biogeochemical proxies (δ^{15}N-Phe$_{zp}$ and TP$_{zp}$) had significant relationships with ChlMD, where δ^{15}N-Phe$_{zp}$ varied inversely (r^2=0.48, p<0.5) and TP directly with ChlMD (r^2=0.31, p<0.5).

Even though it was necessary to reduce the dataset for the PCA and correlation analyses, the tight and significant relationships between MLD and the bulk δ^{15}N values of all five plankton compartments were preserved (Fig. 7.1). Unlike the amino acid N-source proxy δ^{15}N-Phe, bulk δ^{15}N values had no direct relationship with the nutrient and

chlorophyll based variables comprising PC1. The combined impact of both the N-source and trophic effects on bulk mesozooplankton $\delta^{15}N$ values was reflected in the PCA by the placement of the $\delta^{15}N$-$bulk_{zp}$ variable between the $\delta^{15}N$-Phe_{zp} and $\delta^{15}N$-Glu_{zp} (Fig. 7.4).

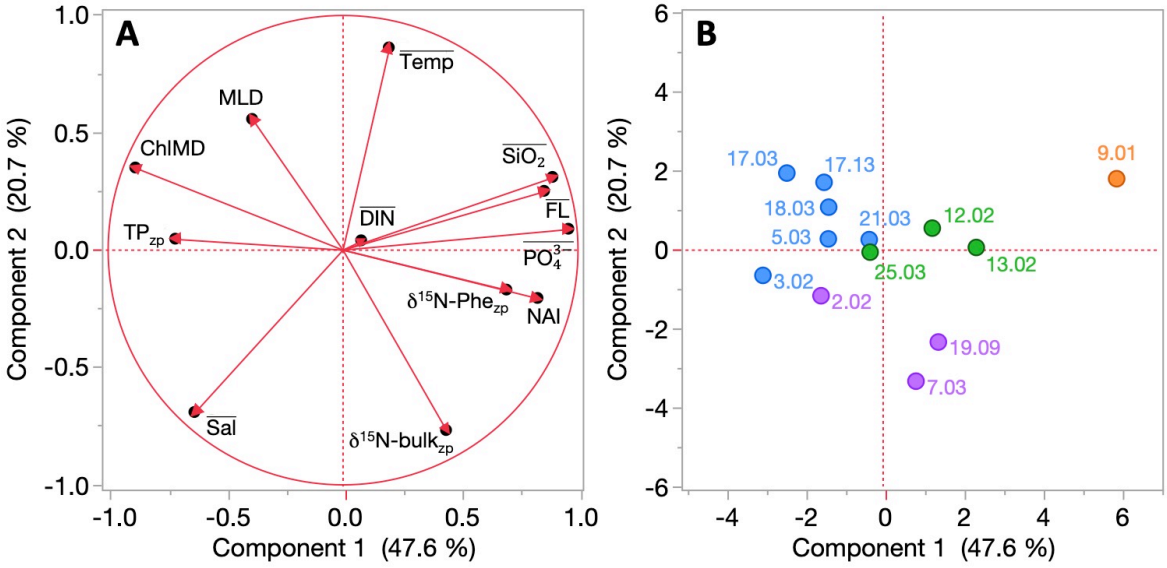

Figure 7.4: **(A-B)** Environmental factors regulating the planktonic food web structure and its nitrogen supply in the Mekong River plume and SCS according to a two-dimensional PCA of 13 environmental variables (Table S7.1). Overlined variables were integrated through the mixed layer, and variables labeled with the subscript "zp" are derived from the 1000-2000 µm mesozooplankton size fraction samples. The score plot **(B)** is a scatter plot of each cast's score according to the first two principal components, where casts are labeled by their station.event numbers and colors correspond to habitat types. Viewed another way, panel **B** shows how the variables measures collected at each station drove the variable relationships displayed in panel **A**. % variation explained by PC1 and PC2 is listed on their respective axes. The relationships displayed in the PCA are also shown in tabular form with a multivariate analysis in the appendix (Fig. S7.1).

7.2. Discussion

With the development of the CSI-AA technique and its application to marine systems, much has been learned about the structure and function of planktonic food webs, but relatively little is known about the environmental controls that govern the trophic position of mesozooplankton. Much of the previous work on this topic has been carried out in relatively stable environments, where the role of stratification and diazotrophy have been identified as key environmental and biological controls on the primary N source to the pelagic food web (Loick-Wilde et al. 2019). These factors consequently reshape energy flow at the base of the food web, causing a trophic shift in the mesozooplankton (Loick-Wilde et al. 2019). Here, we have investigated how these (and other) factors can be used to

characterize other, more variable systems, using the physicochemically diverse waters of the southwestern SCS as a test system.

7.2.1. Nitrogen supply in the habitat types

One benefit of the habitat type approach is that it integrates both MLD and nitrate availability in surface waters (NAI) in defining phytoplankton habitats. Since DIN is often the limiting nutrient for phytoplankton in marine environments (Tyrell 1999), understanding the sources and distribution of DIN in the study region provides a foundation for interpreting nitrogen dynamics in the entire planktonic food web. Based on the NAI values derived from vertical profiles of nitrate concentration (Table 4.1), nitrate availability was highest at MRW and some UpW stations, reaching measurable concentrations in surface waters. Again, this indicates that both the Mekong River and coastal upwelling were important sources of nitrate for local plankton communities at the time of sampling. At the same time, MLD affected the supply of deep nitrate to surface waters, which can in turn greatly influence the composition of surface phytoplankton communities and may establish conditions favorable for nitrogen fixation (Hutchins and Fu 2017) when nitrogen is strongly limiting. For example, with the habitat analysis in Chapter 3, we found that the phytoplankton communities at MRW, OnSW, and UpW habitats (where NAI was relatively high and MLD shallow) were characterized by nitrate-utilizing diatoms possessing a range of salinity tolerances (Fig. 4.3, 4.4). In contrast, OSW stations, which had the lowest nitrate availability and deepest MLD, were occupied by phytoplankton that often included "blue water" species like *Trichodesmium* spp. and prochlorophytes (Fig. 4.3, 4.4). Taken together, a transition from MRW and UpW habitats to the OSW habitat reflects a shift from regions dominated by nitrate-utilization to one in which N_2-fixation was a common metabolic strategy (Fig. 6.2) and an important source of "new N" (Fig. 6.3).

Using the $\delta^{15}N$ signatures of bulk POM_{tow} and zooplankton biomass, we can track the input into the planktonic food web of major N sources that are isotopically unique – like riverine or upwelled nitrate ($\delta^{15}N$ of ~5‰) in contrast to diazotroph N ($\delta^{15}N$ of -2‰) – into the planktonic food web (Montoya et al. 2002). Accordingly, the bulk $\delta^{15}N$ values of the five plankton compartments reflected the general trends described above, with the lowest $\delta^{15}N$ values at OSW stations where diazotrophs were common. The majority of these plankton bulk $\delta^{15}N$ values also correlated negatively and significantly with MLD (Fig. 7.1), which gives strong evidence for the critical role of the MLD in governing the N sources both available to and actually incorporated into the planktonic food web of the SCS.

Isotope mixing of nitrate and diazotroph nitrogen can account for the major trends in bulk $\delta^{15}N$ values of plankton, but transient processes like isotopic fractionation associated with the uptake of nitrate by phytoplankton must also be considered. Isotope theory (Montoya 2007) predicts that when nitrate is injected into a system, for example by a river plume or upwelling, the isotopic composition of the nitrate pool will be modified through time as it is consumed and horizontally advected. Isotopic discrimination against ^{15}N during consumption (ε = 5-10 ‰; Montoya and McCarthy 1995; Waser et al. 1998) transfers N with a low $\delta^{15}N$ to phytoplankton biomass while simultaneously enriching the residual nitrate pool in ^{15}N. If much of this isotopically light phytoplankton N is subsequently removed from the system through sedimentation or grazing, assimilation of the residual, isotopically heavy nitrate will increase the $\delta^{15}N$ of the particulate pool. Both of these ^{15}N-depletion and ^{15}N-enrichment perturbations in the $\delta^{15}N$ of POM will lead to an apparent mismatch between the $\delta^{15}N$ of POM and zooplankton over the time course of nitrate consumption, as zooplankton act as a low-pass filter for changes in the isotopic composition of particles (Montoya 2007). If either perturbation signal in phytoplankton biomass persists long enough relative to the turnover times of zooplankton biomass, these nitrate fractionation signals will propagate up the food web into zooplankton. The extent of this signal propagation in turn provides a qualitative measure of the history of the fractionation process in the nitrate pool, which reflects the time course environmental conditions experienced by the plankton community.

Note that these isotopic variations occurring in horizontal space through time are analogous to those that occur vertically in the water column. In a steady-state system, the upward injection of subthermocline nitrate supports phytoplankton uptake that progressively increases the $\delta^{15}N$ of the residual nitrate toward the top of the nitracline (Altabet 1996; Needoba et al. 2003), resulting in a strong gradient in the $\delta^{15}N$ of nitrate with depth. Loick et al. (2007) has previously shown that this nitrate fractionation mechanism takes place in the water column off Vietnam, producing an increase in nitrate $\delta^{15}N$ values from 3.5‰ below 100 m to > 8.0‰ above 100 m and up to a depth of approximately 50 m. In consequence, phytoplankton can become enriched in ^{15}N due to the constant upward advection of subthermocline nitrate together with the constant isotope fractionation associated with its uptake.

Applying these concepts to our dataset, we might expect to see both low and high plankton $\delta^{15}N$ measurements reflecting different stages of nitrate uptake at sites associated with major nitrate inputs. Indeed, we found very low $\delta^{15}N$ values in POM_{tow} at sites of high

nitrate availability in surface waters of the MRW and young UpW type stations, but not in zooplankton (Fig. 7.1). Since bulk $\delta^{15}N$ values below the nitrate threshold of ~5‰ may be indicative of either N from diazotrophy or from fractionation in the early stages of nitrate consumption, we cannot fully resolve the origin of these low $\delta^{15}N$-POM_{tow} signatures. That said, the contextual clues of high NAI and low $\delta^{15}N$ in POM_{tow} without correspondingly low $\delta^{15}N$ in zooplankton strongly point to a transient process related to nitrate uptake as the primary cause.

Conversely, when the plankton bulk $\delta^{15}N$ values are plotted against MLD, samples with anomalously high $\delta^{15}N$ values become apparent (Fig. 7.1). At OSW Stn. 6, located on the fringes of the upwelling region, all five plankton compartments (from integrated POM_{tow} up though all four zooplankton compartments) were significantly enriched in ^{15}N. Evidence of sustained nitrate fractionation at an oligotrophic OSW habitat type station may seem counterintuitive, but the compilation of satellite SST images in Fig. 3.3 indicates that the waters at Stn. 6 (sampled on June 8) were likely advected from the upwelling region and had only recently shifted from the UpW to the OSW habitat type. In this situation, we would expect that shifts in the plankton community species and isotopic composition would lag behind changes in local chemical and physical properties such that the sampled plankton community retains the imprint of previous conditions. In Chapter 4, we found evidence of such a delay in phytoplankton community response to environmental change at a handful of stations, including Stn. 6. In addition, closer examination of NAI and ChlMD at Stn. 6 reveals a rare discordance between these two variables (not shown), where the relatively shallow position of ChlMD relative to NAI and the broad shape of the fluorescence profiles (not shown) point to a phytoplankton community in transition. Taken together, the evidence at Stn. 6 points to a sustained input of isotopically enriched nitrate via upwelling into the local plankton food web followed by recent advection offshore. Viewed more generally, combining environmental and biological measurements that integrate over multiple time and spatial scales illuminates the ecosystem's complex history.

Disregarding samples that were likely influenced by these nitrate fractionation processes (see Fig. 7.1), we can now more reliably quantify the transfer of fixed nitrogen from diazotrophs into N pools of mesozooplankton using two-source end member mixing stable nitrogen isotope approaches (Montoya et al. 2002). This has only occasionally been identified and quantified for some marine ecosystems like the tropical North Atlantic (Hauss et al. 2013; Landrum et al. 2011; Wannicke et al. 2010), the Amazon River plume (Loick-Wilde et al. 2016), the eastern Indian Ocean (Raes et al. 2014), the southern South

China Sea (Loick et al. 2007), or Baltic Sea (Loick-Wilde et al. 2019). So far the highest measured transfer of diazotroph nitrogen into the upper planktonic food web was 67% in zooplankton from the tropical North Atlantic (Montoya et al. 2002). By comparison, the previously measured maximum of 13% for zooplankton in the South China Sea during SWM seasons was rather low (Loick et al. 2007), and the maximum value of 20% in this study further confirmed this finding (Fig. 7.2). The discrepancy in % diazotroph N inputs between bulk POM_{tow} and zooplankton in this study (Fig. 7.2) points to selective feeding in all habitats, such that diazotroph input is near 0% in coastal habitats despite evidence that diazotrophs were both present (Fig. 5.1) and active (Fig. 6.2). We also note that our approach may overestimate diazotroph N input into POM in areas where DIN was present and actively being drawn down (e.g. MRW stations and UpW Stn. 7), as discussed earlier. The minimal or low contribution of diazotroph N to mesozooplankton biomass despite moderate to high inputs into POM_{tow} may be related to the preferential grazing of the mesozooplankton as discussed below.

7.2.2. Zooplankton diet and environmental regulation of the planktonic food web structure

As a complement to our bulk $\delta^{15}N$ measurements and to provide a more nuanced view of diet and trophic position within the plankton food web, we measured the compound-specific $\delta^{15}N$ signatures of AA in a subset of POM and mesozooplankton (1000-2000 μm) samples. In comparing AA $\delta^{15}N$ values across plankton compartments, we found that the $\delta^{15}N$-Phe values of our samples confirmed the offset in the N source of POM_{tow} versus mesozooplankton. These results support previous findings from Loick et al. (2007), who used bulk $\delta^{13}C$ signatures to show that the POM collected on filters was largely unrepresentative of the mesozooplankton food source in this ecosystem. Importantly, Loick et al. (2007) also found that this was true independently of whether POM was sampled from the surface or deep Chl. *a* max, as we have found here. The lack of connectivity between these two pools may be due in part to the large diversity of phytoplankton cell sizes in the SCS. Zooplankton are known to selectively graze on phytoplankton according to cell size (Hansen et al. 1997), whereas the filtering process for sampling POM will sample all particles larger than the nominal filter pore size. As a result, the food source of a given size fraction of zooplankton may represent only a portion of the bulk POM sampled. This in turn may explain why in regions such as the nutrient-limited subtropical North Atlantic, where phytoplankton are likely smaller and more homogenous in size compared to

phytoplankton in near coastal habitats (Rodríguez et al. 2001), filtered POM is much more representative of the mesozooplankton diet (Landrum et al. 2011).

Only at the OSW habitat type stations where *Trichodesmium* and other diazotrophs shaped the phytoplankton community (Fig. 5.1) did diazotroph N make a significant contribution (up to 20%) to the N biomass of mesozooplankton (Fig. 7.2). This change in N source from nitrate-dependent towards higher diazotroph N input was also associated with a lengthening of the food chain, given the inverse correlation between δ^{15}N-Phe and TP in the 1000-2000 µm size fraction (Fig. 7.4). This phenomenon is likely reflects a combination of two factors: 1) the reduction in (non-diazotroph) phytoplankton cell sizes as conditions become more oligotrophic, allowing for smaller consumers and more links in the food chain (Ryther 1969); and 2) an enhancement of N delivery to consumers via the microbial food web where *Trichodesmium* spp. abundances are more prominent (Mulholland 2007). Most studies suggest that filamentous, N_2-fixing cyanobacteria like *Trichodesmium* spp. are not directly grazed by zooplankton (Motwani et al. 2018; Mulholland 2007; Wannicke et al. 2013) and that diazotroph N exuded or lysed from these communities, in the form of NH_4^+ or DON, enters zooplankton through the microbial food web (Capone et al. 1997). According to trophic analyses of microbial food webs by Steffan et al. (2015), zooplankton should occupy carnivorous TPs when grazing on first-level consumers of microbial food webs (but see also: Décima et al. 2017; Gutiérrez-Rodríguez et al. 2014). This indeed was the case during a highly degraded late stage of a filamentous cyanobacteria bloom in the Baltic Sea, when mesozooplankton clearly occupied carnivorous TPs (Loick-Wilde et al. 2019; Loick‐Wilde et al. 2018). In contrast, many field studies from tropical oceans have demonstrated the dominance of herbivorous and omnivorous zooplankton with a generally narrow range of TPs that rarely reached the carnivorous threshold of TP $\geq$ 3 despite the presence of *Trichodesmium* spp. (Hannides et al. 2009; McClelland et al. 2003; Mompeán et al. 2016), a potentially important source of diazotroph N via the microbial food web.

Our TP estimates generally agree with the previously-noted narrow ranges for tropical zooplankton and indicate that omnivorous feeding behavior was found only at Stns. 1, 3, 17, and 18, which belonged to the OSW habitat characterized by diazotrophs including *Trichodesmium* (Fig. 7.3, Fig. 4.4B). At Stn. 18, detritivory probably played an important role according to the ΣV proxy, but at these other three OSW stations, an increasing reliance on a carnivorous diet supported indirectly by diazotrophy may have increased the mean TPs. At the remaining OSW stations, however, mesozooplankton occupied an

average TP closer to 2, reflecting a dominance of herbivory and a reduction in the role of the microbial pathway of diazotroph N delivery into zooplankton. The dominant pathways of N flow were likely direct grazing on diazotrophs other than *Trichodesmium* (primarily DDAs and UCYNs; Conroy et al. 2016; Hunt et al. 2016; Loick-Wilde et al. 2016) and/or indirect inputs via grazing on non-diazotrophic autotrophs (e.g. diatoms and pico-cyanobacteria, Adam et al. 2016; Bonnet et al. 2016b; Caffin et al. 2018; Klawonn et al. 2019) supported by diazotroph-derived DON and NH_4^+. We additionally note that while diazotrophs like *Trichodesmium* spp. were often abundant at OSW stations, they comprised only a small percentage of the total phytoplankton community biomass (Fig. 5.3), which likely reinforced the relatively low TPs found in all OSW mesozooplankton.

The PCA and bivariate correlations revealed a number of interesting relationships among zooplankton TPs, environmental variables, and the bulk and amino acid-specific $\delta^{15}N$ measurements. The similar behavior of NAI and $\delta^{15}N\text{-}Phe_{zp}$ in the PCA confirmed both variables as independent and robust proxies for the availability of nitrate to phytoplankton and for the incorporation of diazotroph nitrogen in zooplankton, respectively. Furthermore, their significant correlation (r^2=0.30, p<0.05, Fig. S7.2) suggests that NAI may be a good indicator of N sources utilized by the higher plankton food web in the SCS and potentially in other systems.

Interestingly, phosphate was an important driver of PC1, grouping with NAI (r^2=0.49, p<0.05) and $\delta^{15}N\text{-}Phe_{zp}$ (r^2=0.57, p<0.05) and varying strongly and inversely with TP_{zp} (r^2=0.63, p<0.05). Nutrient amendment experiments with phytoplankton during the same cruise suggested that the phytoplankton are co-limited by nitrate and phosphate (see nutrient amendment experiments in appendix, Fig. S8.1, S8.2), which may explain the highly significant relationships between phosphate and the zooplankton N source and trophic position proxies (Fig. S7.2). This is in contrast to the situation in the Baltic Sea where the mean trophic position of mesozooplankton in the summertime had no relationship with phosphate concentrations in the mixed layer (Loick-Wilde et al. 2019). This is possibly because polyphosphate accumulations in the dominant filamentous N_2-fixing cyanobacterium *Nodularia spumigena* (Braun et al. 2018) had released much of the planktonic food web from P-limitation in the Baltic in summer.

The statistical analyses additionally revealed that bulk and AA specific N isotope proxies were not associated with temperature and salinity in the Mekong River plume and adjacent SCS. This result supports the findings of Weber et al. (2019), who showed that the majority of the system's environmental variability was explained by the integrative

properties MLD, ChlMD and NAI, and further supports the habitat type approach as a tool for analyzing plankton food web dynamics. In contrast to the SCS, regions influenced by larger rivers likely have food webs structured more strongly around gradients of temperature and salinity. In the Amazon River plume, phytoplankton communities (Goes et al. 2014; Stukel et al. 2014; Weber et al. 2017; Weber et al. 2019) and mesozooplankton communities (Conroy et al. 2017; Loick-Wilde et al. 2016) are separated largely by salinity. But unlike what was suggested for the DIN-rich, light-limited areas of the Amazon River plume (Coles et al. 2017; Doherty et al. 2017; Satinsky et al. 2017), we found that the zooplankton food webs close to the river mouth of the Mekong were based on autotrophy rather than heterotrophy (i.e., bacterial recycling of organic matter) as indicated by a predominance of herbivorous rather than carnivorous mesozooplankton. Herbivory was somewhat unexpected and yields a testable hypothesis that higher discharges of sediment-carrying river waters may lead to light limitation of autotrophic growth and the biasing of the base of the planktonic food web towards heterotrophy, as has been shown for the Amazon River plume (Lefèvre et al. 2017; Smith and Demaster 1996). Our results can be explained by the relatively low outflow of the Mekong River during our cruise (Thi Ha et al. 2018), though we note that increased dam construction in the upper river basin is drastically reducing riverine sediment loads (e.g. Kummu et al. 2010; Kummu and Varis 2007; Thi Ha et al. 2018; Wang et al. 2011), which can conceivably alter nutrient flow in the coastal plankton food web.

In summary, our analysis provides convincing evidence that diazotrophy is more prevalent in the oligotrophic shelf waters of the SCS than previously thought, supporting up to 20% of zooplankton biomass in the early SWM season. Compound specific isotope analyses on mesozooplankton amino acid N uncovered a concurrent increase in diazotroph-N dependence with mean TP towards oligotrophic waters. These trends underscore recent findings from the Baltic Sea that elevated mesozooplankton TPs are associated with diazotrophy, which may be in part due to the circuitous routing of diazotroph N through the food web via the microbial loop. Mixed layer phosphate concentration also strongly correlated with mesozooplankton TP and may represent a useful indirect indicator of marine food web structure in near-coastal regions. Finally, with the help of the habitat type framework, we have shown that it is possible to tease apart critical plankton food web information in a highly variable environment, demonstrating the usefulness of this approach in studying multiple levels of planktonic food web in physicochemically complex regions.

Conclusions & Perspectives

Q1: What are the relative influences of the Mekong River plume and seasonal coastal upwelling in the southwestern SCS at the time of sampling?

H1a: Both the Mekong River outflow and the coastal upwelling are detectable, but reduced relative to "normal" SWM conditions.

Through a combination of water mass analysis, remote sensing, and analysis of habitat types, I have shown that the conditions sampled in June 2016 were unique compared to those encountered on previous expeditions. Both the Mekong River plume and coastal upwelling were detectable, but due to the timing of our cruise (both early in the SWM season and in a year following a strong ENSO event), the river plume influence on the southwestern SCS was minimal. Counter to expectation, the surface expression of upwelling was more similar to situations encountered during climatically "normal" years. In summary, we sampled at a time when the river outflow and upwelled waters were not yet interacting.

Q2: How do the river plume and upwelling shape the local phytoplankton community and govern the distributions of diazotroph populations?

H2a: Diazotroph abundances are elevated in the Mekong River plume and offshore of the coastal upwelling.

H2b: DDAs are the most active diazotroph group in the study region, particularly in waters affected by the Mekong River plume.

The unique configuration of the river plume and upwelling described above, as well as the biologically relevant habitats generated by the habitat type approach, simplified the biogeographical assessment of the phytoplankton communities. The habitat analysis identified distinct phytoplankton communities associated with the river plume, near-shore, and oligotrophic offshore waters, with common coastal diatom species dominating the river and coastal waters, and diazotrophs like *Trichodesmium* spp. defining the oligotrophic phytoplankton communities. This trend in community composition reflected a transition in the major new N sources at the base of the food web, from predominantly nitrate-based towards an increasing reliance on N_2-fixation.

Even though the Mekong River waters primarily supported coastal diatoms through classical eutrophication, *Rhizosolenia–Richelia* and *Hemiaulus–Richelia* DDAs were both present and actively fixing N_2 within the high-nutrient plume; however, DDAs reached their highest abundances in offshore OSW habitat, indicating that the oligotrophic shelf waters were a more favorable habitat. In contrast to the coastal and offshore habitats, I found no

distinct phytoplankton community associated with the coastal upwelling, and there were no clear signs of the stimulation of diazotrophy by aged upwelled waters. Counter to previous investigations, the highest diazotroph abundances were in the offshore oligotrophic waters, uninfluenced by either the river plume or upwelling, where a mixed community of *Trichodesmium* spp., DDAs, and UCYN groups were actively fixing N_2.

Unexpectedly, N_2-fixation activity was highest in the small size fraction throughout the study region, suggesting that UCYNs contributed the most to community rates of N_2-fixation. Targeted experiments with NanoSIMS to measure cell-specific rates of N_2-fixation would have unambiguously identified the most active diazotroph groups, but unfortunately my attempts at performing these experiments were largely unsuccessful in this regard (and were not included in this thesis). Regardless, the results presented here demonstrate that the shelf waters of the southwestern SCS supported a diverse and active diazotroph community.

Q3: What are the ecosystem impacts of diazotrophy in southwestern SCS in June 2016 and how does it compare with previous expeditions?

H3a: Rates of N_2-fixation are measurable, but reduced compared to previous SWM conditions, and are highest in the aged river plume waters.

H3b: Diazotroph N can be traced into suspended particles, but does not represent the dominant source of N.

H3c: Diazotroph N makes a measurable contribution to zooplankton biomass where diazotroph abundances and activity are highest.

H3d: Mesozooplankton trophic position increases concurrently with reliance on diazotroph N.

Counter to expectation, rates of diazotrophy were appreciable during the early stage of the SWM, which extends the reported annual period over which N_2-fixation supports significant production in the SCS. Since diazotrophs were capable of thriving independent of the Mekong River plume, the 2015 ENSO event had little effect on regional diazotrophy in 2016. In fact, N_2-fixation rates in June 2016 were similar to or higher than those measured previously during climatically "normal" SWM seasons, indicating that diazotrophy along the shelf of Vietnam may be more significant than previously thought.

N stable isotope natural abundance measurements of POM and zooplankton indicated that diazotroph N made its way through the entire planktonic food web. Diazotroph N contributions to the particle field reflected trends in N_2-fixation rates, with $\%N_{diazo}$ estimates around only 10-15% in the OnSW and UpW habitats and reaching over 70% in the OSW habitat, indicating that even modest N_2-fixation activity resulted in the accumulation of diazotroph N within surface waters.

These trends were mirrored by the bulk $\delta^{15}N$ signal of zooplankton at the habitat scale, such that diazotroph inputs to zooplankton were essentially absent near the coast but increased to up to 20% where other measures of diazotroph impacts were highest. Compound specific isotope analyses revealed that this large offset in $\%N_{diazo}$ estimates of POM and zooplankton were due to selective grazing of zooplankton on POM, such that POM was not representative of the mesozooplankton diet. Even so, the $\delta^{15}N$ signature of mesozooplankton phenylalanine, an N-source indicator, decreased concurrently with NAI, meaning that diazotroph N within the mesozooplankton diet increased as nitrate availability to surface waters fell. Excitingly, this significant relationship directly links a habitat-defining variable, NAI – the index that we invented – to N dynamics in the upper plankton food web. We additionally found that mesozooplankton TP was highest in the oligotrophic shelf waters, indicating a lengthening of the food web, but the direct cause for this shift remains unclear.

To conclude, I recognize that the questions and hypotheses posed and addressed in this thesis are quite specific to the study region. This work has helped fill important knowledge gaps related to diazotrophy and food web dynamics in the SCS shelf system, but the process and tools used to get us there were perhaps of greater interest and of larger relevance to the marine science community. I have shown that despite the physicochemical complexity of our test site, we could delineate habitats that were relevant across multiple scales of the system, from the mixing of water masses to phytoplankton community structure to energy flow through the zooplankton food web.

In closing, I would like to point to a few areas of research that I have come to realize, through my work on this thesis, deserve further attention:

My investigation into a link between DDA biogeography and host-symbiont relationships was surficial at best, but it highlights many unknown questions about these fascinating assemblages. For example, do hosts incur costs when forming symbioses? What conditions encourage symbiosis formation and destruction? How do hosts and symbionts come in contact? Can hosts eject their symbionts voluntarily? Answers to these questions will likely shed light on the distributions, success, and diazotrophic activity of DDAs in various environments.

There is continued debate in the SCS over the relative influences of diazotrophy and atmospheric N deposition on the marine N cycle, particularly in the northern SCS off the coast of China. I do not doubt, based on multiple lines of evidence, that diazotrophs are the

primary source of depleted N in the surface waters of our study area, but our estimates are nonetheless complicated by a lack of information on atmospheric N deposition to the region. To my knowledge, there are no direct measurements of atmospheric N deposition to the ocean in the southern South China Sea. A study much like that of Baker et al. (2007), which directly quantifies wet and dry atmospheric N deposition, needs to be performed in order to properly constrain its role in the local and regional N cycle. With this information we could better quantify the larger scale impacts of diazotrophy on the marine food web.

And finally, with the threat of anthropogenic stressors on ecosystems only worsening, it is important now more than ever to gather baseline data on the river-ocean continuum. River systems and coastlines are particularly exposed to such threats, and yet we are only recently coming to understand how they interact with the greater marine environment. Currently, multiple stressors threaten the Mekong Delta region, including rising sea levels from climate change, mangrove destruction from aquaculture expansion, and perhaps most seriously, dam construction along the Mekong River and its major tributaries. The Mekong River currently has over 40 dams in operation with dozens more currently under construction according the Mekong River Commission (www.mrcmekong.org). An abundance of literature has already identified significant reductions to sediment loading and river discharge, which will physically reshape the Delta and alter nutrient loads (Hoa et al. 2007; Kummu et al. 2010; Kummu and Varis 2007; Lu and Siew 2006). Some studies show that dams may preferentially retain phosphate and silica relative to dissolved N species (Maavara et al. 2015), which could significantly raise the N:P ratio of the river water. Such changes have the potential to alter marine phytoplankton community composition and suppress plume-associated diazotrophy. The problem of changing water chemistry due to human activities is a problem that affects many major rivers. Increasing N loads in the Amazon River were recently implicated in massive blooms of the macroalgae *Sargassum* in the tropical North Atlantic (Wang et al. 2019). Sudden and drastic changes to the chemistry of large rivers like the Mekong and Amazon Rivers can fundamentally alter marine ecosystems, and more focus should be paid now to better understanding these linkages.

References

Adam, B. and others 2016. N_2-fixation, ammonium release and N-transfer to the microbial and classical food web within a plankton community. ISME J **10:** 450-459.

Altabet, M. A. 1996. Nitrogen and carbon isotopic tracers of the source and transformation of particles in the deep sea, p. 155-184. *In* V. Ittekkot, P. Schäfer, S. Honjo and P. J. Depetris [eds.], Particle Flux in the Ocean. John Wiley & Sons.

Anderson, M. J., and J. Robinson. 2003. Generalized discriminant analysis based on distances. Australian & New Zealand Journal of Statistics **45:** 301-318.

Anderson, M. J., and T. J. Willis. 2003. Canonical Analysis of Principal Coordinates: A Useful Method of Constrained Ordination for Ecology. Ecology **84:** 511-525.

Baker, A. R., K. Weston, S. D. Kelly, M. Voss, P. Streu, and J. N. Cape. 2007. Dry and wet deposition of nutrients from the tropical Atlantic atmosphere: Links to primary productivity and nitrogen fixation. Deep Sea Research Part I Oceanographic Research Papers **54:** 1704-1720.

Benavides, M., S. Bonnet, I. Berman-Frank, and L. Riemann. 2018. Deep Into Oceanic N2 Fixation. Frontiers in Marine Science **5**.

Benavides, M., D. A. Bronk, N. S. R. Agawin, M. D. Perez-Hernandez, A. Hernandez-Guerra, and J. Aristegui. 2013. Longitudinal variability of size-fractionated N-2 fixation and DON release rates along 24.5 degrees N in the subtropical North Atlantic. J. Geophys. Res.-Oceans **118:** 3406-3415.

Berman-Frank, I., J. T. Cullen, Y. Shaked, R. M. Sherrell, and P. G. Falkowski. 2001. Iron availability, cellular iron quotas, and nitrogen fixation in Trichodesmium. Limnology and Oceanography **46:** 1249-1260.

Berthelot, H., M. Benavides, P. H. Moisander, O. Grosso, and S. Bonnet. 2017. High-nitrogen fixation rates in the particulate and dissolved pools in the Western Tropical Pacific (Solomon and Bismarck Seas). Geophysical Research Letters **44:** 8414-8423.

Berthelot, H., S. Bonnet, M. Camps, O. Grosso, and T. Moutin. 2015. Assessment of the dinitrogen released as ammonium and dissolved organic nitrogen by unicellular and filamentous marine diazotrophic cyanobacteria grown in culture. Frontiers in Marine Science **2**.

Bird, C., J. Martinez Martinez, A. G. O'Donnell, and M. Wyman. 2005. Spatial Distribution and Transcriptional Activity of an Uncultured Clade of Planktonic Diazotrophic γ-Proteobacteria in the Arabian Sea. Appl. Environ. Microbiol. **71:** 2079-2085.

Bombar, D. and others 2010. Sources of new nitrogen in the Vietnamese upwelling region of the South China Sea. J. Geophys. Res.-Oceans **115**.

Bombar, D. and others 2011. Distribution of diazotrophic microorganisms and nifH gene expression in the Mekong River plume during intermonsoon. Marine Ecology Progress Series **424:** 39-U55.

Bombar, D., R. W. Paerl, and L. Riemann. 2016. Marine Non-Cyanobacterial Diazotrophs: Moving beyond Molecular Detection. Trends in Microbiology **24:** 916-927.

Bonnet, S. and others 2016a. Diazotroph derived nitrogen supports diatom growth in the South West Pacific: A quantitative study using nanoSIMS. Limnology and Oceanography **61:** 1549-1562.

Bonnet, S. and others 2016b. Dynamics of N2 fixation and fate of diazotroph-derived nitrogen in a low-nutrient, low-chlorophyll ecosystem: results from the VAHINE mesocosm experiment (New Caledonia). Biogeosciences **13:** 2653-2673.

Braun, P. D., H. N. Schulz-Vogt, A. Vogts, and M. Nausch. 2018. Differences in the accumulation of phosphorus between vegetative cells and heterocysts in the cyanobacterium Nodularia spumigena. Scientific reports **8:** 5651.

Bronk, D. A. 2002. Chapter 5 - Dynamics of DON, p. 153-247. *In* D. A. Hansell and C. A. Carlson [eds.], Biogeochemistry of Marine Dissolved Organic Matter. Academic Press.

Brown, M. T., W. M. Landing, and C. I. Measures. 2005. Dissolved and particulate Fe in the western and central North Pacific: Results from the 2002 IOC cruise. Geochemistry Geophysics Geosystems **6**.

Brzezinski, M. A. 1985. The Si-C-N Ratio of Marine Diatoms - Interspecific Variability and the Effect of Some Environmental Variables. Journal of Phycology **21:** 347-357.

Caffin, M., H. Berthelot, V. Cornet-Barthaux, A. Barani, and S. Bonnet. 2018. Transfer of diazotroph-derived nitrogen to the planktonic food web across gradients of N2 fixation activity and diversity in the western tropical South Pacific Ocean. Biogeosciences **15:** 3795-3810.

Capone, D. G. 2005. Nitrogen fixation by Trichodesmium spp.: An important source of new nitrogen to the tropical and subtropical North Atlantic Ocean. Glob. Biogeochem. Cycle **19**.

Capone, D. G. and others 1998. An extensive bloom of the N-2-fixing cyanobacterium Trichodesmium erythraeum in the central Arabian Sea. Marine Ecology Progress Series **172:** 281-292.

Capone, D. G., J. P. Zehr, H. W. Paerl, B. Bergman, and E. J. Carpenter. 1997. Trichodesmium, a globally significant marine cyanobacterium. Science **276:** 1221-1229.

Caputo, A., M. Stenegren, M. C. Pernice, and R. A. Foster. 2018. A Short Comparison of Two Marine Planktonic Diazotrophic Symbioses Highlights an Un-quantified Disparity. Frontiers in Marine Science **5**.

Carpenter, E. J. 1983. Physiology and Ecology of Marine Planktonic Oscillatoria (Trichodesmium), p. 18. Marine Biology Letters.

Carpenter, E. J., H. R. Harvey, B. Fry, and D. G. Capone. 1997. Biogeochemical tracers of the marine cyanobacterium Trichodesmium. Deep-Sea Research Part I-Oceanographic Research Papers **44:** 27-38.

Carpenter, E. J., J. P. Montoya, J. Burns, M. R. Mulholland, A. Subramaniam, and D. G. Capone. 1999. Extensive bloom of a N2-fixing diatom/cyanobacterial association in the tropical Atlantic Ocean. Marine Ecology Progress Series **185:** 273-283.

Chao, S.-Y., P.-T. Shaw, and S. Y. Wu. 1996. El Nino modulation of the South China Sea circulation. Progress in Oceanography **38:** 51-93.

Chen, M., Y. Lu, N. Jiao, J. Tian, S. J. Kao, and Y. Zhang. 2019. Biogeographic drivers of diazotrophs in the western Pacific Ocean. Limnology and Oceanography **64:** 1403-1421.

Chen, Y. L. L., H. Y. Chen, S. H. Tuo, and K. Ohki. 2008. Seasonal dynamics of new production from Trichodesmium N-2 fixation and nitrate uptake in the upstream Kuroshio and South China Sea basin. Limnology and Oceanography **53:** 1705-1721.

Chikaraishi, Y. and others 2009. Determination of aquatic food-web structure based on compound-specific nitrogen isotopic composition of amino acids. Limnology and Oceanography: Methods **7:** 740-750.

Chikaraishi, Y., N. O. Ogawa, and N. Ohkouchi. 2010. Further evaluation of the trophic level estimation based on nitrogen isotopic composition of amino acids, p. 37-51. *In* N. Ohkouchi, I. Tayasu and K. Koba [eds.], Earth, life, and isotopes. Kyoto University Press.

Chin, T. M., J. Vazquez-Cuervo, and E. M. Armstrong. 2017. A multi-scale high-resolution analysis of global sea surface temperature. Remote Sensing of Environment **200:** 154-169.

Church, M. J., K. M. Björkman, D. M. Karl, M. A. Saito, and J. P. Zehr. 2008. Regional distributions of nitrogen-fixing bacteria in the Pacific Ocean. Limnology and Oceanography **53:** 63-77.

Church, M. J., C. Mahaffey, R. M. Letelier, R. Lukas, J. P. Zehr, and D. M. Karl. 2009. Physical forcing of nitrogen fixation and diazotroph community structure in the North Pacific subtropical gyre. Glob. Biogeochem. Cycle **23**.

Church, M. J., C. M. Short, B. D. Jenkins, D. M. Karl, and J. P. Zehr. 2005. Temporal Patterns of Nitrogenase Gene nifH Expression in the Oligotrophic North Pacific Ocean. Appl. Environ. Microbiol. **71:** 5362-5370.

Clark, D. R., A. P. Rees, and I. Joint. 2008. Ammonium regeneration and nitrification rates in the oligotrophic Atlantic Ocean: Implications for new production estimates. Limnology and Oceanography **53:** 52-62.

Codispoti, L. A. 2007. An oceanic fixed nitrogen sink exceeding 400 Tg Na-1 vs the concept of homeostasis in the fixed-nitrogen inventory. Biogeosciences **4:** 233-253.

Coles, V. and others 2017. Ocean biogeochemistry modeled with emergent trait-based genomics. Science **358:** 1149-1154.

Conroy, B. J., D. K. Steinberg, B. Song, A. Kalmbach, E. J. Carpenter, and R. A. Foster. 2017. Mesozooplankton Graze on Cyanobacteria in the Amazon River Plume and Western Tropical North Atlantic. Frontiers in microbiology **8:** 1436.

Conroy, B. J., D. K. Steinberg, M. R. Stukel, J. I. Goes, and V. J. Coles. 2016. Meso- and microzooplankton grazing in the Amazon River plume and western tropical North Atlantic. Limnology and Oceanography **61:** 825-840.

Cullen, J. J. 2015. Subsurface Chlorophyll Maximum Layers: Enduring Enigma or Mystery Solved? Annual Review of Marine Science **7:** 207-239.

Décima, M., M. R. Landry, C. J. Bradley, and M. L. Fogel. 2017. Alanine $\delta^{15}N$ trophic fractionation in heterotrophic protists. Limnology and Oceanography **62:** 2308-2322.

DeMaster, D. J., W. O. Smith, D. M. Nelson, and J. Y. Aller. 1996. Biogeochemical processes in Amazon shelf waters: Chemical distributions and uptake rates of silicon, carbon and nitrogen. Cont. Shelf Res. **16:** 617-&.

Deniro, M. J., and S. Epstein. 1981. Influence of diet on the distribution of nitrogen isotopes in animals. Geochim. Cosmochim. Acta **45:** 341-351.

Deutsch, C., J. L. Sarmiento, D. M. Sigman, N. Gruber, and J. P. Dunne. 2007. Spatial coupling of nitrogen inputs and losses in the ocean. Nature **445:** 163-167.

Dippner, J. W., D. Bombar, N. Loick-Wilde, M. Voss, and A. Subramaniam. 2013. Comment on "Current separation and upwelling over the southeast shelf of Vietnam in the South China Sea" by Chen et al. J. Geophys. Res.-Oceans **118:** 1618-1623.

Dippner, J. W., and N. Loick-Wilde. 2011. A redefinition of water masses in the Vietnamese upwelling area. Journal of Marine Systems **84:** 42-47.

Dippner, J. W., K. V. Nguyen, H. Hein, T. Ohde, and N. Loick. 2007. Monsoon-induced upwelling off the Vietnamese coast. Ocean Dynamics **57:** 46-62.

Doherty, M. and others 2017. Bacterial Biogeography across the Amazon River-Ocean Continuum. Frontiers in Microbiology **8**.

Duce, R. A. and others 2008. Impacts of Atmospheric Anthropogenic Nitrogen on the Open Ocean. Science **320:** 893-897.

Duce, R. A. and others 1991. The atmospheric input of trace species to the world ocean. Glob. Biogeochem. Cycle **5:** 193-259.

Dugdale, R. C. 1967. Nutrient Limitation in the Sea: Dynamics, Identification, and Signficance. Limnology and Oceanography **12:** 685-695.

Dugdale, R. C., and J. J. Goering. 1967. Uptake of New and Regenerated Forms of Nitrogen in Primary Productivity. Limnology and Oceanography **12:** 196-206.

Dyhrman, S. T. and others 2006. Phosphonate utilization by the globally important marine diazotroph Trichodesmium. Nature **439:** 68-71.

Eglite, E. and others 2018. Strategies of amino acid supply in mesozooplankton during cyanobacteria blooms: a stable nitrogen isotope approach. Ecosphere.

Eppley, R., and B. Peterson. 1979. Particulate Organic-Matter Flux and Planktonic New Production In the Deep Ocean. Nature **282:** 667-680.

Eppley, R. W., and W. H. Thomas. 1969. Comparison of Half-saturation Constants for Growth and Nitrate Uptake of Marine Phytoplankton. Journal of Phycology **5:** 375-&.

Faith, D. P., P. R. Minchin, and L. Belbin. 1987. Compositional dissimilarity as a robust measure of ecological distance. Vegetatio **69:** 57-68.

Falkowski, P. G. 1983. Enzymology of Nitrogen Assimilation, p. 839-868. *In* E. J. Carpenter and D. G. Capone [eds.], Nitrogen in the Marine Environment. Academic Press.

---. 1997. Evolution of the nitrogen cycle and its influence on the biological sequestration of CO2 in the ocean. Nature **387:** 272.

Fernandez, C., L. Farias, and O. Ulloa. 2011. Nitrogen Fixation in Denitrified Marine Waters. Plos One **6:** 9.

Foster, R. A., G. D. O'Mullan, D. G. Capone, D. A. Bronk, M. R. Mulholland, and E. J. Carpenter. 2008. Nitrogen-Fixing And Nitrifying Symbioses In The Marine Environment.

Foster, R. A., A. Subramaniam, C. Mahaffey, E. J. Carpenter, D. G. Capone, and J. P. Zehr. 2007. Influence of the Amazon River plume on distributions of free-living and symbiotic cyanobacteria in the western tropical north Atlantic Ocean. Limnology and Oceanography **52:** 517-532.

Foster, R. A., A. Subramaniam, and J. P. Zehr. 2009. Distribution and activity of diazotrophs in the Eastern Equatorial Atlantic. Environmental microbiology **11:** 741-750.

Foster, R. A., and J. P. Zehr. 2006. Characterization of diatom-cyanobacteria symbioses on the basis of nifH, hetR and 16S rRNA sequences. Environmental Microbiology **8:** 1913-1925.

Fry, B. 1988. Food web structure on Georges Bank from stable C, N, and S isotopic compositions. Limnology and Oceanography **33:** 1182-1190.

Fry, B. 2006. Stable isotope ecology. Springer.

Gattuso, J.-P. and others 2015. Contrasting futures for ocean and society from different anthropogenic CO_2 emissions scenarios. Science **349:** aac4722.

Gill, A. E., and W. L. Donn. 1982. Atmosphere‐Ocean Dynamics, International Geophysics. Academic Press.

Glibert, P. M., and D. A. Bronk. 1994. Release of Dissolved Organic Nitrogen by Marine Diazotrophic Cyanobacteria, Trichodesmium spp. Appl. Environ. Microbiol. **60:** 3996-4000.

Glibert, P. M., J. J. Middelburg, J. W. McClelland, and M. J. Vander Zanden. 2019. Stable isotope tracers: Enriching our perspectives and questions on sources, fates, rates, and pathways of major elements in aquatic systems. Limnology and Oceanography **64:** 950-981.

Goes, J. I. and others 2014. Influence of the Amazon River discharge on the biogeography of phytoplankton communities in the western tropical north Atlantic. Progress in Oceanography **120:** 29-40.

Gomes, H. d. R., Q. Xu, J. Ishizaka, E. J. Carpenter, P. L. Yager, and J. I. Goes. 2018. The Influence of Riverine Nutrients in Niche Partitioning of Phytoplankton Communities–A Contrast Between the Amazon River Plume and the Changjiang (Yangtze) River Diluted Water of the East China Sea. Frontiers in Marine Science **5**.

Grabowski, M. N. W., M. J. Church, and D. M. Karl. 2008. Nitrogen fixation rates and controls at Stn ALOHA. Aquatic Microbial Ecology **52:** 175-183.

Grosse, J., D. Bombar, N. D. Hai, N. N. Lam, and M. Voss. 2010. The Mekong River plume fuels nitrogen fixation and determines phytoplankton species distribution in the South China Sea during low- and high-discharge season. Limnology and Oceanography **55:** 1668-1680.

Grosskopf, T. and others 2012. Doubling of marine dinitrogen-fixation rates based on direct measurements. Nature **488:** 361-364.

Gruber, N. 2008. The Marine Nitrogen Cycle: Overview and Challenges, p. 1-50. *In* D. G. Capone, D. A. Bronk, M. R. Mulholland and E. J. Carpenter [eds.], Nitrogen in the Marine Environment (Second Edition). Academic Press.

Gruber, N., and J. L. Sarmiento. 1997. Global patterns of marine nitrogen fixation and denitrification. Glob. Biogeochem. Cycle **11:** 235-266.

Gruber, N., and J. L. Sarmiento. 2002. Large-Scale Biogeochemical-Physical Interactions In Elemental Cycles. The Sea **12**.

Gutiérrez-Rodríguez, A., M. Décima, B. N. Popp, and M. R. Landry. 2014. Isotopic invisibility of protozoan trophic steps in marine food webs. Limnology and Oceanography **59:** 1590-1598.

Hannides, C. C., B. N. Popp, M. R. Landry, and B. S. Graham. 2009. Quantification of zooplankton trophic position in the North Pacific Subtropical Gyre using stable nitrogen isotopes. Limnology and Oceanography **54:** 50-61.

Hansen, P. J., P. K. Bjornsen, and B. W. Hansen. 1997. Zooplankton grazing and growth: Scaling within the 2-2,000- mu m body size range. Limnol. Oceanogr. **42:** 687-704.

Harding, K., K. A. Turk-Kubo, R. E. Sipler, M. M. Mills, D. A. Bronk, and J. P. Zehr. 2018. Symbiotic unicellular cyanobacteria fix nitrogen in the Arctic Ocean. Proceedings of the National Academy of Sciences **115:** 13371-13375.

Hauss, H., J. M. Franz, T. Hansen, U. Struck, and U. Sommer. 2013. Relative inputs of upwelled and atmospheric nitrogen to the eastern tropical North Atlantic food web: spatial distribution of δ 15 N in mesozooplankton and relation to dissolved nutrient dynamics. Deep Sea Research Part I: Oceanographic Research Papers **75:** 135-145.

Hawser, S. P., J. M. Oneil, M. R. Roman, and G. A. Codd. 1992. Toxicity of Blooms of the Cyanobacterium Trichodesmium to Zooplankton. Journal of Applied Phycology **4:** 79-86.

Hewson, I., S. R. Govil, D. G. Capone, E. J. Carpenter, and J. A. Fuhrman. 2004. Evidence of Trichodesmium viral lysis and potential significance for biogeochemical cycling in the oligotrophic ocean. Aquatic Microbial Ecology **36:** 1-8.

Hilton, J. A., R. A. Foster, H. James Tripp, B. J. Carter, J. P. Zehr, and T. A. Villareal. 2013. Genomic deletions disrupt nitrogen metabolism pathways of a cyanobacterial diatom symbiont. Nature Communications **4:** 1767.

Hoa, L. T. V., N. H. Nhan, E. Wolanski, T. T. Cong, and H. Shigeko. 2007. The combined impact on the flooding in Vietnam's Mekong River delta of local man-made structures, sea level rise, and dams upstream in the river catchment. Estuarine Coastal and Shelf Science **71:** 110-116.

Honjo, S., S. J. Manganini, R. A. Krishfield, and R. Francois. 2008. Particulate organic carbon fluxes to the ocean interior and factors controlling the biological pump: A synthesis of global sediment trap programs since 1983. Progress in Oceanography **76:** 217-285.

Howarth, R. W., and R. Marino. 2006. Nitrogen as the limiting nutrient for eutrophication in coastal marine ecosystems: Evolving views over three decades. Limnology and Oceanography **51:** 364-376.

Hu, J., H. Kawamura, H. Hong, and Y. Qi. 2000. A Review on the Currents in the South China Sea: Seasonal Circulation, South China Sea Warm Current and Kuroshio Intrusion. Journal of Oceanography **56:** 607-624.

Hunt, B. P. V., S. Bonnet, H. Berthelot, B. J. Conroy, R. A. Foster, and M. Pagano. 2016. Contribution and pathways of diazotroph-derived nitrogen to zooplankton during the VAHINE mesocosm experiment in the oligotrophic New Caledonia lagoon. Biogeosciences **13:** 3131-3145.

Hutchins, D. A., and F. Fu. 2017. Microorganisms and ocean global change. Nature microbiology **2:** 17058.

Jahnke, R. A. 2010. Global Synthesis, p. 597-615. *In* K.-K. Liu, L. Atkinson, R. Quiñones and L. Talaue-McManus [eds.], Carbon and Nutrient Fluxes in Continental Margins: A Global Synthesis. Springer Berlin Heidelberg.

Janson, S., J. Wouters, B. Bergman, and E. J. Carpenter. 1999. Host specificity in the Richelia - diatom symbiosis revealed by hetR gene sequence analysis. Environmental Microbiology **1:** 431-438.

Jayakumar, A., B. X. Chang, B. Widner, P. Bernhardt, M. R. Mulholland, and B. B. Ward. 2017. Biological nitrogen fixation in the oxygen-minimum region of the eastern tropical North Pacific ocean. Isme j **11:** 2356-2367.

Jeffrey, S. W., R. F. C. Mantoura, and S. W. Wright. 1997. Phytoplankton Pigments in Oceanography: Guidelines to Modern Methods. UNESCO Publishing.

Jewett, L., and A. Romanou. 2017. Ocean acidification and other ocean changes, p. 364–392. *In* D. J. Wuebbles et al. [eds.], Climate Science Special Report: Fourth National Climate Assessment. U.S. Global Change Research Program.

Kalnay, E. and others 1996. The NCEP/NCAR 40-Year Reanalysis Project. Bulletin of the American Meteorological Society **77:** 437-472.

Kana, T. M., P. M. Glibert, R. Goericke, and N. A. Welschmeyer. 1988. Zeaxanthin and ß-carotene in Synechococcus WH7803 respond differently to irradiance. Limnology and Oceanography **33:** 1623-1626.

Karl, D., R. Letelier, L. Tupas, J. Dore, J. Christian, and D. Hebel. 1997. The role of nitrogen fixation in biogeochemical cycling in the subtropical North Pacific Ocean. Nature **388:** 533-538.

Karl, D. M., M. J. Church, J. E. Dore, R. M. Letelier, and C. Mahaffey. 2012. Predictable and efficient carbon sequestration in the North Pacific Ocean supported by symbiotic nitrogen fixation. Proc Natl Acad Sci U S A **109:** 1842-1849.

Kim, T.-W., K. Lee, R. Duce, and P. Liss. 2014. Impact of atmospheric nitrogen deposition on phytoplankton productivity in the South China Sea. Geophysical Research Letters **41:** 3156-3162.

Klawonn, I. and others 2019. Untangling hidden nutrient dynamics: rapid ammonium cycling and single-cell ammonium assimilation in marine plankton communities. The ISME Journal.

Knapp, A. 2012. The sensitivity of marine N2 fixation to dissolved inorganic nitrogen. Frontiers in Microbiology **3**.

Konno, U. and others 2010. Determination of total N ₂ fixation rates in the ocean taking into account both the particulate and filtrate fractions. Biogeosciences **7:** 2369-2377.

Krauk, J. M., T. A. Villareal, J. A. Sohm, J. P. Montoya, and D. G. Capone. 2006. Plasticity of N : P ratios in laboratory and field populations of Trichodesmium spp . Aquatic Microbial Ecology **42:** 243-253.

Kummu, M., X. X. Lu, J. J. Wang, and O. Varis. 2010. Basin-wide sediment trapping efficiency of emerging reservoirs along the Mekong. Geomorphology **119:** 181-197.

Kummu, M., and O. Varis. 2007. Sediment-related impacts due to upstream reservoir trapping, the Lower Mekong River. Geomorphology **85:** 275-293.

Landolfi, A., P. Kahler, W. Koeve, and A. Oschlies. 2018. Global Marine N-2 Fixation Estimates: From Observations to Models. Frontiers in Microbiology **9**.

Landrum, J. P., M. A. Altabet, and J. P. Montoya. 2011. Basin-scale distributions of stable nitrogen isotopes in the subtropical North Atlantic Ocean: Contribution of diazotroph nitrogen to particulate organic matter and mesozooplankton. Deep-Sea Research Part I-Oceanographic Research Papers **58:** 615-625.

Lefèvre, N. and others 2017. Net Heterotrophy in the Amazon Continental Shelf Changes Rapidly to a Sink of CO2 in the Outer Amazon Plume. Frontiers in Marine Science **4**.

Liu, K.-K., and I. R. Kaplan. 1989. The eastern tropical Pacific as a source of ^{15}N-enriched nitrate in seawater off southern California. Limnology and Oceanography **34:** 820-830.

Lohrenz, S. E., D. G. Redalje, P. G. Verity, C. N. Flagg, and K. V. Matulewski. 2002. Primary production on the continental shelf off Cape Hatteras, North Carolina. Deep-Sea Res. Part II-Top. Stud. Oceanogr. **49:** 4479-4509.

Loick, N., J. Dippner, H. N. Doan, I. Liskow, and M. Voss. 2007. Pelagic nitrogen dynamics in the Vietnamese upwelling area according to stable nitrogen and carbon isotope data. Deep-Sea Research Part I-Oceanographic Research Papers **54:** 596-607.

Loick-Wilde, N. and others 2017. Microplankton biomass and diversity in the Vietnamese upwelling area during SW monsoon under normal conditions and after an ENSO event. Progress in Oceanography **153:** 1-15.

Loick-Wilde, N. and others 2019. Stratification, nitrogen fixation, and cyanobacterial bloom stage regulate the planktonic food web structure. Global Change Biology **25:** 794-810.

Loick-Wilde, N. and others 2016. Nitrogen sources and net growth efficiency of zooplankton in three Amazon River plume food webs. Limnology and Oceanography **61:** 460-481.

Loick‐Wilde, N. and others 2018. De novo amino acid synthesis and turnover during N2 fixation. Limnology and Oceanography **63:** 1076-1092.

Longhurst, A. 1995. Seasonal cycles of pelagic production and consumption. Progress in Oceanography **36:** 77-167.

Lu, X. X., and R. Y. Siew. 2006. Water discharge and sediment flux changes over the past decades in the Lower Mekong River: possible impacts of the Chinese dams. Hydrol. Earth Syst. Sci. **10:** 181-195.

Luo, Y. W. and others 2012. Database of diazotrophs in global ocean: abundance, biomass and nitrogen fixation rates. Earth Syst. Sci. Data **4:** 47-73.

Maavara, T. and others 2015. Global phosphorus retention by river damming. Proceedings of the National Academy of Sciences **112:** 15603-15608.

Mahaffey, C., A. F. Michaels, and D. G. Capone. 2005. The conundrum of marine N2 fixation. American Journal of Science **305:** 546-595.

Mahowald, N. M. and others 2005. Atmospheric global dust cycle and iron inputs to the ocean. Glob. Biogeochem. Cycle **19**.

Martinez-Perez, C. and others 2016. The small unicellular diazotrophic symbiont, UCYN-A, is a key player in the marine nitrogen cycle. Nat Microbiol **1:** 16163.

McCarthy, M. D., R. Benner, C. Lee, and M. L. Fogel. 2007. Amino acid nitrogen isotopic fractionation patterns as indicators of heterotrophy in plankton, particulate, and dissolved organic matter. Geochim. Cosmochim. Acta **71:** 4727-4744.

McClelland, J. W., C. M. Holl, and J. P. Montoya. 2003. Nitrogen sources to zooplankton in the Tropical North Atlantic: Stable isotope ratios of amino acids identify strong coupling to N_2-fixation. Deep-Sea Res. I **50:** 849-861.

McClelland, J. W., and J. P. Montoya. 2002. Trophic relationships and the nitrogen isotopic composition of amino acids in plankton. Ecology **83:** 2173-2180.

McCutchan Jr, J. H., W. M. Lewis Jr, C. Kendall, and C. C. McGrath. 2003. Variation in trophic shift for stable isotope ratios of carbon, nitrogen, and sulfur. Oikos **102:** 378-390.

Messer, L. F. and others 2016. High levels of heterogeneity in diazotroph diversity and activity within a putative hotspot for marine nitrogen fixation. The ISME Journal **10:** 1499-1513.

Minagawa, M., and E. Wada. 1984. Stepwise enrichment of N-15 along food-chains - Further evidence and the relation between delta-N-15 and animal age. Geochim. Cosmochim. Acta **48:** 1135-1140.

Mohr, W., T. Grosskopf, D. W. R. Wallace, and J. LaRoche. 2010. Methodological Underestimation of Oceanic Nitrogen Fixation Rates. Plos One **5:** 7.

Moisander, P. H. and others 2010. Unicellular Cyanobacterial Distributions Broaden the Oceanic N-2 Fixation Domain. Science **327:** 1512-1514.

Moisander, P. H., R. A. Beinart, M. Voss, and J. P. Zehr. 2008. Diversity and abundance of diazotrophic microorganisms in the South China Sea during intermonsoon. ISME Journal **2:** 954-967.

Moisander, P. H., M. Benavides, S. Bonnet, I. Berman-Frank, A. E. White, and L. Riemann. 2017. Chasing after Non-cyanobacterial Nitrogen Fixation in Marine Pelagic Environments. Frontiers in Microbiology **8**.

Moisander, P. H., T. Serros, R. W. Paerl, R. A. Beinart, and J. P. Zehr. 2014. Gammaproteobacterial diazotrophs and nifH gene expression in surface waters of the South Pacific Ocean. The ISME Journal **8:** 1962-1973.

Mompeán, C., A. Bode, E. Gier, and M. D. McCarthy. 2016. Bulk vs. amino acid stable N isotope estimations of metabolic status and contributions of nitrogen fixation to size-fractionated zooplankton biomass in the subtropical N Atlantic. Deep Sea Research Part I: Oceanographic Research Papers **114:** 137-148.

Montoya, J. P. 2007. Natural abundance of 15N in marine planktonic ecosystems. Wiley-Blackwell.

---. 2008. Nitrogen Stable Isotopes in Marine Environments. Nitrogen in the Marine Environment, 2nd Edition**:** 1277-1302.

Montoya, J. P., E. J. Carpenter, and D. G. Capone. 2002. Nitrogen fixation and nitrogen isotope abundances in zooplankton of the oligotrophic North Atlantic. Limnology and Oceanography **47:** 1617-1628.

Montoya, J. P., C. M. Holl, J. P. Zehr, A. Hansen, T. A. Villareal, and D. G. Capone. 2004. High rates of N-2 fixation by unicellular diazotrophs in the oligotrophic Pacific Ocean. Nature **430:** 1027-1031.

Montoya, J. P., J. P. Landrum, and S. C. Weber. In press. Amazon River Influence on Nitrogen Fixation in the Western Tropical North Atlantic. The Sea.

Montoya, J. P., and J. J. McCarthy. 1995. Isotopic fractionation during nitrate uptake by phytoplankton grown in continuous culture. J. Plankton Res. **17:** 439-464.

Montoya, J. P., M. Voss, P. Kahler, and D. G. Capone. 1996. A simple, high-precision, high-sensitivity tracer assay for N-2 fixation. Appl. Environ. Microbiol. **62:** 986-993.

Moore, C. M. and others 2009. Large-scale distribution of Atlantic nitrogen fixation controlled by iron availability. Nat. Geosci. **2:** 867-871.

Motwani, N. H., J. Duberg, J. B. Svedén, and E. Gorokhova. 2018. Grazing on cyanobacteria and transfer of diazotrophic nitrogen to zooplankton in the Baltic Sea. Limnology and Oceanography **63:** 672-686.

Mulholland, M. R. 2007. The fate of nitrogen fixed by diazotrophs in the ocean. Biogeosciences **4:** 37-51.

Mulholland, M. R., P. W. Bernhardt, C. A. Heil, D. A. Bronk, and J. M. O'Neil. 2006. Nitrogen fixation and release of fixed nitrogen by Trichodesmium spp. in the Gulf of Mexico. Limnology and Oceanography **51:** 1762-1776.

Mulholland, M. R. and others 2014. Contribution of diazotrophy to nitrogen inputs supporting Karenia brevis blooms in the Gulf of Mexico. Harmful Algae **38:** 20-29.

Mulholland, M. R. and others 2019. High Rates of N2 Fixation in Temperate, Western North Atlantic Coastal Waters Expand the Realm of Marine Diazotrophy. Glob. Biogeochem. Cycle **33:** 826-840.

Mulholland, M. R., and D. G. Capone. 2000. The nitrogen physiology of the marine N2-fixing cyanobacteria Trichodesmium spp. Trends in Plant Science **5:** 148-153.

Mulholland, M. R., K. Ohki, and D. G. Capone. 2001. Nutrient Controls on Nitrogen Uptake and Metabolism by Natural Populations and Cultures of Trichodesmium (Cyanobacteria). Journal of Phycology **37:** 1001-1009.

Needoba, J. A., R. A. Foster, C. Sakamoto, J. P. Zehr, and K. S. Johnson. 2007. Nitrogen fixation by unicellular diazotrophic cyanobacteria in the temperate oligotrophic North Pacific Ocean. Limnology and Oceanography **52:** 1317-1327.

Needoba, J. A., N. A. Waser, P. J. Harrison, and S. E. Calvert. 2003. Nitrogen isotope fractionation in 12 species of marine phytoplankton during growth on nitrate. Marine Ecology Progress Series **255:** 81-91.

O'Reilly, C. M., R. E. Hecky, A. S. Cohen, and P.-D. Plisnier. 2002. Interpreting stable isotopes in food webs: Recognizing the role of time averaging at different trophic levels. Limnology and Oceanography **47:** 306-309.

O'Neil, J. M. 1999. Grazer interactions with nitrogen-fixing marine cyanobacteria: Adaptation for N-acquisition? Bull. Inst. Oceanogr. **19:** 293-317.

O'Neil, J. M., and M. R. Roman. 1992. Grazers and Associated Organisms of Trichodesmium, p. 61-73. *In* E. J. Carpenter, D. G. Capone and J. G. Rueter [eds.], Marine Pelagic Cyanobacteria: Trichodesmium and other Diazotrophs. Springer Netherlands.

Ohki, K. 1999. A possible role of temperate phage in the regulation of Trichodesmium biomass. Bull. Inst. Oceanogr. **19:** 235-256.

Ohkouchi, N. and others 2017. Advances in the application of amino acid nitrogen isotopic analysis in ecological and biogeochemical studies. Organic Geochemistry **113:** 150-174.

Paerl, H. W. 1997. Coastal eutrophication and harmful algal blooms: Importance of atmospheric deposition and groundwater as “new” nitrogen and other nutrient sources. Limnology and Oceanography **42:** 1154-1165.

Paerl, H. W., and J. Huisman. 2008. Climate. Blooms like it hot. Science **320** 57-58.

Raes, E. J. and others 2014. Changes in latitude and dominant diazotrophic community alter N2 fixation. Mar. Ecol. Prog. Ser.

Redfield, A. C. 1958. The Biological Control of Chemical Factors in the Environment. Am. Scientist **46:** 205-221.

Reygondeau, G., O. Maury, G. Beaugrand, J. M. Fromentin, A. Fonteneau, and P. Cury. 2012. Biogeography of tuna and billfish communities. Journal of Biogeography **39:** 114-129.

Rodríguez, J. and others 2001. Mesoscale vertical motion and the size structure of phytoplankton in the ocean. Nature **410:** 360.

Rouyer, T., J. M. Fromentin, N. C. Stenseth, and B. Cazelles. 2008. Analysing multiple time series and extending significance testing in wavelet analysis. Marine Ecology Progress Series **359:** 11-23.

Roy, T. and others 2011. Regional impacts of climate change and atmospheric CO_2 on future ocean carbon uptake: A multimodel linear feedback analysis. J. Clim. **24:** 2300-2318.

Ryther, J. H. 1969. Photosynthesis and Fish Production in the Sea. Science **166:** 72-76.

Ryther, J. H., and W. M. Dunstan. 1971. Nitrogen, Phosphorus, and Eutrophication in the Coastal Marine Environment. Science **171:** 1008-1013.

Sathyendranath, S., A. Longhurst, C. M. Caverhill, and T. Platt. 1995. Regionally and seasonally differentiated primary production in the North Atlantic. Deep Sea Research Part I: Oceanographic Research Papers **42:** 1773-1802.

Satinsky, B. M. and others 2017. Expression patterns of elemental cycling genes in the Amazon River Plume. The ISME journal **11:** 1852.

Savoye, N., A. Aminot, P. Tréguer, M. Fontugne, N. Naulet, and R. Kérouel. 2003. Dynamics of particulate organic matter δ15N and δ13C during spring phytoplankton blooms in a macrotidal ecosystem (Bay of Seine, France). Marine Ecology Progress Series **255:** 27-41.

Scharek, R., L. M. Tupas, and D. M. Karl. 1999. Diatom fluxes to the deep sea in the oligotrophic North Pacific gyre at Station ALOHA. Marine Ecology Progress Series **182:** 55-67.

Schulz, J. and others 2012. Spatial and temporal habitat partitioning by zooplankton in the Bornholm Basin (central Baltic Sea). Progress in Oceanography **107:** 3-30.

Sharp, J. H. 1983. The distribution of inorganic nitrogen and dissolved and particulate organic nitrogen in the sea, p. 1-35. *In* E. J. Carpenter and D. G. Capone [eds.], Nitrogen in the Marine Environment. Academic Press.

Shiozaki, T. and others 2018. Diazotroph community structure and the role of nitrogen fixation in the nitrogen cycle in the Chukchi Sea (western Arctic Ocean). Limnology and Oceanography **63:** 2191-2205.

Shiozaki, T., T. Nagata, M. Ijichi, and K. Furuya. 2015. Nitrogen fixation and the diazotroph community in the temperate coastal region of the northwestern North Pacific. Biogeosciences **12:** 4751-4764.

Sigman, D. M., M. A. Altabet, D. C. McCorkle, R. Francois, and G. Fischer. 2000. The delta N-15 of nitrate in the Southern Ocean: Nitrogen cycling and circulation in the ocean interior. J. Geophys. Res.-Oceans **105:** 19599-19614.

Sipler, R. E. and others 2017. Preliminary estimates of the contribution of Arctic nitrogen fixation to the global nitrogen budget. Limnology and Oceanography Letters **2:** 159-166.

Smith, W. O., and D. J. Demaster. 1996. Phytoplankton biomass and productivity in the Amazon River plume: Correlation with seasonal river discharge. Cont. Shelf Res. **16:** 291-319.

Snidvongs, A., and S.-K. Teng. 2006. Global International Waters Assessment Mekong River, GIWA Regional assessment, p. 75.

Sohm, J. A., J. A. Hilton, A. E. Noble, J. P. Zehr, M. A. Saito, and E. A. Webb. 2011a. Nitrogen fixation in the South Atlantic Gyre and the Benguela Upwelling System. Geophysical Research Letters **38**.

Sohm, J. A., C. Mahaffey, and D. G. Capone. 2008. Assessment of relative phosphorus limitation of Trichodesmium spp. in the North Pacific, North Atlantic, and the north coast of Australia. Limnology and Oceanography **53:** 2495-2502.

Sohm, J. A., A. Subramaniam, T. E. Gunderson, E. J. Carpenter, and D. G. Capone. 2011b. Nitrogen fixation by Trichodesmium spp. and unicellular diazotrophs in the North Pacific Subtropical Gyre. Journal of Geophysical Research: Biogeosciences **116**.

Sohm, J. A., E. A. Webb, and D. G. Capone. 2011c. Emerging patterns of marine nitrogen fixation. Nature Reviews Microbiology **9:** 499-508.

Sournia, A. 1970. Cyanophyceae in the marine plankton.

Steffan, S. A. and others 2015. Microbes are trophic analogs of animals. Proceedings of the National Academy of Sciences **112:** 15119-15124.

Steffan, S. A., Y. Chikaraishi, P. S. Dharampal, J. N. Pauli, C. Guédot, and N. Ohkouchi. 2017. Unpacking brown food‐webs: Animal trophic identity reflects rampant microbivory. Ecology and evolution **7:** 3532-3541.

Steinberg, D. K., and M. R. Landry. 2017. Zooplankton and the ocean carbon cycle. Annual Review of Marine Science **9:** 413-444.

Steinberg, D. K., and G. K. Saba. 2008. Nitrogen consumption and metabolism in marine zooplankton, p. 1135-1196. *In* D. G. Capone, D. A. Bronk, M. R. Mulholland and E. J. Carpenter [eds.], Nitrogen in the marine environment. Elsevier Academic Press.

Stenegren, M., A. Caputo, C. Berg, S. Bonnet, and R. A. Foster. 2017. Distribution and drivers of symbiotic and free-living diazotrophic cyanobacteria in the Western Tropical South Pacific. Biogeosciences Discuss. **2017:** 1-47.

Stukel, M. R., V. J. Coles, M. T. Brooks, and R. R. Hood. 2014. Top-down, bottom-up and physical controls on diatom-diazotroph assemblage growth in the Amazon River plume. Biogeosciences **11:** 3259-3278.

Subramaniam, A. and others 2008. Amazon River enhances diazotrophy and carbon sequestration in the tropical North Atlantic Ocean. Proc. Natl. Acad. Sci. U. S. A. **105:** 10460-10465.

Tang, W., and N. Cassar. 2019. Data-Driven Modeling of the Distribution of Diazotrophs in the Global Ocean. Geophysical Research Letters **46:** 12258-12269.

Tang, W. and others 2019. Revisiting the distribution of oceanic N2 fixation and estimating diazotrophic contribution to marine production. Nature Communications **10:** 831.

Teh, L. S. L., A. Witter, W. W. L. Cheung, U. R. Sumaila, and X. Yin. 2017. What is at stake? Status and threats to South China Sea marine fisheries. Ambio **46:** 57-72.

Thi Ha, D., S. Ouillon, and G. Van Vinh. 2018. Water and Suspended Sediment Budgets in the Lower Mekong from High-Frequency Measurements (2009-2016). Water **10**.

Thornton, S. F., and J. McManus. 1994. Application of organic-carbon and nitrogen stable-isotope and C/N ratios as source indicators of organic-matter provenance in estuarine systems - Evidence from the Tay Estuary, Scotland. Estuarine Coastal and Shelf Science **38:** 219-233.

Tyrell, T. 1999. The relative influences of nitrogen and phosphorus on oceanic primary production. Nature **400:** 525-531.

Vander Zanden, M. J., and J. B. Rasmussen. 2001. Variation in delta N-15 and delta C-13 trophic fractionation: Implications for aquatic food web studies. Limnology and Oceanography **46:** 2061-2066.

Vidussi, F., H. Claustre, B. B. Manca, A. Luchetta, and J.-C. Marty. 2001. Phytoplankton pigment distribution in relation to upper thermocline circulation in the eastern Mediterranean Sea during winter. Journal of Geophysical Research: Oceans **106:** 19939-19956.

Villareal, T. A. 1989. Division Cycles in the Nitrogen-Fixing Rhizosolenia (Bacillariophyceae) Richelia (Nostocaceae) Symbiosis. British Phycological Journal **24:** 357-365.

Villareal, T. A. 1992. Marine Nitrogen-Fixing Diatom-Cyanobacteria Symbioses, p. 163-175. *In* E. J. Carpenter, D. G. Capone and J. G. Rueter [eds.], Marine Pelagic Cyanobacteria: Trichodesmium and other Diazotrophs. Springer Netherlands.

Villareal, T. A. 1994. Widespread occurrence of the Hemiaulus-cyanobacterial symbiosis in the Southwest North Atlantic Ocean. Bull. Mar. Sci. **54:** 1-7.

Villareal, T. A., and E. J. Carpenter. 2003. Buoyancy regulation and the potential for vertical migration in the oceanic cyanobacterium Trichodesmium. Microb. Ecol. **45:** 1-10.

Voss, M., D. Bombar, J. W. Dippner, D. N. Hai, N. N. Lam, and N. Loick-Wilde. 2014. The Mekong River and its influence on the nutrient chemistry and matter cycling in the Vietnamese coastal zone. Biogeochemical Dynamics at Major River-Coastal Interfaces: Linkages with Global Change**:** 296-320.

Voss, M., D. Bombar, N. Loick, and J. W. Dippner. 2006. Riverine influence on nitrogen fixation in the upwelling region off Vietnam, South China Sea. Geophysical Research Letters **33:** L07604.

Voss, M., P. Croot, K. Lochte, M. Mills, and I. Peeken. 2004. Patterns of nitrogen fixation along 10°N in the tropical Atlantic. Geophysical Research Letters **31:** n/a-n/a.

Wada, E., M. Terazaki, Y. Kabaya, and T. Nemoto. 1987. 15N and 13C abundances in the Antartic Ocean with emphasis on the biogeochemical structure of the food web. Deep Sea Research Part A. Oceanographic Research Papers **34:** 829-841.

Walsby, A. E. 1978. The properties and buoyancy-providing role of gas vacuoles in Trichodesmium Ehrenberg. British Phycological Journal **13:** 103-116.

Wang, H., Y. Saito, Y. Zhang, N. Bi, X. Sun, and Z. Yang. 2011. Recent changes of sediment flux to the western Pacific Ocean from major rivers in East and Southeast Asia. Earth-Science Reviews **108:** 80-100.

Wang, M., C. Hu, B. B. Barnes, G. Mitchum, B. Lapointe, and J. P. Montoya. 2019. The great Atlantic Sargassum belt. Science **365:** 83-87.

Wannicke, N., M. Benavides, T. Dalsgaard, J. W. Dippner, J. P. Montoya, and M. Voss. 2018. New Perspectives on Nitrogen Fixation Measurements Using 15N2 Gas. Frontiers in Marine Science **5**.

Wannicke, N., B. P. Koch, and M. Voss. 2009. Release of fixed N-2 and C as dissolved compounds by Trichodesmium erythreum and Nodularia spumigena under the influence of high light and high nutrient (P). Aquatic Microbial Ecology **57:** 175-189.

Wannicke, N., F. Korth, I. Liskow, and M. Voss. 2013. Incorporation of diazotrophic fixed N_2 by mesozooplankton - Case studies in the southern Baltic Sea. Journal of Marine Systems **117–118:** 1-13.

Wannicke, N., I. Liskow, and M. Voss. 2010. Impact of diazotrophy on N stable isotope signatures of nitrate and particulate organic nitrogen: case studies in the north-eastern tropical Atlantic Ocean. Isotopes in Environmental and Health Studies **46:** 337-354.

Ward, B. A., S. Dutkiewicz, C. M. Moore, and M. J. Follows. 2013. Iron, phosphorus, and nitrogen supply ratios define the biogeography of nitrogen fixation. Limnology and Oceanography **58:** 2059-2075.

Waser, N. A. D., P. J. Harrison, B. Nielsen, S. E. Calvert, and D. H. Turpin. 1998. Nitrogen isotope fractionation during the uptake and assimilation of nitrate, nitrite, ammonium, and urea by a marine diatom. Limnology and Oceanography **43:** 215-224.

Webb, E. A., R. W. Jakuba, J. W. Moffett, and S. T. Dyhrman. 2007. Molecular assessment of phosphorus and iron physiology in Trichodesmium populations from the western Central and western South Atlantic. Limnology and Oceanography **52:** 2221-2232.

Weber, S. C., E. J. Carpenter, V. J. Coles, P. L. Yager, J. Goes, and J. P. Montoya. 2017. Amazon River influence on nitrogen fixation and export production in the western tropical North Atlantic. Limnology and Oceanography **62:** 618-631.

Weber, S. C. and others 2019. Habitat Delineation in Highly Variable Marine Environments. Frontiers in Marine Science **6**.

Wen, L. S., K. T. Jiann, and P. H. Santschi. 2006. Physicochemical speciation of bioactive trace metals (Cd, Cu, Fe, Ni) in the oligotrophic South China Sea. Mar. Chem. **101:** 104-129.

Wu, C.-R., P.-T. Shaw, and S.-Y. Chao. 1998. Seasonal and interannual variations in the velocity field of the South China Sea. Journal of Oceanography **54:** 361-372.

Wu, J. F., E. Boyle, W. Sunda, and L. S. Wen. 2001. Soluble and colloidal iron in the olgotrophic North Atlantic and North Pacific. Science **293:** 847-849.

Wu, J. F. and others 2003. Dissolved inorganic phosphorus, dissolved iron, and Trichodesmium in the oligotrophic South China Sea. Glob. Biogeochem. Cycle **17**.

Wu, S. P. and others 2018. Atmospheric ammonia measurements along the coastal lines of Southeastern China: Implications for inorganic nitrogen deposition to coastal waters. Atmos. Environ. **177:** 1-11.

Wyrtki, K. 1961. Physical Oceanography of the Southeast Asian waters.

Xie, S. P., Q. Xie, D. X. Wang, and W. T. Liu. 2003. Summer upwelling in the South China Sea and its role in regional climate variations. J. Geophys. Res.-Oceans **108:** 13.

Yang, J. Y. T., S. C. Hsu, M. H. Dai, S. S. Y. Hsiao, and S. J. Kao. 2014. Isotopic composition of water-soluble nitrate in bulk atmospheric deposition at Dongsha Island: sources and implications of external N supply to the northern South China Sea. Biogeosciences **11:** 1833-1846.

Zehr, J. P. and others 2008. Globally Distributed Uncultivated Oceanic N2-Fixing Cyanobacteria Lack Oxygenic Photosystem II. Science **322:** 1110-1112.

Zehr, J. P., M. T. Mellon, and S. Zani. 1998. New nitrogen-fixing microorganisms detected in oligotrophic oceans by amplification of nitrogenase (nifH) genes. Appl. Environ. Microbiol. **64:** 3444-3450.

Zehr, J. P., I. N. Shilova, H. M. Farnelid, M. d. C. Muñoz-Marín, and K. A. Turk-Kubo. 2016. Unusual marine unicellular symbiosis with the nitrogen-fixing cyanobacterium UCYN-A. Nature Microbiology **2:** 16214.

Zehr, J. P., and P. J. Turner. 2001. Nitrogen fixation: Nitrogenase genes and gene expression, p. 271-286. Methods in Microbiology. Academic Press.

Zehr, J. P. and others 2001. Unicellular cyanobacteria fix N2 in the subtropical North Pacific Ocean. Nature **412:** 635-638.

Zhang, R. H., A. Sumi, and M. Kimoto. 1996. Impact of El Nino on the East Asian monsoon: A diagnostic study of the '86/87 and '91/92 events. Journal of the Meteorological Society of Japan **74:** 49-62.

Acknowledgements

There are too many people to thank over these last four years, particularly when I'm writing this at the very last moment. Maren Voss and Joachim Dippner, thank you for being wonderful mentors, but also something like tough-loving parents. You've helped me grow here in Germany and in the very least have made me more comfortable listening in German. Maren, I look forward to the years ahead as collaborators. Joe Montoya, thank you for your continue advisement and for keeping track of my slow transition to a Germanic writing style. Ajit Subramaniam, always a pleasure. I thoroughly enjoyed our paper discussions and hope there will be more to come. Natalie Loick-Wilde, the long science and life chats have kept my interests in this career burning, even in times of doubt. Your friendship and mentorship have been a gift. Thank you to the lab members for keeping me functional, particularly in my first year. And thank you to my family, for putting up with seeing me so irregularly and for your endless support from across the pond. And lastly, thank you to my new wife, Domenika Karwowski, for…. everything. You've kept me alive and, most importantly, happy. Love you.

Appendix

CHAPTER 1 – Introduction

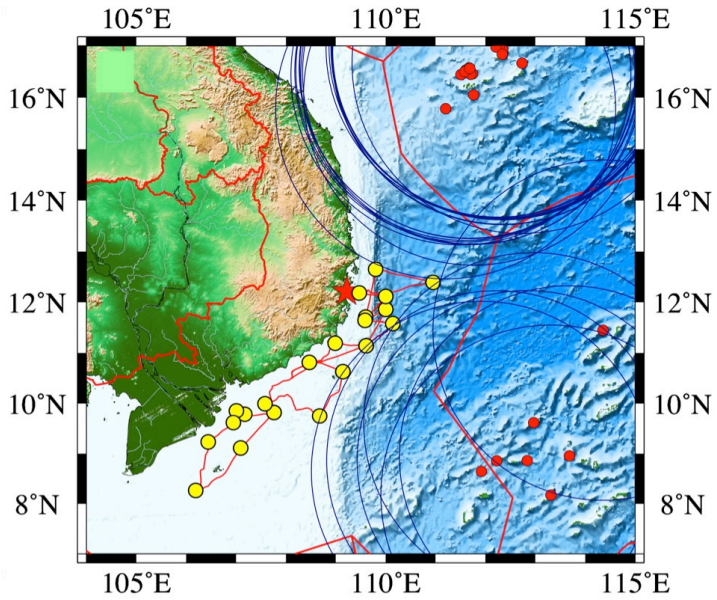

Figure S1.1: Station map (yellow circles) and cruise track (red lines between stations) of cruise FK160603. Large blue circles denote the 200 nm exclusion zones around disputed landmasses (red circles) at the time of sampling. The city of Nha Trang is marked with red star.

CHAPTER 2 –Materials & Methods

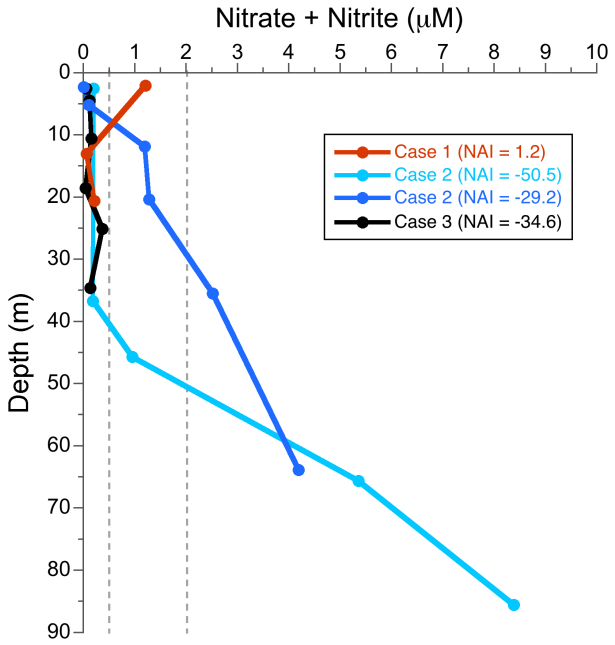

Figure S2.1: Exemplar profiles of $NO_{2/3}$ concentrations demonstrating how the nitrate availability index (NAI) was calculated. The three cases correspond to the methods description and grey dashed lines denote the case boundaries (0.5 and 2 μM $NO_{2/3}$). The deepest measured nutrient sample for all profiles was collected either between 85-100m or just above bottom (whichever was deeper). Exemplar profiles are from casts 11.03 (red), 18.03 (light blue), 7.03 (dark blue), and 8.02 (black).

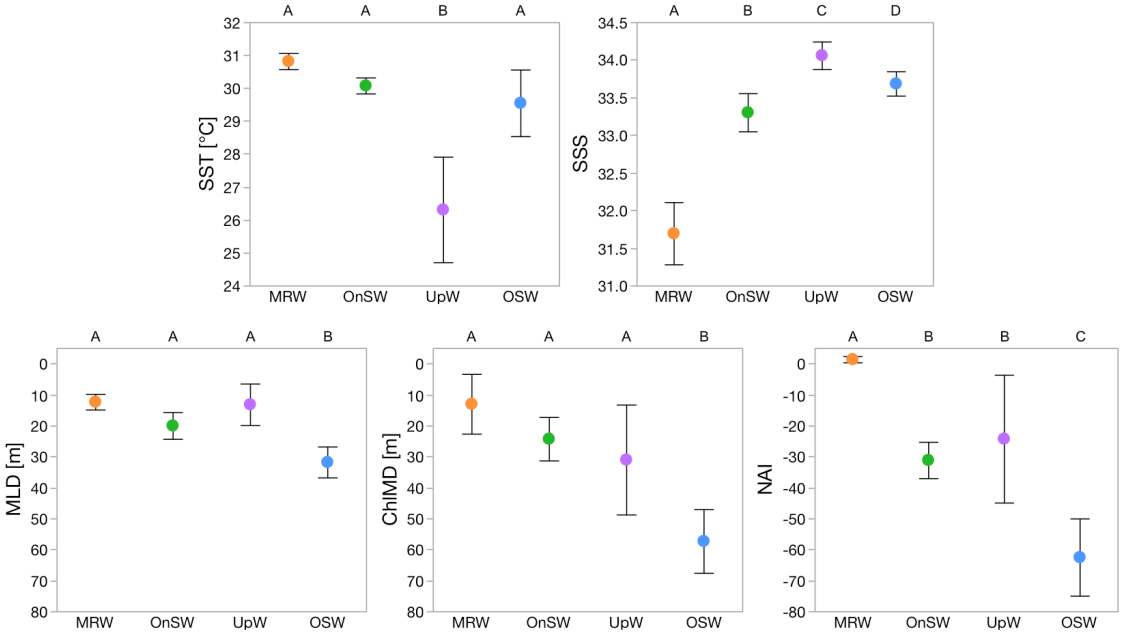

Figure S2.2: Graphical representations of Table 4.1, where habitat-defining variables are grouped by habitat. Note that the y-axis is flipped for MLD and ChlMD. Error bars show the standard deviation of the mean. Letters along the top of each plot indicate significant differences for a given variable between habitats, where habitats with different letters are significantly different (Tukey-Kramer tests, $p<0.05$).

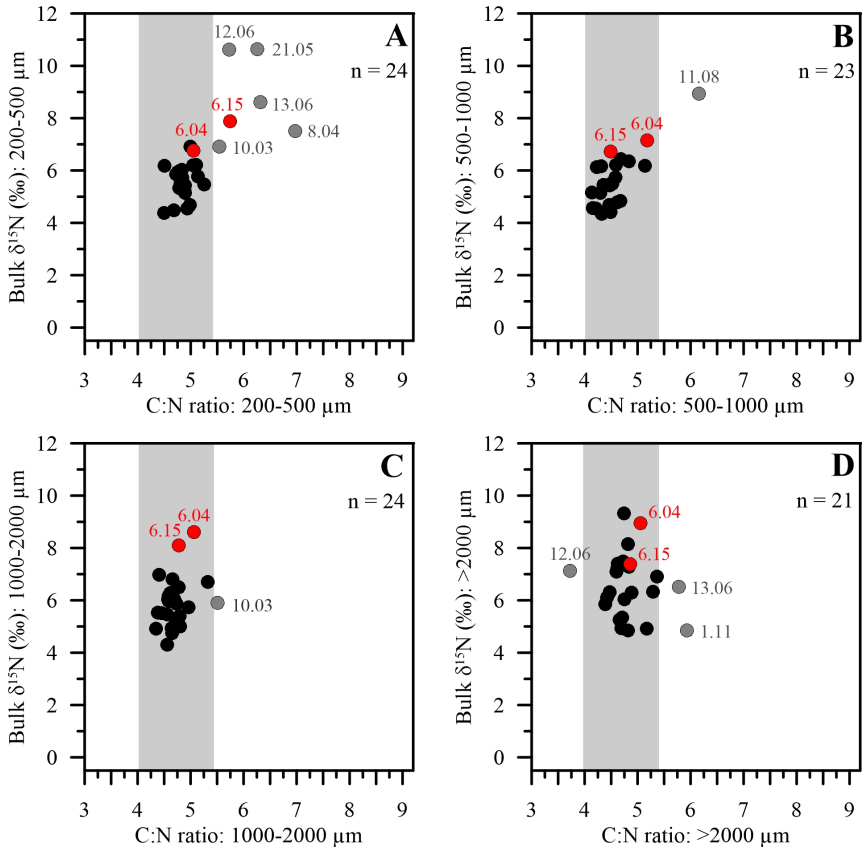

Figure S2.3: Determination of contamination in zooplankton samples from the four size fractions: **(A)** 200-500 µm, **(B)** 500-1000 µm, **(C)** 1000-2000 µm, and **(D)** >2000 µm. The expected range in the elemental C:N ratio of zooplankton biomass is between 4 and 5.4 (Steinberg and Saba 2007). Sample C:N values below this range is indicative of fish contamination and above this range is indicative of phytoplankton contamination. Samples outside of this range are marked with gray. Stn. 6 samples are marked in red. Marked samples are labeled with their event number.

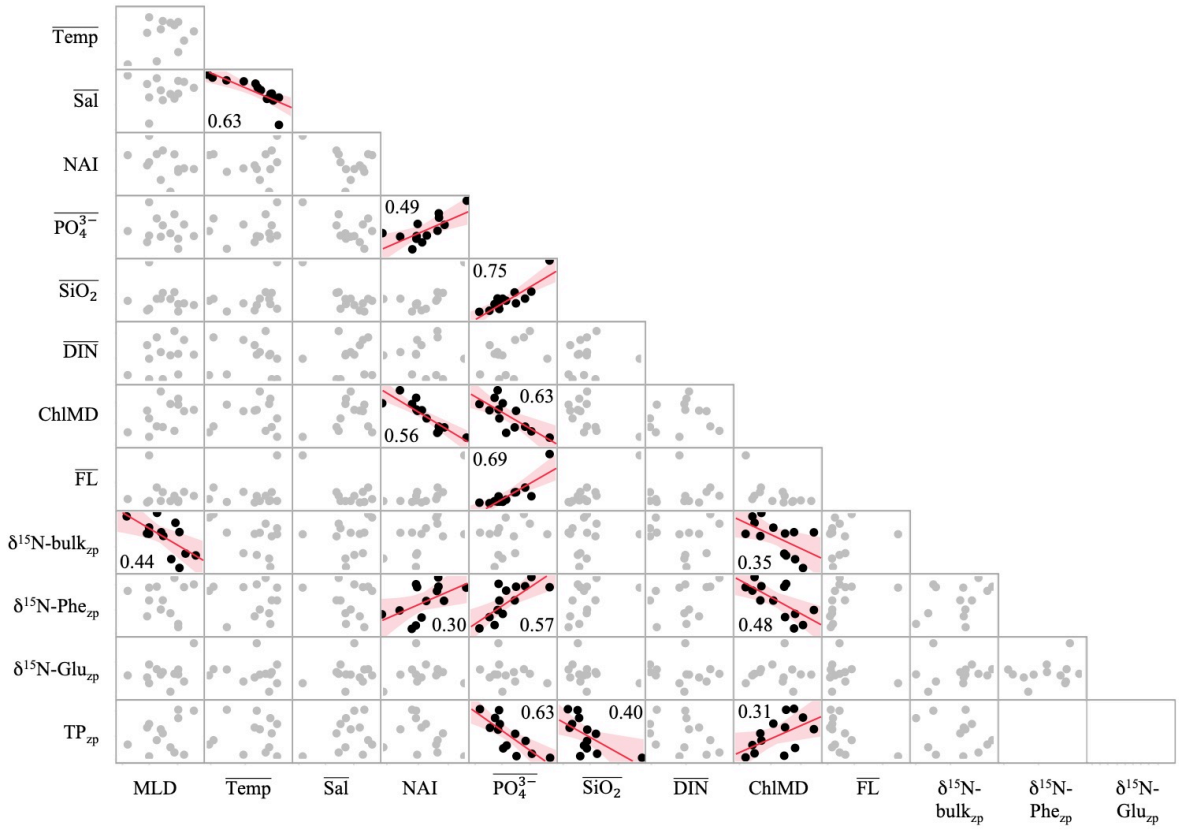

Figure S2.4: Scatterplot matrix of multivariate linear correlations between the 13 biotic and abiotic variables from 15 stations shown in the PCA. Data were normalized prior to the analysis. The scatterplots of significantly correlated variables ($p \geq 0.5$) include the linear fit with r^2 values.

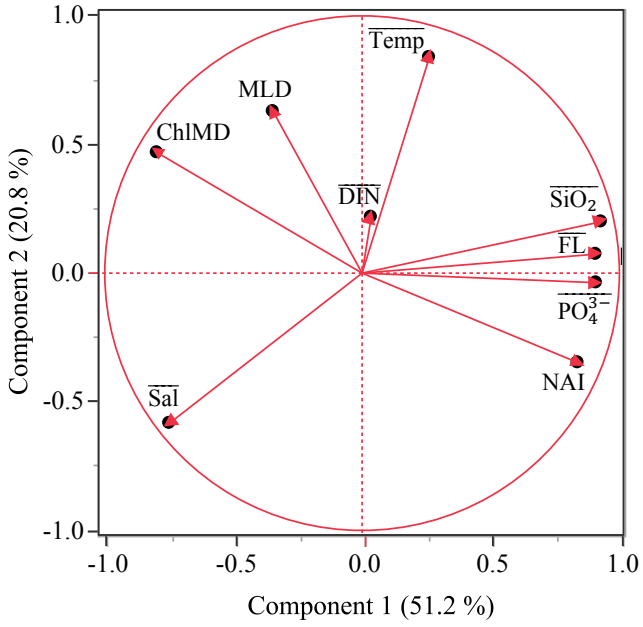

Figure S2.5: PCA of the nine environmental variables collected from CTD casts corresponding to zooplankton net tows, representing a subset of the variables included in the multivariate analysis (Fig. 7.4). Inclusion of zooplankton measures does not significantly influence the PCA results. Overlined variables were integrated through the mixed layer. See Fig. 7.4 and Table 7.1 for more information.

CHAPTER 3 – Characterization of the study site

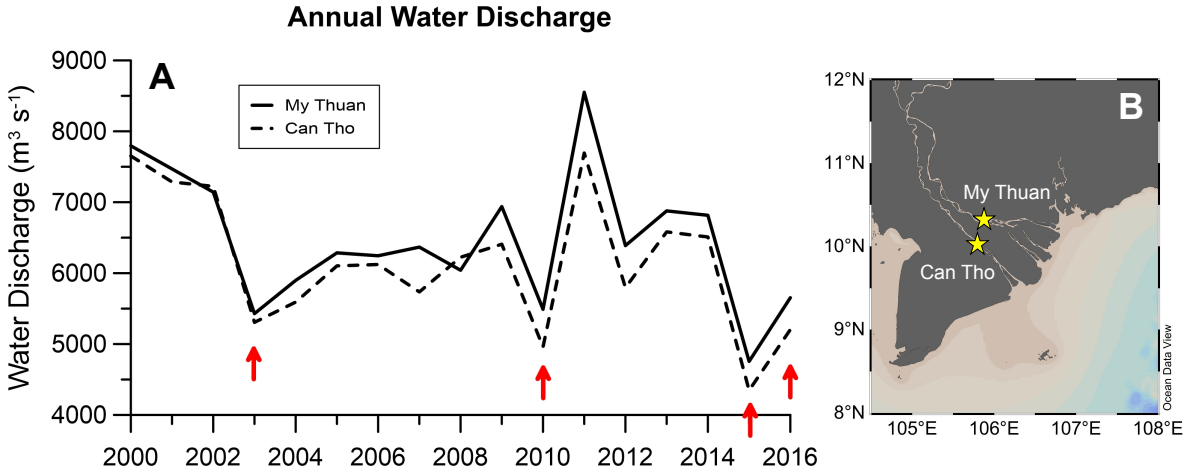

Figure S3.1: **(A)** Annual water discharge of the Mekong River measured at My Thuan and Can Tho stations from 2000-2016. Red arrows indicate post-ENSO years. Modified figure from Thi Ha et al. (2018). **(B)** Locations of My Thuan and Can Tho stations along the Mekong River.

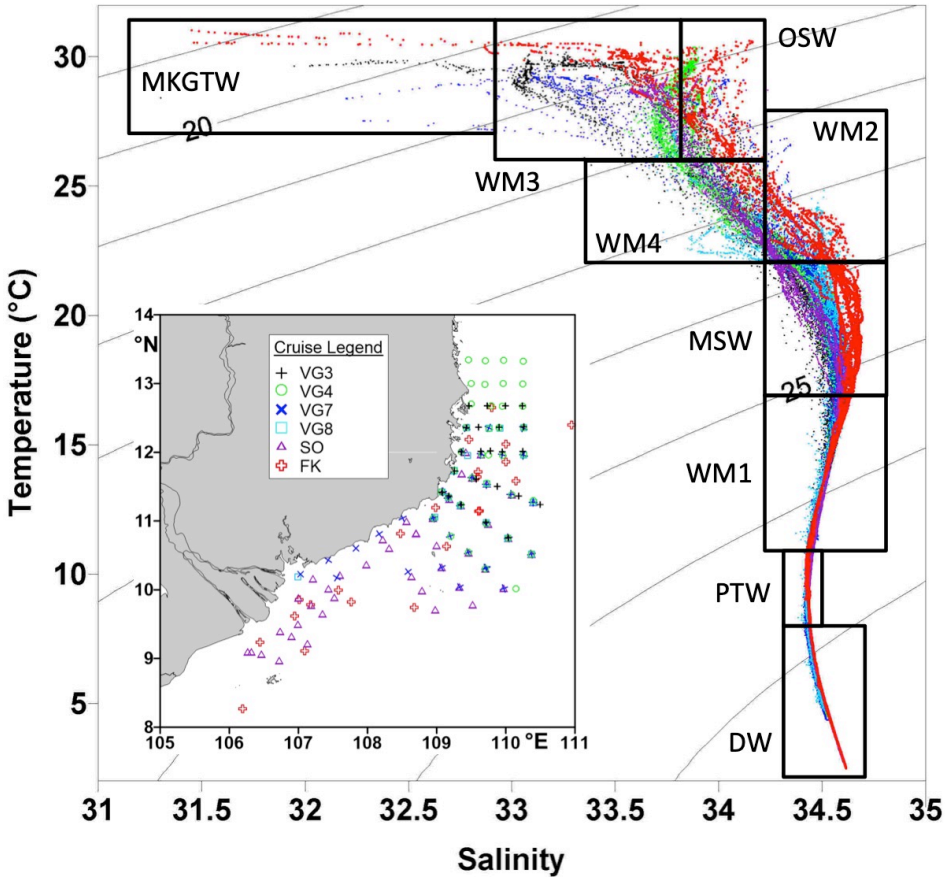

Figure S3.2: TS–Diagram for all cruises in the Vietnamese upwelling area. Boxes show modified definitions of characteristic SCS water masses originally given in Dippner and Loick–Wilde (2011): Deep Water (DW), Permanent Thermocline Water (PTW), Maximum Salinity Water (MSW), Open Sea Water (OSW), Mekong/Gulf of Thailand Water (MKGTW), Water Mass 1 (WM1): mixed water between MSW and PTW, WM2: mixed water between MSW and OSW, WM3: mixed water between OSW and MKGTW, and WM4: mixed water between OSW, MKGTW and MSW. Casts from each cruise are colored according to the map in the inset. VG3, VG7, and FK (red) represent cruises during the SWM season in 2003, 2004, and 2016, respectively. The isolines mark the density in σt units.

The slight water mass boundary modifications accommodated saltier Maximum Salinity Water (MSW) in June 2016, which is the core of the upwelling water (Dippner and Loick-Wilde 2011). Since MSW does not reach the surface in 2016 (or in any previously surveyed year), this modification does not affect surface water mass definitions.

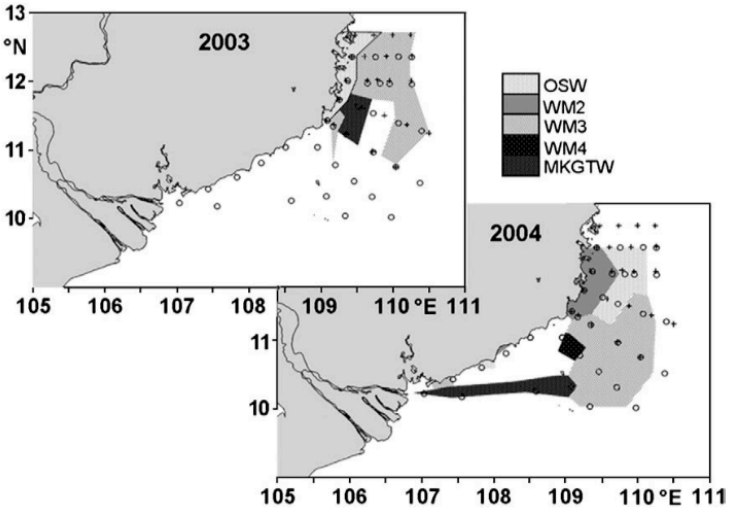

Figure S3.3: Surface maps showing the distributions of water masses defined by Dippner and Loick-Wilde (2011) during the July SWM seasons in 2003 and 2004. 2003 was a post-ENSO year. Sampling stations are marked by crosses and circles, respectively. Figure taken directly from Dippner and Loick-Wilde (2011).

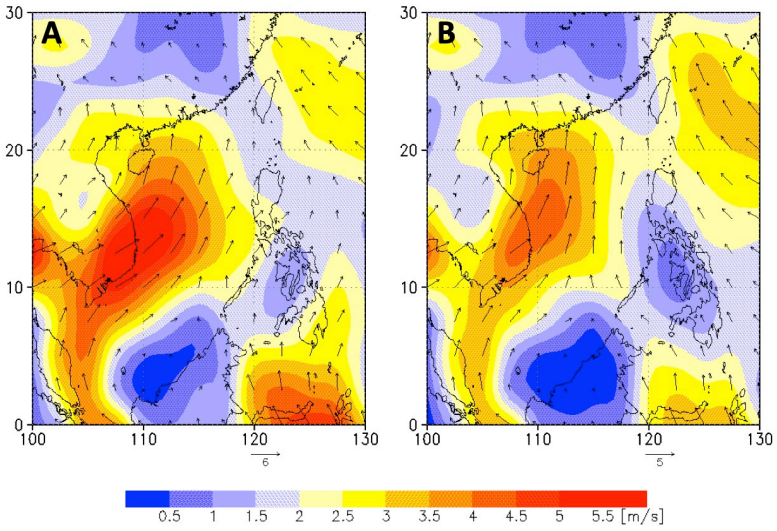

Figure S3.4: Comparison of wind strength averaged over the SWM season (MJJAS) **(A)** from 1948–2018 and **(B)** over the six strongest post-ENSO years over that timespan (1973, 1983, 1992, 1998, 2010, 2016) based on MAE and Niño3.4 indices. Wind magnitude is indicated by color and wind vector by arrows, though note the slight difference in vector scale between plots. Plots were made courtesy of Joachim Dippner using NCEP/NCAR Reanalysis data (Kalnay et al. 1996).

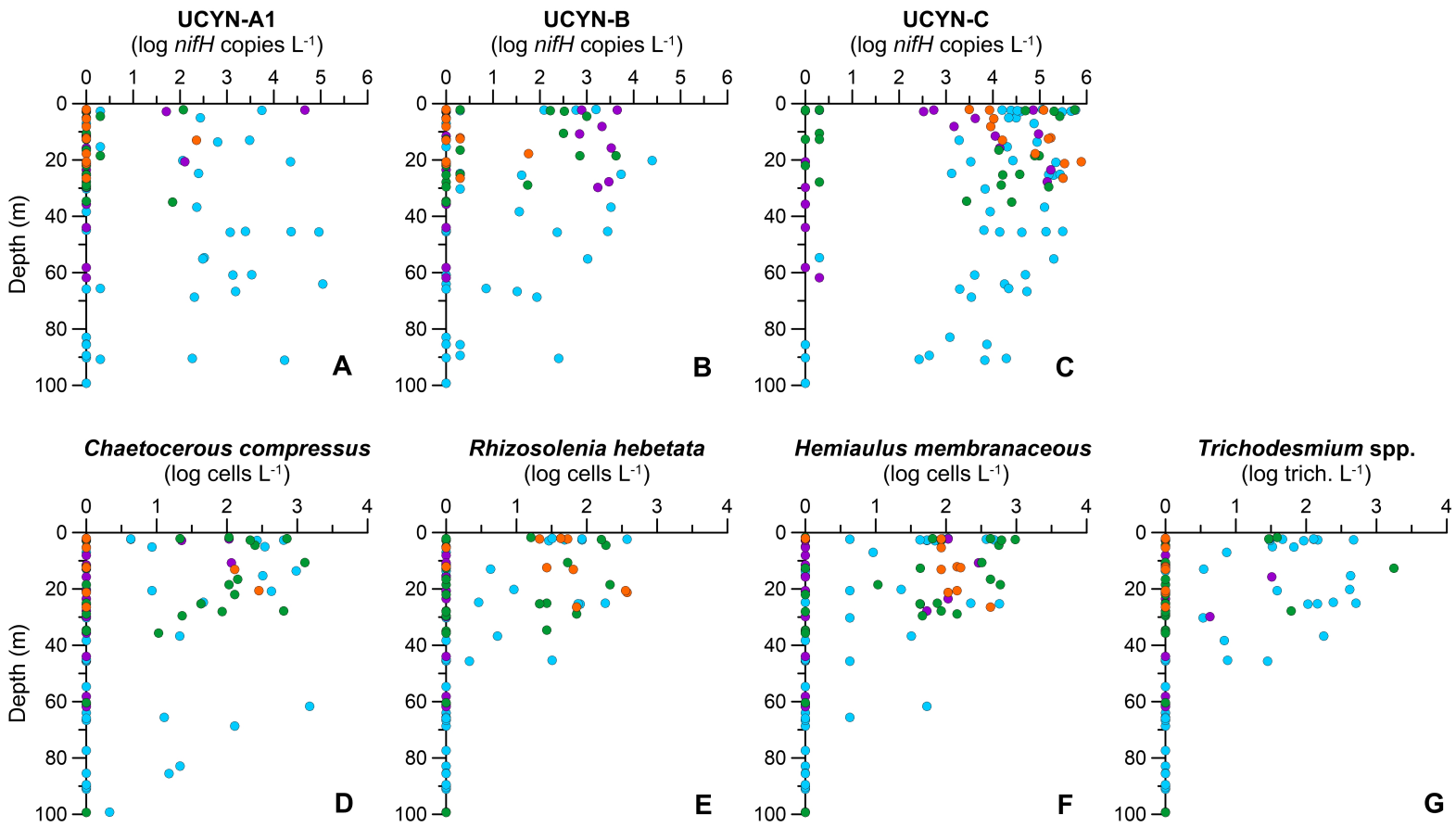

Figure S5.1: Water column abundances of the most prevalent groups of diazotrophs and diazotroph hosts as determined through *nifH* gene copy abundances of unicellular groups **(A-C)**, cell counts of DDA host species **(D-F)**, and trichome counts of *Trichodesmium* spp. **(G)**. Markers are colored according to their habitat types.

CHAPTER 6 – Diazotroph activity & contributions to POM

Supplemental Table 6.1: Summary of whole community areal activity integrated over the top 100 m of the water column or deepest depth sampled where the water column is shallower. For each measure, the habitat mean ± stdev is shown on the first line and the range of observed values in parenthesis is shown on the second line.

	Habitat Types			
	MRW	OnSW	UpW	OSW
# of profiles	3	4	3	9
Integration depth (m)	22 --	33 ± 3 (30 – 35)	52 ± 19 (30 – 65)	95 ± 8 (85 – 100)
Areal N_2-Fix (μmol N m^{-2} d^{-1})	82 ± 21 (65 – 106)	122 ± 29 (89 – 148)	96 ± 23 (77 – 121)	274 ± 164 (163 – 647)
Areal PP (mmol C m^{-2} d^{-1})	125 ± 86 (42– 214)	40 ± 23 (21 – 72)	43 ± 19 (25 – 63)	29 ± 14 (12 – 58)
$\%PP_{diazo}$	0.6 ± 0.4 (0.3 – 1.0)	2.5 ± 1.2 (1.3 – 4.0)	1.8 ± 1.2 (0.9 – 3.2)	6.7 ± 3.1 (2.9 – 12.1)

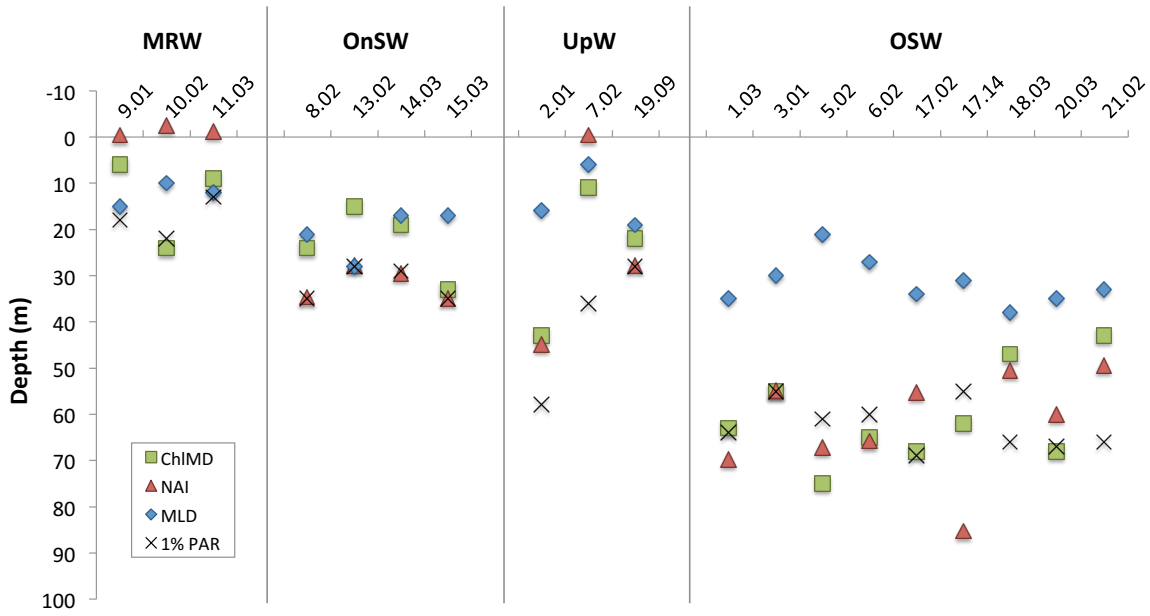

Figure S6.1: Compilation of chlorophyll max depth (ChlMD), nitrate availability index (NAI), mixed layer depth (MLD), and the depth of the 1% PAR (photosynthetically active radiation) light level across all stations, organized by habitat type.

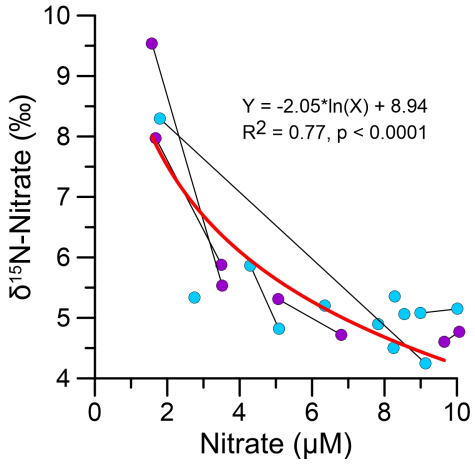

Figure S6.2: Pooled nitrate $\delta^{15}N$ measurements and concentrations from the top 100 m. Samples collected from the same CTD cast are connected with a black line and markers are colored according to their habitat type. The natural log fit of all data is shown in red, giving an isotope fractionation value (ε) of 2‰.

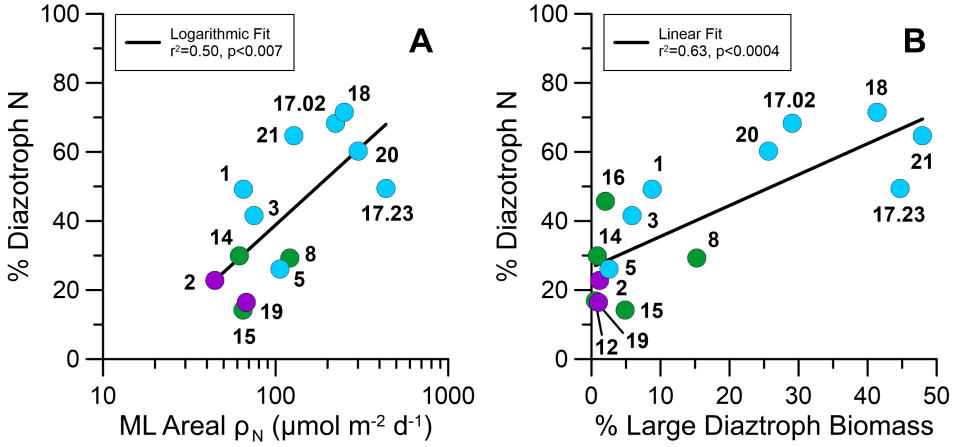

Figure S6.3: Relationship between the percentage of diazotrophic nitrogen in POM ($\%N_{diazo}$) to areal volumetric rates of nitrogen fixation integrated through the mixed layer **(A)** and to the proportion of large diazotroph biomass to total community biomass based on cell carbon estimates derived from microscopy counts **(B)**. Markers are labeled with their station number and colored according to habitat type. Logarithmic and linear fits are shown with the black lines (see plots for details). Stations whose $\delta^{15}N$-POM values may have been influenced by nitrate fractionation are not included (see Methods).

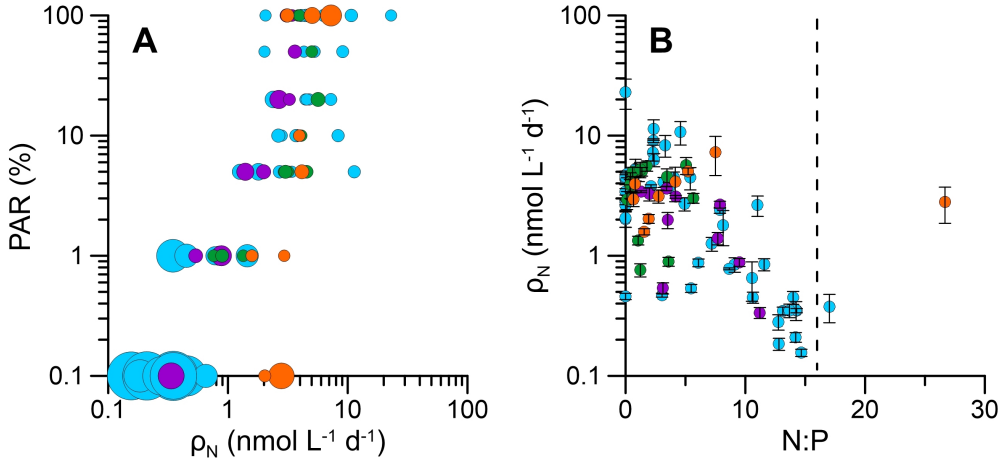

Figure S6.4: **(A)** Relationship of volumetric rates of total nitrogen fixation (bubbles) with photosynthetically active radiation (PAR, relative to surface) and $NO_{2/3}$ concentration. **(B)** Log volumetric rates of total nitrogen fixation versus N:P ratio, where error bars represent the standard deviation of replicates and the dashed line marks the Redfield ratio (16:1). All data are from the top 100 m (or deepest depth sampled) of the water column. Markers are colored according to habitat type.

Investigation of POM sources

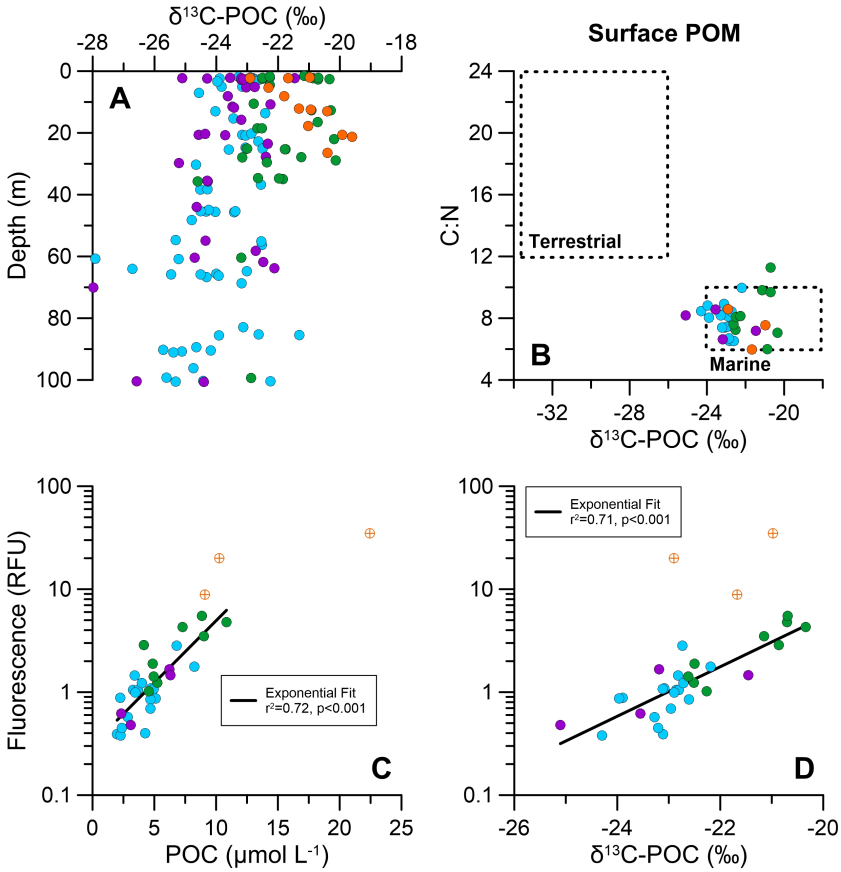

Figure S6.5: **(A)** $\delta^{13}C$ signatures of POM from the top 100m. **(B)** Source determination of surface POM based on C:N and $\delta^{13}C$ of particles, where boxes roughly delineate POM from terrestrial and marine sources. See text for details. Relationship of surface fluorescence (log scale) with POC **(C)** elemental concentration and **(D)** $\delta^{13}C$ signatures. MRW stations (orange, marked with cross) were excluded from correlation analyses; see plots. Markers in all panels are colored by habitat type.

The $\delta^{13}C$ of POC in the top 100 m ranged from -28.0 to -19.6‰, with the majority of surface values between -25 to -20‰ (Fig. S6.5A). Samples from the MRW and OnSW habitats tended to the have the heaviest (most positive) signatures. An analysis of carbon sources using the $\delta^{13}C$ signatures and C:N of surface POM (Fig. S6.5B) revealed that the particles were of primarily marine origin. The C:N values varied between roughly 5 to 11, which straddle the Redfield ratio of 6.6 for marine OM, but are mostly below the thresholds often used for terrestrial OM (> 12; e.g. Thornton and McManus 1994).

The isotopic signatures of C and N stable isotopes in POM can unravel isotopically distinct sources of organic material to a system. Given the proximity of some stations to the Mekong River and coast of Vietnam, a primary question underpinning interpretations in this study concerns the relative contributions of allochthonous POM (originating from land) and autochthonous POM (grown *in situ*) to the study site. One common approach to addressing this question is to use C and N elemental and isotopic ratios of POM. Terrestrial POM delivered by rivers and coastal runoff primarily reflects the surrounding plant life and thus tends to have a higher C:N (>12) than marine POM (C:N ≈ 6 – 10) (e.g. Savoye et al. 2003; Thornton and McManus 1994). Since an elevated C:N may also result from the degradation of autochthonous material (Bordovskiy 1965; Smith et al. 1992), the $\delta^{13}C$ of POM provides an additional useful tracer. Previous studies have shown that the $\delta^{13}C$ of POC in the Mekong estuary is heavily influenced by the natural vegetation (e.g. grasses, mangroves) and crops (e.g. rice) grown in the Mekong Delta (Borges et al. 2018), which are primarily C3 plants and thus have $\delta^{13}C$ signatures of -33 to -24‰ (O'Leary 1988). Conversely, marine phytoplankton tend to have more positive $\delta^{13}C$ signatures due to reduced discrimination against ^{13}C in their carbon source. As such, a $\delta^{13}C$ signature of < -26‰ is often used to distinguish terrestrial POM from marine ($\delta^{13}C$ > -24‰) (e.g. Savoye et al. 2003). Applying these source identifiers to our dataset, we see that the POM from surface waters in our study site – where an allochthonous signal would likely be strongest – is of predominantly marine origin.

Interestingly, the trends in near-surface $\delta^{13}C$ (Fig. 6.5A, B) are actually opposite of what we would expect from allochthonous inputs, since POC from the MRW and OnSW habitats was isotopically the heaviest (most positive) measured. These heavy signatures must instead reflect variation related to phytoplankton community composition and/or physiology. Coccolithophores, which are known to reach appreciable abundances in nutrient rich waters of the SCS (Jin et al. 2016, Hai Doan-Nhu personal comm.), have calcium carbonate shells that would increase the $\delta^{13}C$ of POC. Unfortunately, coccolithophores were not enumerated with microscopy surveys and acidification of surface POC samples was inconclusive.

Other factors that can increase $\delta^{13}C$ of phytoplankton biomass include larger cell size and high primary production, since both lower the cells' internal DIC concentration, which in turn reduces the expression of ^{13}C-discrimination associated with carbon fixation (Fry 1996; Fry and Wainright 1991). An investigation into the cell sizes of particularly abundant species was inconclusive, likely in large part because the species enumerated via

microscopy always accounted for < 25% of the total surface POC (not shown). We additionally found no significant relationship of surface δ^{13}C-POC with our primary production rates (not shown), though this is not altogether surprising since these rates reflect activity over the course of one day, whereas POC pools may integrate over multiple days to weeks. We did, however, find that both POC elemental and ^{13}C-isotope abundances scaled directly with log fluorescence (r^2=0.72, p<0.001 and r^2=0.71, p<0.001, respectively; Fig. S6.5C, D) when MRW stations with particularly high surface fluorescence were excluded, suggesting that the observed trends in δ^{13}C of POC are related to phytoplankton.

References

Bordovskiy, O. K. 1965. Accumulation of organic matter in bottom sediments. Marine Geology **3:** 33-82.

Borges, A. V., G. Abril, and S. Bouillon. 2018. Carbon dynamics and CO2 and CH4 outgassing in the Mekong delta. Biogeosciences **15:** 1093-1114.

Fry, B. 1996. 13C/12C fractionation by marine diatoms. Marine Ecology Progress Series **134:** 283-294.

Fry, B., and S. C. Wainright. 1991. Diatom sources of 13C-rich carbon in marine food webs. Marine Ecology Progress Series **76:** 149-157.

Jin, X., C. Liu, A. J. Poulton, M. Dai, and X. Guo. 2016. Coccolithophore responses to environmental variability in the South China Sea: species composition and calcite content. Biogeosciences **13:** 4843-4861.

O'Leary, M. H. 1988. Carbon Isotopes in Photosynthesis: Fractionation techniques may reveal new aspects of carbon dynamics in plants. BioScience **38:** 328-336.

Savoye, N., A. Aminot, P. Tréguer, M. Fontugne, N. Naulet, and R. Kérouel. 2003. Dynamics of particulate organic matter δ15N and δ13C during spring phytoplankton blooms in a macrotidal ecosystem (Bay of Seine, France). Marine Ecology Progress Series **255:** 27-41.

Smith, D. C., M. Simon, A. L. Alldredge, and F. Azam. 1992. Intense hydrolytic enzyme activity on marine aggregates and implications for rapid particle dissolution. Nature **359:** 139-142.

Thornton, S. F., and J. McManus. 1994. Application of organic-carbon and nitrogen stable-isotope and C/N ratios as source indicators of organic-matter provenance in estuarine systems - Evidence from the Tay Estuary, Scotland. Estuarine Coastal and Shelf Science **38:** 219-233.

CHAPTER 7 – Diazotroph inputs to the planktonic food web

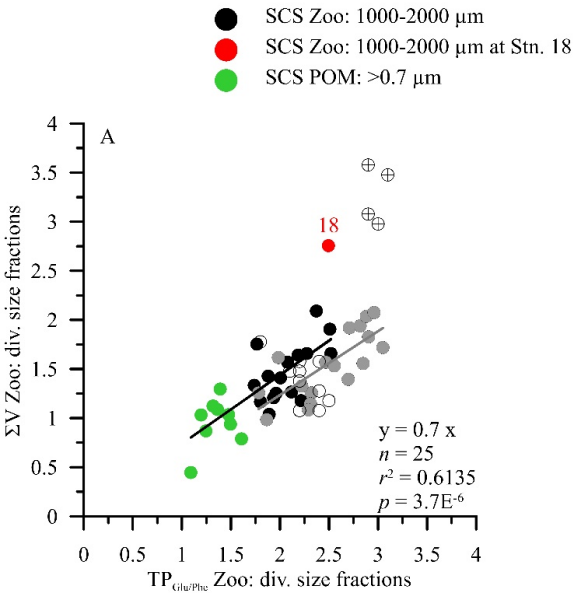

Figure S7.2: The composite relationships between $TP_{Glu/Phe}$ and the heterotrophic microbial re-synthesis proxy (ΣV) in this dataset (POM and zooplankton 1000-2000 µm) in comparison to mesozooplankton data sets with intensive microbial re-synthesis from the suboxic zone of the Baltic Sea (Eglite et al. 2018) and with no microbial re-synthesis from the tropical North Pacific (Monpéan et al. 2016). ΣV values of maximum 2 and coupled ΣV and TP values indicate the absence of intensive heterotrophic microbial re-synthesis of amino acids (Ohkouchi et al. 2017).

BONUS: Nutrient Amendment Experiments

I carried out a series of nutrient amendment experiments (NAEs) in an attempt to answer the following for our surveyed region: (i) which nutrients (N, P, Si) limit phytoplankton growth, (ii) are there group specific responses within the phytoplankton communities to nutrient additions, (iii) are the composition and abundance of diazotroph communities influenced by nutrient additions, and (iv) can the experimental outcomes be extrapolated to the natural conditions encountered on the cruise?

In brief, a total of three NAEs were conducted at the following stations: UpW Stn. 3, OnSW Stn. 8, and OSW Stn. 17. For each experiment, twenty-four 2-L Whirl-pak® bags were filled with surface seawater from a single CTD cast and amended with nitrate ($NaNO_3$, final conc. of 16 μM), phosphate (KH_2PO_4, final conc. of 1 μM), and silicate (Na_2SiO_3, final conc. of 16 μM) following a factorial design (in triplicate) with one control (Cntl) and seven treatments: (+N), (+P), (+Si), (+N,P), (+N,Si), (+P,Si), (+N,P,Si). After spiking the seawater, the bags were sealed by rolling down the top at least three times, allowing some air to remain inside for gas exchange and to serve as a leak indicator. The bags were then placed in an on-deck, flow-through incubator (unshaded, covered by an acrylic incubator lid). Samples for monitoring phytoplankton activity and community structure were collected approx. 36 (T_{36}) and 72 (T_{72}) hours after the start of incubation (Table S1). Baseline (T_0) samples were collected directly from the CTD Niskin bottles. Nutrient concentrations at T_0 were not measured directly, but were calculated based on the addition of the ambient nutrient concentrations at the surface at the time of collection plus the concentration of nutrients added for each treatment.

Table 8.1: Methods explanation

Sample Type	**T_0**	**T_{36}**	**T_{72}**
Nutrients	50 mL	50 mL	50 mL
Phytoplankton counts/ID	45 mL	45 mL	45 mL
Pigments	1 L	--	1 L
nifH assessment	1L	--	Rem. Vol.*

*combined remaining volume of replicates, ~0.5L each

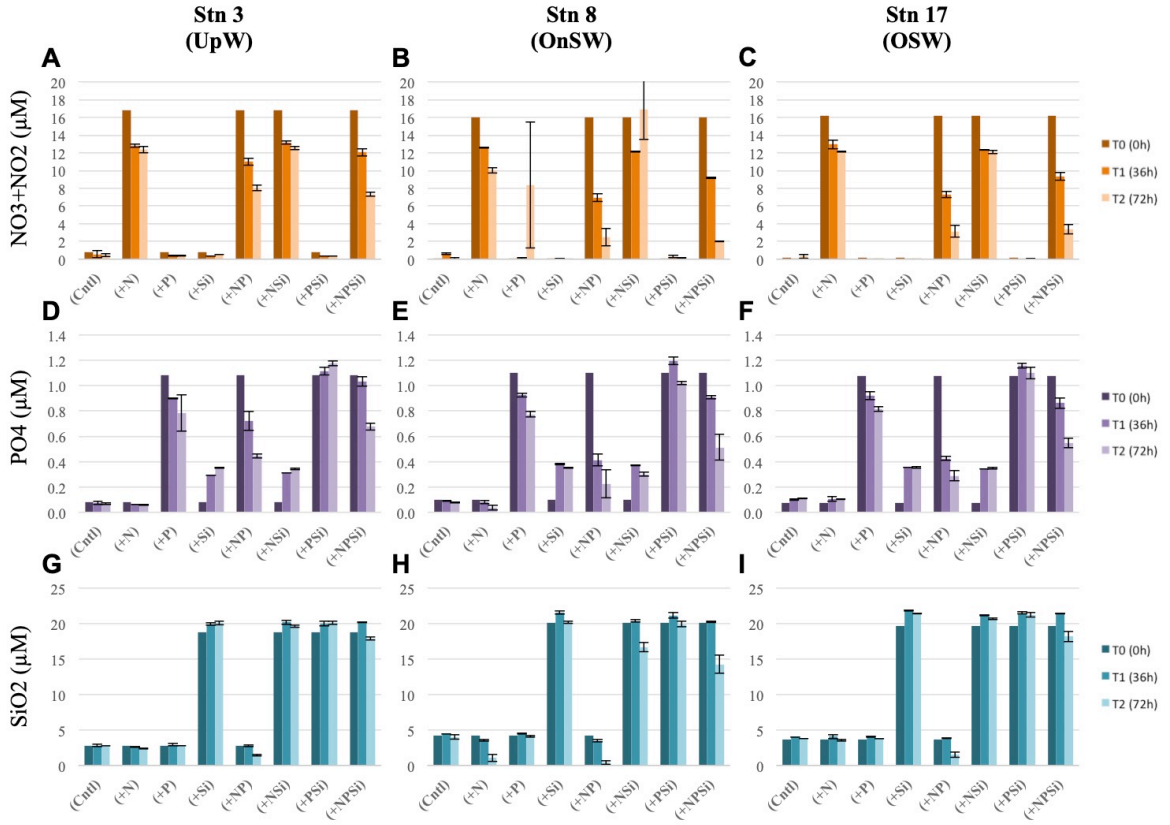

Figure S8.1: Concentrations of $NO_{2/3}$ **(A-C)**, PO_4^{3-} **(D-F)**, and SiO_2 **(G-I)** across all treatments and controls (x-axes) at three time points (see legends) in all three NAEs at Stns. 3 (first column), 8 (middle column), and 17 (last column). Error bars show std dev of experimental triplicates.

Nutrient concentrations show the fastest depletion of both N and P in N+P treatments, suggesting co-limitation of N and P. The strongest drawdown of nutrients tended to occur within the first 36 hours. I suspect that there was a minor P contamination in the Si stock, which complicates interpretations.

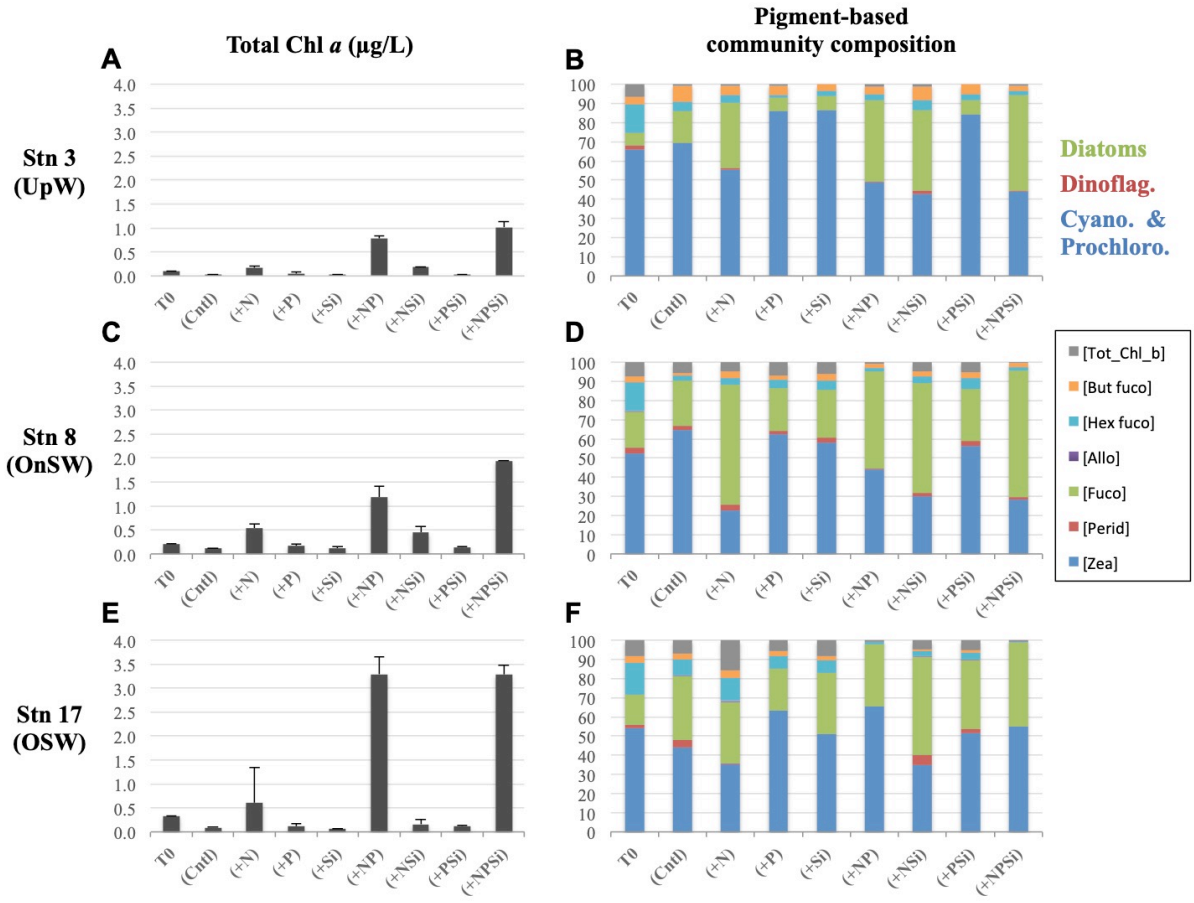

Figure S8.2: Total chlorophyll a concentrations **(A, C, E)** and relative community composition based on diagnostic pigment concentrations (see figure legends and Methods chapter) across all treatments (x-axes) for all three NAEs at UpW **(A, B)**, OnSW **(C, D)**, and OSW **(E, F)** stations. Data are shown for time points T0 and T72 and represent averages of experimental triplicates.

Based on total Chl a concentrations, phytoplankton responded the strongest to N+P treatments, again suggesting co-limitaion of N and P. There was also a modest signal in +N only treatments in most experiments. Interestingly, Chl a responses were the weakest at the UpW station, whereas phytoplankton responded the strongest at the OSW station. The majority of the stimulated community consisted of diatoms, particularly in any treatment with N, suggesting this group is well suited to rapid N use.

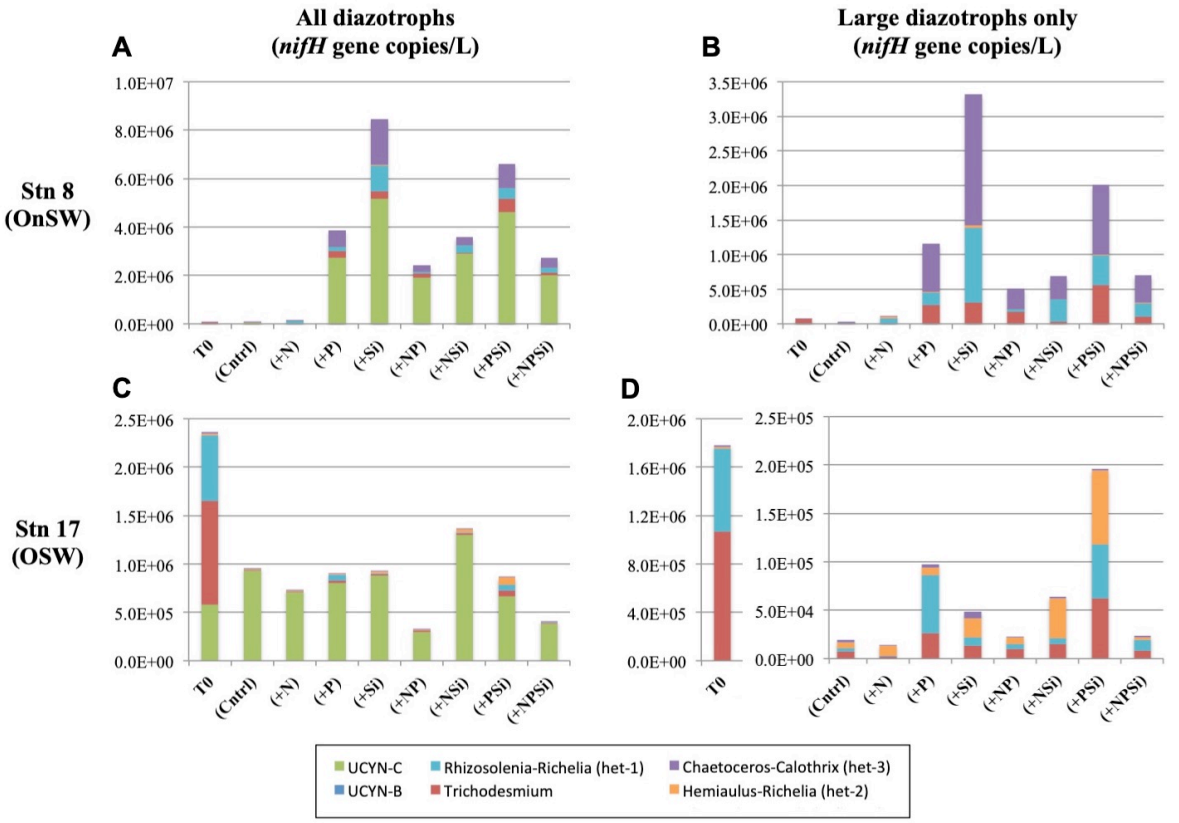

Figure S8.3: Diazotroph community composition and estimated absolute abundances based on *nifH* gene analyses for all diazotrophs examined (see legend) **(A, C)** and for the large diazotrophs only (excluding unicellular groups) **(B, D)**. Molecular data is available only for Stn. 8 **(A, B)** and Stn. 17 **(C, D)** at time points T0 and T72.

I have *nifH* gene copy abundances from only two of the experiments, but there are interesting similarities nonetheless. UCYN-C overwhelmingly dominated nearly all treatments, indicating that they could compete even in high N conditions in the presence of rapidly growing diatoms. They may be well suited to the incubation bags, but the above statement holds true nonetheless. Out of the large diazotrophs, dominant species differed between experiments, with Chaetoceros-Calothrix domination Si (+P) treatments in OnSW waters. Diversity was high among the large diazotrophs, and growth responses tended to be greatest when P was added, indicating P limitation.

Declaration

I hereby affirm that I have produced the present work independently and have written it without outside help, that I have used only the aids and sources indicated by me for this purpose, and that I have appropriately cited passages taken either directly or borrowed from in terms of content.

Rostock, 21.01.2020